2021

Experimental Methods To Support Robot Behavior Design For Legged Locomotion On Granular Media

Sonia Roberts
University of Pennsylvania

Experimental Methods To Support Robot Behavior Design For Legged Locomotion On Granular Media

Abstract

Most models of legged locomotion assume a rigid ground contact, but this is not a reasonable assumption for robots in unstructured, outdoor environments, and especially not for field robots in dry desert environments. Locomotion on sand, a highly dissipative substrate, presents the additional challenge of a high energetic cost of transport. Many legged robots can be adapted for desert locomotion by simple morphological changes like increasing foot size or gearing down the motors. However, the Minitaur robot has direct-drive (no gearbox) legs which are sensitive enough to measure ground properties of interest to geoscientists, and its legs would lose their sensitivity if they were geared down or the footsize increased substantially. This thesis has two main contributions. First, a controller for jumping on sand with a direct-drive robot that saves significant energy in comparison to a nominal compression-extension Raibert-style controller without sacrificing jump height. This controller was developed by examining the complex interaction between the jumping leg and the ground, and devising a force to add to the leg controller which will push the robot's foot into a more favorable state that does not transfer as much energy to the ground. The second contribution is a ground emulator robot which can be programmed to exert ground force functions of arbitrary shape. With the ground emulator, it is possible for a robot on a linear rail to jump dozens of times per experiment, whereas traditional experiments on granular media would require the ground to be reset between individual jumps. Results from the simulation experiments used to develop the controller and the ground emulator experiments used to test it on a physical robot leg are validated with experiments on a prepared granular media bed. Finally, the contributions of this thesis are contextualized in a broader project of building explainable artificially intelligent systems by composing robust, mostly reactive controllers.

Degree Type

Dissertation

Degree Name

Doctor of Philosophy (PhD)

Graduate Group

Electrical & Systems Engineering

First Advisor

Daniel E. Koditschek

Second Advisor

Cynthia Sung

Keywords

energy, granular, legged

Subject Categories

Robotics

EXPERIMENTAL METHODS TO SUPPORT ROBOT BEHAVIOR DESIGN FOR LEGGED LOCOMOTION ON GRANULAR MEDIA

Sonia F. Roberts

A DISSERTATION

in

Electrical and Systems Engineering

Presented to the Faculties of the University of Pennsylvania

in

Partial Fulfillment of the Requirements for the

Degree of Doctor of Philosophy

2021

Daniel E. Koditschek, Supervisor of Dissertation
Professor of Electrical and Systems Engineering

Alejandro Ribeiro, Graduate Group Chairperson
Professor of Electrical and Systems Engineering

Dissertation Committee:

Cynthia Sung, Professor of Mechanical Engineering, University of Pennsylvania
Marc Miskin, Professor of Electrical and Systems Engineering, University of Pennsylvania
Tonia Hsieh, Professor of Biology, Temple University

EXPERIMENTAL METHODS TO SUPPORT ROBOT BEHAVIOR DESIGN FOR LEGGED LOCOMOTION ON GRANULAR MEDIA

This thesis is dedicated to the people who passed away during its completion.

Robin Harris

Ron Hamilton

Henry Smith

Carolyn Hamilton

Doug Hamilton

Tom Dodson

Andres Gutierrez

Acknowledgments

Thank you to the National Science Foundation, which made this work possible with NSF NRI-2.0 grant #1734355 and NSF INSPIRE grant #1514882. Thank you to my mentors, and especially my adviser, Dan Koditschek. I am also grateful for the machining support I received from Terry Kientz and Jeremy Wang. Thank you to Diedra Krieger for your administrative support. Thank you to my colleagues in Kodlab, Modlab, and the IGERT Fellowship. Thank you to my stitching group, my contra dance friends, my Quizo team, my artist friends in Philadelphia, my climbers and barbequeuers, and my gamers. Thank you to the partners who have supported me at different points during this long journey through the dissertation. And thank you to my family.

ABSTRACT

EXPERIMENTAL METHODS TO SUPPORT ROBOT BEHAVIOR DESIGN FOR LEGGED LOCOMOTION ON GRANULAR MEDIA

Sonia F. Roberts

Daniel E. Koditschek

Most models of legged locomotion assume a rigid ground contact, but this is not a reasonable assumption for robots in unstructured, outdoor environments, and especially not for field robots in dry desert environments. Locomotion on sand, a highly dissipative substrate, presents the additional challenge of a high energetic cost of transport. Many legged robots can be adapted for desert locomotion by simple morphological changes like increasing foot size or gearing down the motors. However, the Minitaur robot has direct-drive (no gearbox) legs which are sensitive enough to measure ground properties of interest to geoscientists, and its legs would lose their sensitivity if they were geared down or the foot size increased substantially.

This thesis has two main contributions. First, a controller for jumping on sand with a direct-drive robot that saves significant energy in comparison to a nominal compression-extension Raibert-style controller without sacrificing jump height. This controller was developed by examining the complex interaction between the jumping leg and the ground, and devising a force to add to the leg controller which will push the robot's foot into a more favorable state that does not transfer as much energy to the ground. The second contribution is a ground emulator robot which can be programmed to exert ground force functions of arbitrary shape. With the ground emulator, it is possible for a robot on a linear rail to jump dozens of times per experiment, whereas traditional experiments on granular media would require the ground to be reset between individual jumps. Results from the simulation experiments used to develop the controller and the ground emulator experiments used to test it on a physical robot leg are validated with experiments on a prepared granular media bed. Finally, the contributions of this thesis are contextualized in a broader project of building explainable artificially intelligent systems by composing robust, mostly reactive controllers.

Contents

List of Tables

List of Figures

Part I

Introduction, Motivation, Preliminaries

Chapter 1

Introduction

1.1 Organization and contributions

This thesis presents three contributions, each of which has its own section after this introductory chapter and a chapter summarizing locomotion problems for legged robots in desert field work (Chapter 2). The main contribution is a reactive controller for jumping on sand with a direct-drive robot which significantly reduces energetic cost of transport without reducing jump height. This controller was tested in simulation (Fig. 3.9), physical emulation (Fig. 4.6), and in experiments on prepared granular media (Fig. 5.3). The second contribution is the design (Fig. 4.1) and validation (Fig. 4.5) of an experimental platform for testing vertical hopping on ground with arbitrary force functions. This is a novel method for performing experiments on compressible, dissipative substrates. The final contrbution is the contextualization of the approach to robot behavior design employed in this thesis in the broader project of building explainable artificially intelligent systems (Chapter 6).

The next chapter briefly summarizes some of the motivations and applications of this work as part of a larger project adapting legged robots for geoscientific field work (Chapter 2.1), describes of the difficulty of designing controllers for complex limb-environment interactions like locomotion on natural sand [103, 105, 107] (Chapter 2.2), and contextualizes the contributions with related work (Chapter 2.3). A table summarizing the contributions to the literature that accompany this thesis is in Appendix A. The direct-drive Minitaur's [70] legs can be used as shear sensors to measure the erodibility of the ground – a quantity of interest to our geoscientific collaborators [97, 102]. However, because of these direct-drive legs, Minitaur overheats very quickly in the desert and cannot reliably transport itself between testing locations. As a result, our team of geoscientists currently uses a single Minitaur limb attached to the back of a heavily geared RHex [42] robot which can locomote more effectively than a Minitaur in the desert and over longer distances. A preferable solution would be a team of robots: One with sensitive legs which could transport itself quickly through the desert and make quick measurements of erodibility over a large area, and a slower, heavily geared robot that could follow it while carrying heavy sensing equipment to measure things like wind speed and direction, airborne sand grains, and soil moisture content. This thesis thus focuses on locomotion with sensitive, direct-drive legs on highly dissipative substrates like sand.

The simplest form of unstructured, soft ground is dry, homogeneous granular media, an idealized form of what one might find in a desert. This ground type is not "simple" because the reaction forces it exerts upon intrusion are simple, but rather because there are analytic models describing these forces. Whereas the behavior of more complex ground types cannot even be simulated without appeal to discrete element models, it is possible to simulate dry, homogeneous granular media much more quickly and efficiently without loss of accuracy. It is thus possible to conceive of sand as a type of "spring" with complex stiffness and damping functions, and no restoring forces (Chapter 3.1.2). A robot attempting to locomote over sand is, in a sense, loading the ground's lossy spring with energy which – unlike on rigid ground – will not be returned.

The difficulty of designing controllers for complex limb-ground interactions is resolved by developing a method for designing reactive controllers on the energetic cost landscape of the limb-ground interaction [106] (Chapter 3). A Raibert-style hopper uses a simple but robust spring-based controller that commands the robot leg to exert a soft spring force during the compression mode of stance and a stiff spring force during the extension mode (Chapter 3.1.1). The trajectory of the robot's foot in state space can then be mapped onto the energetic cost landscape while the robot performs a single jump on simulated granular media. It is then possible to identify the times during the jump that were most energetically costly, and write a control law to push the robot foot away from locations in its state space that transfer large quantities of energy to the ground (Chapter 3.2.3). The resulting "active damping" controller operates on the robot's leg spring by modulating the damping in the proportional-derivative controller, and significantly reduces the energetic cost to perform a single jump on granular media.

The second section discusses a novel experimental apparatus (Chapter 4) and protocol designed for testing complex limb-ground interactions [108]. Previous methods for developing and testing robot controllers for granular media are limited in two ways. First, in order to obtain consistent behavior, granular media must be completely refluidized between every experiment. Fluidizing granular media beds are complex and expensive to build, requiring precise manufacturing, specialty materials like porous plastic sheeting, and large air compressors. This is the minimum required for consistent behavior from the granular media. Second, in order to test a controller over a range of different granular media force responses, researchers often modulate the compaction of one type of granular media (often poppyseeds) by sending small puffs of air into the granular media bed or shaking the bed with an additional motor. However, there is no way to decouple the stiffness and damping force responses by modulating the granular media compaction. The only way to accomplish this is to switch out the granular media in the bed and perform experiments on a variety of media with different grain properties, like density and friction.

To address these limitations, I developed a robotic "platform" that can emulate arbitary ground force functions [108] (Chapter 4). The platform consists of a nearly direct-drive (low gearbox ratio) robot "leg" attached to a vertical rail via a gantry plate (Chapter 4.2.2). The leg actuates a platform which is constrained to move up and down along the rail. The platform uses a proportional-derivative controller with simplified granular media stiffness and damping functions to hold a nominal position, and a ratchet mechanism prevents the platform from producing restoring forces (Chapter 4.2.3). Physical experiments to fit the stiffness and damping functions validated the emulation capabilities (Chapter 4.2.6). Another single robot leg can be attached to the vertical rail with a second gantry plate, and allowed to jump on the platform (Chapter 4.2.5). Using this platform in place of physical granular media, it is possible to perform multiple jumping experiments in a row without refluidizing a granular media bed, and a variety of experiments with different ground force functions without having to switch out the physical granular media.

Results from the platform have been validated with experiments in prepared granular media, a commonly accepted method for studying locomotion on granular media [109] (Chapter 5). Consistent preparation is achieved by stirring and smoothing the surface of the media between jumps and by using media with a large enough grain diameter that it can only occupy a tight range of volume fractions, which determine the ground stiffness.

After these two sections, a concluding section contextualizes the contributions of this thesis into a larger project of designing robust robot behavior using structured compositions of mostly reactive controllers, applying concepts from ecological psychology and philosophy to engineering [113, 114] (Chapter 6). Most modern robot behavior design, including previous research on efficient jumping on granular media, relies heavily on equipping the robot with an elaborate model of its environment. I suggest instead that simple and robust control, particularly for tasks like locomotion, can be achieved by modeling relevant aspects of the robot-environment interaction and developing controllers that operate in this space. Such controllers arguably exploit *affordances* (Chapter 6), which are defined as perceptually stable opportunities for purposeful action in an agent-environment system.

Chapter 2

Application of legged robot locomotion to geoscientific research

This chapter begins with a discussion of the applications of legged robot locomotion to geoscientific research, and specifically the motivating application driving the research presented in this thesis. This is followed by a brief description of three natural desert sites and a summary of observations and a few experiments performed at these sites. Finally, the work in this thesis is contextualized by some related work.

2.1 Multi-robot team and multidisciplinary collaboration

I worked with a team of geoscientists, cognitive scientists, and other roboticists [97] to develop a heterogeneous team of robots to collect data relevant to geoscientific experiments in hostile environments such as deserts. The two robots used were a "pack mule" X-RHex [42] robot carrying large payload of sensors [101, 112] and a fast, dynamic Ghost[1] Minitaur [70] robot with four legs that can be used as force sensors to quickly measure ground properties relevant to erodibility over a large area [97] due to the proprioceptive transparency [69] of its direct-drive legs. The Minitaur robot can be programmed for purposes of locomotion using the composition of virtual damped springs [36]. However, due to the inefficiency of motors

[1] Ghost Robotics, 3401 Grays Ferry Ave, Philadelphia, PA 19146 http://www.ghostrobotics.io

in the high-torque, low-velocity regime required for direct-drive legged robot locomotion, Minitaur is currently unable to run in the highly taxing desert environment. This inefficiency of the motors causes intense thermal loading from joule heating, which ultimately causes damage to the robot. As a result, force-sensing experiments in the field are currently conducted with a single direct-drive Minitaur leg mounted on the back of a heavily geared X-RHex, leaving little room for additional sensors. In this thesis, I target the Minitaur robot, aiming to improve its locomotion capabilities in the desert.

In previous experiments using robots to collect data in deserts, X-RHex was made desert-ready with an increase to its gearbox ratio, wider feet, and stiffer legs [97], but these options are undesirable choices for Minitaur. The addition of a gearbox would reduce actuator transparency [69] and make the robot unable to act as a force sensor; the foot size can be increased by about a factor of two, but too large a foot and the inertia will again render the force sensor useless; and stiffening the legs comes at a high cost from the battery, since the spring force is virtual rather than mechanical. The increase in gearbox ratio has also slowed X-RHex down significantly: whereas a standard X-RHex can keep up with a jogging or running human on rugged terrain [61], the highly geared desert version has a top speed at best closer to human walking speed [97]. As Minitaur cannot be geared down without reducing its desired functionality, it is a prime candidate for a fast-running “scout” robot to act in concert with the slower “pack mule” RHex, covering a large area quickly and taking many measurements with the same legs it uses to transport itself and marking areas of interest for RHex to investigate with a wider complement of sensors.

2.2 Field trips to deserts and dune systems suggest challenges for locomotion on natural sand

Fieldwork trips with the RHex [42, 118] robot to dune systems in China and the United States heavily informed the assumptions and work in this thesis. This section describes the environments I visited, generally with a team of engineers and other scientists. I then summarize the relevant experiments and observations from these field trips.

2.2.1 Descriptions of natural dune systems visited

The study site at the Tengger

This study site was the Chinese Academy of Sciences Shapotou Desert Research and Experiment Station, which is located in the southeastern part of the Tengger Desert, in Zhongwei, Ningxia Province, People's Republic of China. According to local meteorological records (as cited in [77]), the annual rainfall is 180.2mm with an annual potential evaporation of 2900mm. The area is characterized as between a steppified and a sandy desert, with short (< 1m) bushes scattering the study site and a range of elevations between 1300 and 1350m.

During our field trip to this desert [101], we spent two days at the Shapotou Research Station (pictured in Figure 2.1). Two days before our arrival, heavy rainfall raised the water table sufficiently high that a human or a robot walking on the surface of the dune could step on wet sand. The rain also compacted the sand dune surface. Over the two days of experiments, we experienced a large range of sand compactions and cohesiveness as the water evaporated and the sand dried. By the end of the second day, the sand was quite dry and loose again. Overall, the sand at the Tengger was very fine, light, and soft.

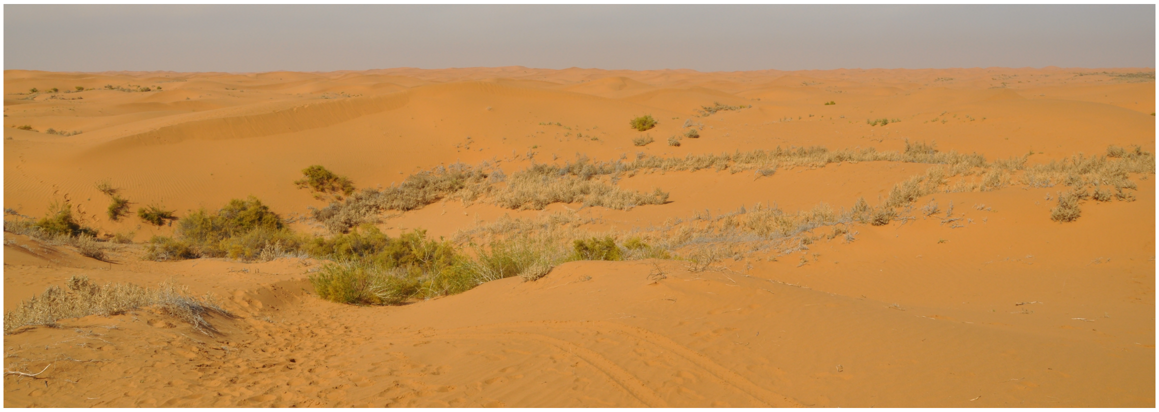

Figure 2.1: The Tengger landscape at the Shapotou Desert Research and Experiment Station [101].

The study site at White Sands National Monument

The White Sands dunefield is the largest known gypsum dunefield in the world and covers an area of 500 km^2. It is located in the topographically-closed Tularosa Basin of the Rio Grande

Rift in southern New Mexico. The dunefield is comprised of a central area of crescentic dunes up to 15m high, flanked on its north, east, and south sides by partially vegetated parabolic dunes. To the west is an extensive deflation plain (Alkali Flat), which constitutes the main source of sediment for the dunefield. The dominant winds in the basin are from the SW and W during winter, with N-NW winds in the fall and winter and S-SSE in summer.

As a result of these conditions, the dunes are highly variable. The changing wind directions and large range of the dune field created from localized sediment results in dunes that vary widely in size and shape, with dunes that have maximum 29 degree slopes very near shallow dunes with slopes not exceeding 20 degrees. The ground conditions in relatively flat areas are also highly variable, including hard, compacted sand between dunes, interdune areas that have been encroached upon by the shallow sloping feet of typical crescentic dunes, large playas, vegetated areas with bushes that catch sand and create small hills, and compacted ripples left behind by migrating dunes. This variety makes it possible to test a robot on many different varieties of desert landscape in one day. We visited this site in 2014 to run preliminary tests with RHex [112] and again in 2016 to perform further experiments with RHex and make preliminary observations about Minitaur's performance on sand.

The study site at the Jornada Experimental Range

The Jornada Experimental Range is managed by the USDA Agricultural Research Service Range Management Research Unit established to produce new knowledge of ecosystem processes for the development of technologies for remediation and management of desert rangelands. The Jornada conducts world-class research as demonstrated by its designations as a USDA Long-Term Agriculatural Research site (LTAR), an NSF Long-Term Ecological Research site (LTER), and an NSF National Ecological Observatory Network (NEON) participant. The Jornada Experimental Range occupies an area 783km^2 located 40 km north of Las Cruces, NM. It is on the Jornada del Muerto Plain in the northern Chihuahuan Desert [53]. The region has abundant sunlight, low air humidity and wide ranges in daily temperature. The sand composition is more typical for the area and does not have an unusual localized sediment source like the Alkali Flats provides for White Sands.

The dunes in the Jornada are very small, at most a few feet in height, and the area is heavily vegetated. The sand is also significantly stiffer than at White Sands, with more hard interdune areas. We visited this site at the same times that we visited White Sands [111], but spent less time here because the environment was less challenging for the robots.

The study site at Oceano Dunes

The Oceano Dunes State Vehicular Recreation Area is a state park in part of the Guadalupe-Nipomo dune system in central California. The Guaalupe-Nipomo dune system is the second-largest dune system in the state of California and covers approximately 89 km^2 [5]. The Ocean Dunes SVRA has been used for off-road recreational vehicle activities since 1982, but concerns about the ecological impact of off-road vehicles have led to plans to close the park for off-road vehicles within the next three years [5, 115].

The source of the sand is primarily the San Lucia Mountains, and consists mostly of quartz and other minerals such as feldspar and hematite. The dune field is directly east of the Pacific Ocean, and the winds coming from the ocean to the west are extremely dominant. Due to this consistent dominant wind vector, we observed much more similarity in dune conditions in different parts of the park than we had observed in either the Jornada or White Sands. As the Oceano Dunes are a coastal dune system, there was also higher humidity and more cloud cover closer to the water. We visited Oceano Dunes in 2016 to field-test modifications made to adapt RHex to desert and dune research and to gather observations about Minitaur's behavior on natural sand.

Visits to other field sites

In addition to the Tengger, White Sands, the Jornada, and Oceano, our team visited Zzyzx in 2016 to test the RHex robots on dunes in the Mojave National Preserve. Zzyzx is located in southeastern California near the southernmost tip of Nevada and is home to the California State University Desert Studies Center. In 2014 I also separately visited Revolution Recovery, a recycling center in Philadelphia, and drove the RHex robot up piles of wood chips, gypsum sheets, concrete pieces, and other separated recyclable materials. I did not gain unique insights into robot locomotion at these sites and I will therefore not discuss them in detail, but it should be noted that the robot had similar locomotion issues in all of these very different environments.

2.2.2 Observations about locomotion in the desert with RHex

Sand dune substrate differs wildly within one robot body length, within one step, and within short time periods

Variations in the sand at all sites were observed on the order of half a robot body length. The slope measurably varied in both the vertical and horizontal directions on the order of a half a robot body length due to the curved nature of many of the dunes. In particular, the slope varied at the tops and bottoms of the dunes, with sudden or gradual transformations from gentle 20-degree slopes for the majority of the dune to steep angles up to 30 degrees immediately at the top of the slip face. A qualitative observation of sand compaction found it to differ between lee and windward sides. There were also noticeable variations in the compacted sand layer depth within a dune vertically (towards the crest vs. towards the bottom) and horizontally, in particular between the ends of the dune and the middle, and also between the windward and the lee sides.

In the Tengger, where it had rained just before our arrival, variations in the sand were also observed between days 1 and 2 in the field. Rainfall the day before we reached the field resulted in compacted and cohesive sand on day 1. On day 2, the surface of the dunes was noticeably drier with a cohesive and compacted sand layer underneath. The cohesive and compacted sand layer receded noticeably during the day as the dune dried.

The substrate is also not consistent vertically within a single footstep. In the Tengger, the recent rainfall raised the water table to a sufficient height that the robot's legs were able to interact with it. In fact, in one head-to-head comparison between the robot with the standard-sized legs and the robot with widened legs, the robot with thinner legs was able to reach the wet, cohesive sand under the surface and "walk" up the dune. The robot with wider legs failed to climb the dune. We determined this by observing the wetness of the sand kicked back by the robot. In White Sands, we saw another example of vertical heterogeneity in the natural desert substrate: A bio-film crust on the surface of the sand. In this case, there was fine, soft sand underneath a hard crust which snapped under pressure. Substrates near the feet of the dunes were also often heterogeneous vertically, with the soft foot of the dune covering a compacted interdune area.

Behavioral responses to seemingly similar substrates vary wildly

We observed highly variable robot behavior on similar virgin slopes of approximately the same slope angle (within 2 degrees), on the same dune face (within 3 meters) or adjacent dune faces (within 10 meters), and within 30 minutes from first to last experiment. In one comparison experiment between identical robots with wider and thinner legs at the Tengger, the wide-legged robot was able to travel approximately half a body length further vertically up a dune when the robots were placed half a body length away from each other. We were then unable to replicate these results either by moving the robots down the same slope by one body length or by moving the robots to an adjacent virgin slope with a similar slope angles (within 1 degree): In both of these attempted replications, both robots performed the same. We were unable to determine in the uncontrolled natural desert environment whether this variation in robot behavior was due to differences in sand compaction, cohesiveness, minor variations in slope angle, or minor differences in robot orientation or other initial conditions. However, given the observed differences between different dune portions, we hypothesize that the variation results at least in part from the substrate differences.

Thermal loading of the motors on natural sand is a challenge even for robots which can normally perform long-distance hikes

The RHex robot is generally able to locomote continuously in excess of 30 minutes, including overcoming small hills and obstacles such as curbs. In 2013-2015, our lab group conducted semi-weekly hikes with the robot around Philadelphia, usually in the neighborhood around the engineering building but also occasionally in forested hillslope environments such as the Wissahickon city park. The robot has a temperature sensor and shuts off its legs when the temperature climbs dangerously high. These “stalls" are extremely rare during normal hikes on city streets or with occasional hills.

On the dunes at White Sands in 2014, we observed frequent motor stalls, particularly in the rear legs. The rear motors consistently stalled while climbing dunes, but the choice of gait did have an effect. When the back legs were supported by the other legs, such as in a crawl (one leg moving at a time) or a slow pronk (all legs moving at once), the robot was able to climb slightly steeper dunes than when using the standard alternating tripod gait [112].

The center of mass location appeared to be the primary cause of the robot's difficulty in climbing inclined natural sand. At high inclinations, the front legs appeared to disengage from the substrate as the robot pitched back, putting more weight on the rear legs and requiring the rear legs to exert substantially more torque to produce forward locomotion [101]. As the legs are made of compliant fiberglass, the rear legs compressed further under the extra weight, compounding the problem. We added an 8.5 kg weight to the front of the robot in the Tengger desert in 2014 and found that the robot's rear legs stalled out less on similar dunes even though it was carrying a payload [101]. However, since there is substantial variability in the natural dune system, the conclusions that we can draw from these experiments are limited.

2.2.3 Morphological modifications to RHex to enable better locomotion on sand

In response to the preliminary observations with RHex in the Tengger, Jornada, and White Sands, we made several morphological modifications to the robot's body and legs. For each modification, we either tested the benefit experimentally in a natural desert or report observations of the robot's behavior after the modification was made. The changes were an increase in leg width, an increase in the gear ratio of the motors in the legs, and an increase in the passive stiffness of the C-shaped legs.

Wider legs result in a lower specific resistance on natural sand

We measured the specific resistance of two identical RHex robots with different leg widths at the Tengger over a 30-minute run, walking both robots together in a single-file line over 430 meters of a modestly challenging dune environment (see Figure 2.2). The robot with wider legs had a specific resistance [140] of 1.1, as compared with the robot with the thin legs, which had a specific resistance of 1.3. This 0.2 advantage in specific resistance that the wide-legged robot had was evident in its speed: For a given gait frequency it traveled noticeably faster than the thin-legged robot. We hypothesize that the wider legs afford better leg friction and reduced leg sinkage, allowing the robot to travel farther in a single gait cycle. If true, this would indicate a significant affordance provided by the wider legs as they would allow for a 20% increase in energy efficiency, expanding the robot's range during operations.

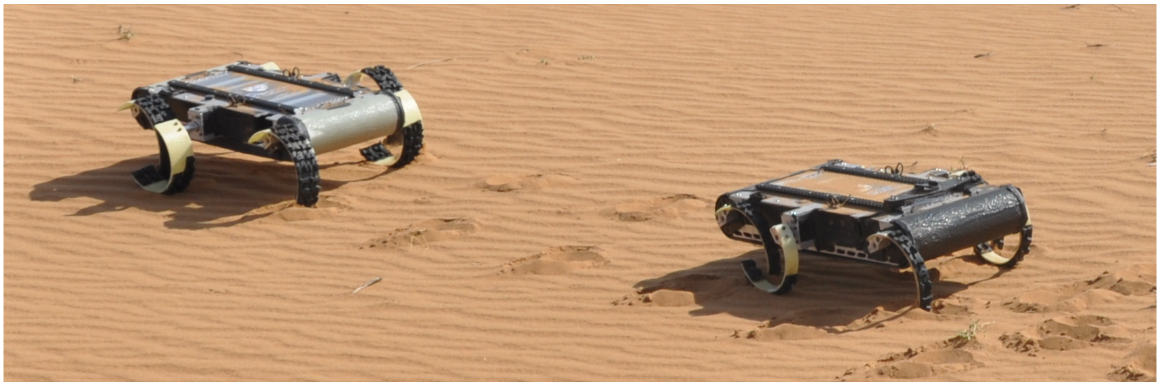

Figure 2.2: Specific resistance experiment in which the two robots walked together for 30 minutes over the same territory [110].

A higher gear ratio reduces frequency of motors overheating while traversing sand dunes

We increased the gear ratio in the RHex robot by a factor of almost 3, from 28:1 to 79:1. This slowed the robot's top speed from a human jogging or running speed to a human walking speed. However, it also moved the motors into a more efficient operational mode due to the increased operational speed and allowed the robot to exert more torque with each step.

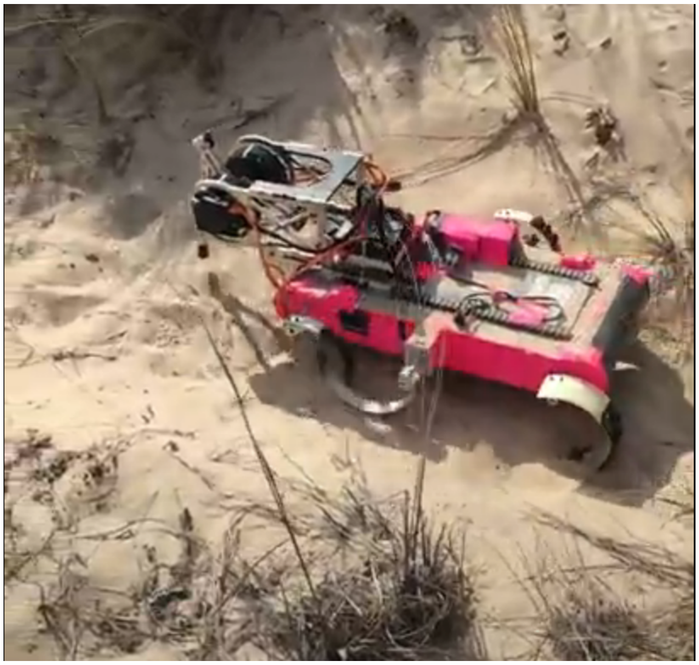

Figure 2.3: RHex carries a payload and walks along a human trail up and down the crests of multiple dunes to reach a study site in Oceano Dunes in 2016. The hike lasted 17 minutes, after which the robot continued to operate for another hour as it was used to take samples. It was able to make these repeated ascents in large part due to the increase in gearbox ratio from 28:1 to 79:1.

This substantially improved the thermal loading problem for RHex. Whereas the robot had needed time to cool its motors between single dune ascents in 2014 when using 28:1 gearbox motors, we were able to run the robot continuously along a human trail across multiple dune crests while carrying a payload in Oceano Dunes in 2016 (see Figure 2.3). The trail led from our vehicle to a test site and the hike lasted 17 minutes. After completing the hike, the robot did not need to rest and cool down, but was immediately ready to walk between sample locations at the relatively flat study site.

Stiffer legs improve dune-climbing capabilities

The compliance in RHex's legs compounded the issue of placing the center of mass rear-ward on the robot when it climbed inclines. We were able to mitigate this issue by adding strips of spring steel to the robot's legs. The spring steel was placed inside the C-shape, tucked under the seal that attached the tread and the joint that connected it to the hip of the robot, and then held in place with zipties. Adding spring steel to only the rear legs was sufficient to provide benefit to the robot in climbing slopes. Having stiff rear legs lifted the back end of the robot and moved the center of mass forward.

I first tested this modification in an outdoor tilting sand box in Philadelphia that was large enough for the RHex robot to begin locomotion, take a few steps, and then end locomotion and sit down. I used crushed quartz sand in the box and prepared it by hand between each experiment, either mixing and smoothing it or mixing, smoothing, and then compressing it. I observed a decrease in the difference in current draw between the front and rear motors when stiffening either all of the legs or just the rear legs. However, the difficulty in controlling the sand conditions in this outdoor sand box made it impossible to draw firm conclusions about the benefit of using stiffened legs overall.

We brought leg stiffening strips of spring steel on our 2016 trips to White Sands and Oceano. We observed that a higher leg stiffness slightly improved the locomotion capabilities of the robot even after the improvements from the increased gear ratio. Increasing the width of the rear legs also decreased the amount of leg sinkage and therefore moved the center of mass forward. In Oceano in 2016, we used the standard width robot legs for the first four legs and stiffened, wide rear legs when ascending dunes, including on our long hike.

2.2.4 Preliminary observations of Minitaur in natural deserts

In 2016, we brought a Minitaur robot on our return trip to White Sands and our inaugural trip to Oceano Dunes. The robot was driven by Turner Topping, an expert Minitaur operator who was involved in the development of the robot and has used it to perform novel and difficult behaviors [131–134]. We ran Minitaur on shallow dune slopes, hard interdune areas, and soft interdune areas.

We observed that Minitaur was able to run effectively on hard interdune areas. However, when there was a soft layer of sand on top of the hard interdune area, the robot's legs did not trigger their thrust modes appropriately. In one instance, the robot appeared to engage in an unstable trot-like behavior (where diagonal pairs of legs move together) instead of a stable bound (where the front and back pairs of feet move together). In another instance, the robot flipped itself onto its side – a locomotion failure case from which it cannot recover –

because its leg thrust modes were inappropriately triggered. See Fig. 2.4 for examples. Our expert robot operator's opinion was that this problem arose from the locomotion controller, which had been developed assuming hard ground. The typical locomotion controller for Minitaur triggers a retraction and then a push for each pair of legs based on a small average deflection of the two legs. If one side of the robot is on a softer patch of ground than the other side, this causes the robot's legs to trigger at different times, leading to the observed unstable behavior.

When we attempted to run Minitaur up shallow slopes, or on softer interdune areas with a larger layer of soft sand, the robot's motors quickly overheated. We were unable to run the robot for more than a few minutes before needing to break and let the robot cool down. The two major problems for Minitaur's locomotion on sand were therefore identified as a gain-tuning issue causing inappropriate triggering of the thrust modes, and the thermal loading of the motors from protracted locomotion on soft surfaces. I addressed the gain-tuning issue by using a controller that triggers a thrust based on a large deflection in the leg rather than a small deflection (Chapter 3), isolating the main issue as the thermal loading of the motors.

2.2.5 Conclusions about locomotion problems on natural sand

Through observing the behavior of the RHex and Minitaur robots in desert environments, it is clear that the outcome of the same programmed behavior depends strongly on ground conditions and that the ground conditions vary within short distances. This implies that any useful adaptations for sand locomotion will have to be consistent across a variety of ground conditions, such as increasing the foot size which decreases the amount that the robot sinks into the sand. While the robot may be able to sense information relevant to its current step, the assumption that a following step will have similar conditions to the current step is not reasonable.

Thermal loading is an issue for all robots locomoting in natural deserts, but it is particularly problematic for direct-drive robots like Minitaur. Typical adaptations to increase motor efficiency in general and locomotor capacity on sand in particular include gearing down the robot's motors and increasing the size of the feet. However, both of these op-

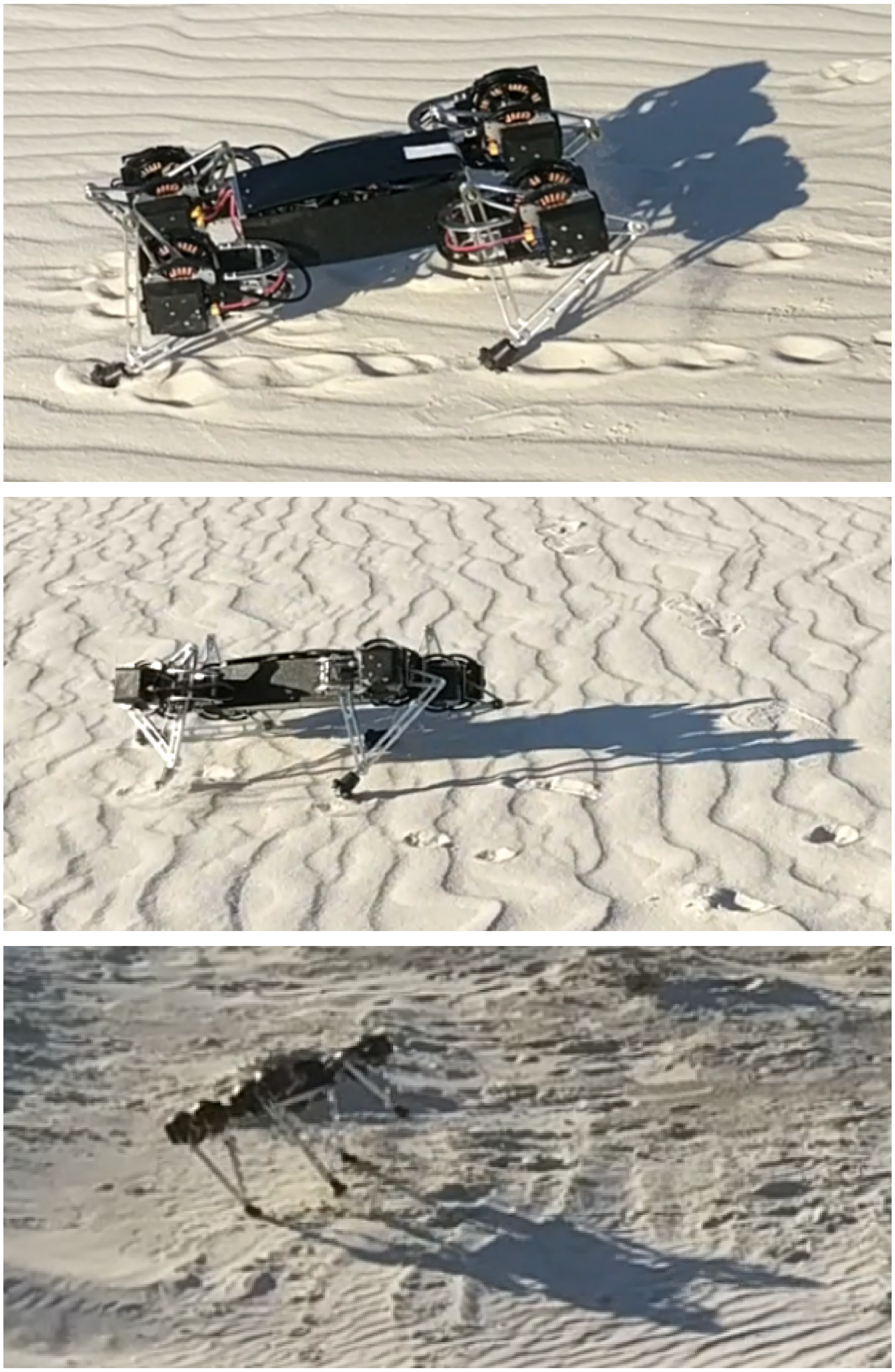

Figure 2.4: In the top image, Minitaur's rear two legs are in sync but its front two legs are triggering at different times because the soft ground does not consistently trigger the legs to jump. In the middle image, Minitaur's front and back pairs of legs have both gotten out of sync. In the bottom image, Minitaur is in the process of flipping itself onto its side after encountering ground that is softer on one side than the other. All images are from either a semi-compacted shallow dune or a very compacted interdune area.

tions would substantially reduce the proprioceptive sensitivity of the Minitaur robot and thus render it no longer useful as a self-transporting force sensor [69, 97]. A change to the programming but not the physical instantiation of the robot is needed.

2.3 Related work

Reactive control for legged robots jumping with virtual springs has roots as far back in the 1980s in Marc Raibert's work [100]. Compositions of simple controllers for hop height and pitch enabled the experimenter to independently control the height of the robot and its forward speed. More recent work with the Minitaur [70] and Jerboa [34] robots has shown how simple reactive controllers for jumping can be composed in multi-legged robots to generate a variety of gaits like bounding, trotting, and pronking [36] depending on how the simple hopping controllers are composed. The default gait used by Minitaur is a bound, and there is some evidence that symmetric gaits may be advantageous for locomotion on granular media [125].

Roboticists are beginning to carefully examine the interaction between the robot and its environment. By understanding this interaction as an energy landscape, it is possible to describe complex behaviors like self-righting relatively simply [87]. By studying the emergent cyclic behavior resulting from repeated interactions with environmental elements, it is possible to "program" the agent-environment system to produce locomotion in a desired direction [95]. The utility of these approaches for more abstract navigation tasks is even more well supported [61, 138, 139].

Legged robot locomotion is notoriously difficult because of the complexity of the granular media's response to intrusion [1, 75, 76]. The work most closely related to that presented in this thesis involves vertical jumping on prepared granular media [16, 17, 57]. However, that work takes a completely different approach to the work presented in this thesis: The robot is assumed to know the approximate shape of the force functions the ground exerts, and the authors show that after it jumps once on a given ground preparation, it is able to jump to a specified height after learning a single fitting parameter [16]. The robot can also be programmed to jump to a specified height if the ground is completely known [57], or can learn the exerted forces well enough to jump to a controlled height after a limited number of hops [17]. A benefit of this body of work is how well it demonstrates the accuracy of the analytic force models used to describe the behavior of the granular media. However, it is limited because it relies on consistent ground conditions, which is not a reliable property in most natural outdoor environments.

My work is different from this existing body of research in a subtle but fundamental way: I reduce the energetic cost of transport for a robot jumping to a specific height, but do not control that height. In other words, in a comparison between my active damping controller and a nominal, robust reactive controller for jumping on rigid ground, the robot will jump to the same height using each controller but will take less energy to do so using my controller. Other controllers developed for jumping on granular media have focused on the problem of getting the robot to jump to a specific height rather than the problem of getting the robot to jump in an energy-efficient way. Granular media is highly dissipative and jumping on it is energetically very costly, which is especially important for a direct-drive robot like Minitaur. My controller could be composd with a feedback controller on the jump height, as in the classic Raibert control scheme, if it is necessary to jump to a specified height.

Part II

Simulation, emulation, and physical experiments demonstrating reduced energetic cost of transport with the active damping controller

Chapter 3

Developing a reactive controller for jumping on granular media in simulation

As we saw in the previous chapter, robot locomotion on granular media is energetically costly. Any adaptations for robots tasked with locomoting over sand will need to work consistently across a variety of conditions due to the variation in natural environments.

This chapter begins with an introduction of the nominal compression-extension controller for robust locomotion on rigid ground and a description of the force model of sand used for this work, which I will use to develop the active damping controller. I will then describe two sets of jumping simulations described in [106] and [109] to suggest the utility of this controller for jumping on granular media with direct-drive legged robots.

3.1 Developing the active damping controller

I will first introduce the basic reactive controller used for locomotion in this thesis. Then, I will reframe the analytic models that describe the forces granular media exerts in response to intrusion as a stiffness-like and a damping-like function, and use these to plot the energy landscape of the robot's interaction with its environment. I will then introduce the model of robot locomotion that I used in simulation to develop the contributed active damping controller. I will then describe the active damping controller, and give some intuition for why it is effective at reducing the energetic cost of transport. A brief analysis gives us conditions under which the active damping controller will transfer less energy to the ground than the comparison controller. The next two sections will describe simulation experiments that demonstrate the utility of the active damping controller in simulation.

3.1.1 Raibert-style hopping control

As the nominal comparison controller for Minitaur running on sand, I use a simple compression-extension spring control law proposed originally by Raibert [100] and used for a suite of behaviors and applications, including recently, parallel compositions of behaviors [34–36]. A soft compliance gain during the first part of stance allows the virtual leg spring to compress. Once the rate of change of the leg length goes to zero, the programmed leg stiffness increases by a large amount instantaneously, injecting a large quantity of potential energy into the virtual spring. This causes the robot to jump. During the switch from soft compression spring to stiff extension spring on sand, in addition to causing the robot's body to accelerate upwards, the forces from the leg spring also push the foot further into the sand. (See Figure 3.1.)

3.1.2 Reframing of analytic force models for sand

Bulk-behavior models of granular media developed for the purposes of modeling animal and robot locomotion characterize ground reaction forces in response to intrusion by a limb [1, 76]. In general, bulk-behavior models of the plastic flows of granular media are accurate when the size of the intruder far exceeds the size of the grains [65], and the results scale well with different sizes and masses of intruders [124]. Bulk-behavior models can now predict the terrain response with sufficient accuracy to allow optimal control methods to generate robot motion trajectories that result in jumps to a desired height [16, 57]. Although powerful, results using optimal control have limited applicability to robot locomotion on real deserts, as they assume granular media preparations that are homogeneous within and between steps

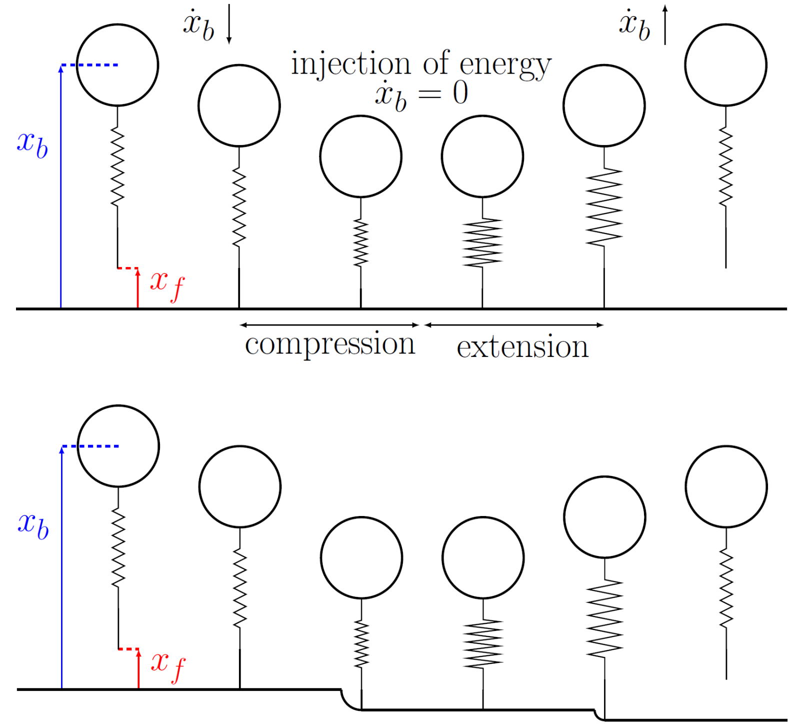

Figure 3.1: A Raibert-style compression-extension spring controller on rigid (top) and compressible ground (bottom). The soft (narrow) virtual leg spring compresses easily. When fully compressed, the virtual spring is instantaneously switched to a very stiff (wide) virtual spring [106].

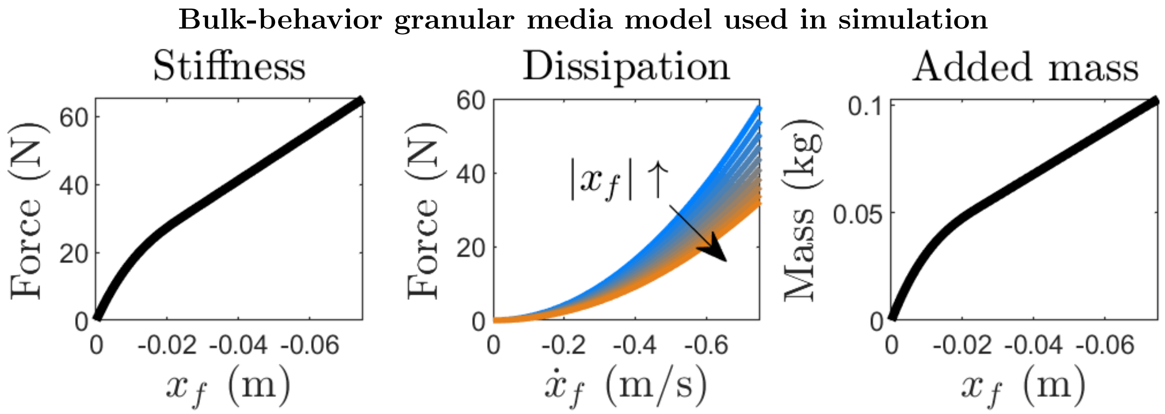

Figure 3.2: The stiffness, dissipation, and added mass functions of the simulated granular media. The stiffness function is transiently nonlinear while the cone of grains accelerated with the foot is still forming. The depth-dependent dissipation function is quadratic in velocity, with a higher coefficient while the cone forms. The added mass function is not constant after the cone forms because the cone continues to shed and gain material throughout intrusion [106].

– an assumption which cannot be made for locomotion in real deserts with unknown ground properties [97, 101, 112] – and experiments in the laboratory are not much affected by the dissipation of electrical energy to heat, which is a very real concern for a robot running long distances in a desert.

I use the same added-mass bulk-behavior model [1] that was validated in the highly dynamic regime by its use in optimal control experiments. Three forces comprise the bulk-behavior model: A stiffness function only of depth, $k_g(x)$; an inertial drag energy dissipation term which is a function of depth and velocity, $d_g(x)\dot{x}^2$; and an added mass term, $m_a(x)\ddot{x}$, which describes the mass of the grains recruited to a stagnant “cone”-shaped clump of grains accelerated underneath the intruding robot foot. The full model [1] is therefore:

$$F_g = k_g(x) + d_g(x)\dot{x}^2 + m_a(x)\ddot{x}.$$

I will now describe the three terms in detail.

The depth-dependent stiffness function, $k_g(x)$

The depth-dependent force described in the added-mass model uses Resistive Force Theory (RFT) [76], a bulk-behavior model describing the hydrostatic-like forces of granular media in response to intrusion. The force response is transiently nonlinear when depths are very low, which is attributed to the growth of the cone of grains accelerating along with the intruding foot. Once the cone is fully formed, the force response is linear in depth, with $k_g(x) = k_{gc} \cdot x$ for some constant k_{gc}. The force response scales with the surface area of the foot, and thus the projected area of the cone of grains moving under the foot, with a larger foot surface area for a given animal or robot significantly improving locomotion capability [96]. RFT models the force response at arbitrary depths and angles using experimentally determined or measured parameters about the individual grains. These hydrostatic-like forces during vertical intrusion have recently been modeled in a universally scalable form using only the internal friction angle, that is, the angle relative to the normal force obtained at the point of failure of the granular media in response to a shearing stress [66].

The depth-dependent inertial drag term, $d_g(x)\dot{x}^2$

This term describes the hydrodynamic-like forces arising from the inertia of the grains accelerated underneath the robot's foot and recruited into the cone of added mass. The form of the term arises from the rate at which the mass is added through the recruitment of grains and then the shearing (and continued recruitment and shedding) of grains along the sides of the cone. While the cone is forming, the depth-dependent function describing the rate of recruitment of grains contributes a transient nonlinearity to the $d_g(x)$ term. Once the cone is formed, this term is constant in depth and quadratic in velocity. Studies of energy dissipation from high-velocity vertical collisions [8, 22] support the interpretation of this term as a dissipation function.

The added mass term, $m_a(x)$

The added mass term describes the mass of the developing cone of grains that are accelerated along with the robot's foot. The development of this cone of grains, and the shearing forces along the cone once it is fully developed, are also modeled in the depth-dependent inertial drag energy dissipation term: the transient non-linearity in $d_g(x)$ is explained as the growth of the cone, and the linearity thereafter is explained as the recruitment and shedding of

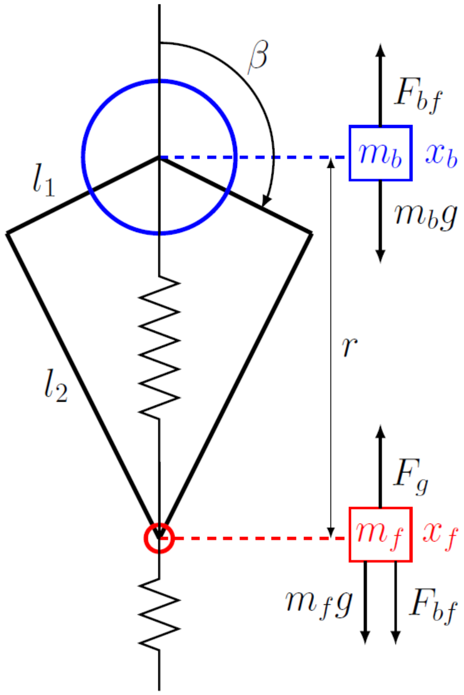

Figure 3.3: The kinematic diagram of the simulated one-legged hopper shows the virtual spring created by a simple linkage using two opposing motors, and the forces from the robot's leg, the ground, and the masses of the body and foot during stance [106].

grains along the shearing plane of the cone of grains pushed down under the foot.

3.1.3 Nonlinear two-spring model of Minitaur locomotion on granular media

I assume a one-dimensional hopping robot with a body mass of 1.75 kg and a foot mass of 0.175 kg (10% of body mass) constrained to move vertically. The robot is modeled on one quarter of a lightweight, desert-ready version of the Minitaur robot currently under development. Connecting the body and foot masses is a programmable leg spring with rest length $l = 0.27$m which can measure its own length and velocity, with an update loop of 1 kHz (achievable on Minitaur robots [70]) and a stiffness of k_l. The leg spring has a small linear dissipation coefficient, $d_l > 0$. To implement the contributed controller, I assume that the robot can sense the depth of its foot in an inertial frame.

A hop has two modes: Stance, during which time the robot's foot is in contact with the ground, and flight, when the robot's body and foot are both aerial. The dynamics of the two modes are as follows:

Stance

The accelerations of the body and foot are governed by a two-mass, two-spring nonlinear dynamical system (see Figure 3.3). Letting x_b^n, x_f^n be the robot body and foot centers of mass at time n, k_l and d_l the linear stiffness and damping coefficients of the robot leg, with g the gravitational constant, I can define first the forces of the virtual leg spring,

$$F_{bf} = -k_l(x_b - x_f - l) - d_l(\dot{x}_b - \dot{x}_f). \tag{3.1}$$

Adding now $m_b, m_f^n = m_f(x_f^n)$ the masses of the robot body and foot respectively and $k_g^n = k_g(x_f^n), d_g^n = d_g(x_f^n)$ and with it, I define the accelerations of body and foot at time n in stance:

$$\begin{aligned} \ddot{x}_b^n &= -\frac{F_{bf}}{m_b} - g \\ \ddot{x}_f^n &= \frac{F_{bf}}{m_f^n} - \frac{F_g}{m_f^n} - g \end{aligned}$$

The switch from stance to flight mode occurs when the following condition is met, for δ the leg spring compression due to gravity from the body's mass: $k_l(x_b^n - x_f^n - (l - \delta)) + d_l(\dot{x}_b^n - \dot{x}_f^n) > m_f^n g$. In flight, the ground stiffness and dissipation functions go to zero, and the added mass is immediately lost.

Ballistic flight

Once the foot lifts off from the compressed ground, the virtual leg spring switches to its soft compression gain. The body and foot are considered to be in free flight and their trajectories determined by standard flight dynamics. The transition from flight to stance occurs when the foot touches the ground, $x_f = 0$, and the body velocity is negative.

3.1.4 The “active damping” controller adds damping to the leg spring when the foot compresses the ground while pushing off

The nominal compression-extension controller and the contributed active damping controller differ only in the extension portion of stance and only when the velocity of the foot in the inertial world frame is negative. Under these conditions, the active damping controller adds this force:

$$F_{AD} = -(b_{AD} \cdot \dot{x}_f) \cdot (\dot{x}_b - \dot{x}_f), \qquad \dot{x}_f < 0. \tag{3.2}$$

We can see the effect of adding this force in Figure 3.4. When using the compression-extension controller (dashed line), the robot’s foot pushes down further into the sand, as we saw in Figure 3.1. However, adding active damping (dotted line) changes the trajectory of the foot moving through the granular media: It no longer pushes down further after the robot switches to its stiff leg spring. This is beneficial for two reasons which i will address in the next subsection.

3.1.5 Mechanical energy losses to the ground are incurred both from the ground’s dissipation function and from plastic ground deformation

To understand why the active damping controller may be beneficial to use when locomoting on granular media, we must first understand where the energy is lost during a jump. Examining the total mechanical energy of the system, there are six relevant energies:

1. LSP (leg spring potential): $0.5 \cdot k_l \cdot (x_b - x_f - l)^2$

2. KB (kinetic energy of body): $0.5 \cdot m_b \cdot \dot{x}_b^2$

3. GB (gravitational potential energy of body): $m_b \cdot g \cdot x_b$

4. GSP (ground “spring potential”): $\int_0^{|x_f|} k_g(z)dz$
   (recall that x_f is negative)

5. KT (kinetic energy of foot): $0.5 \cdot m_f \cdot \dot{x}_f^2$

6. GT (gravitational potential energy of foot): $m_f \cdot g \cdot x_f$

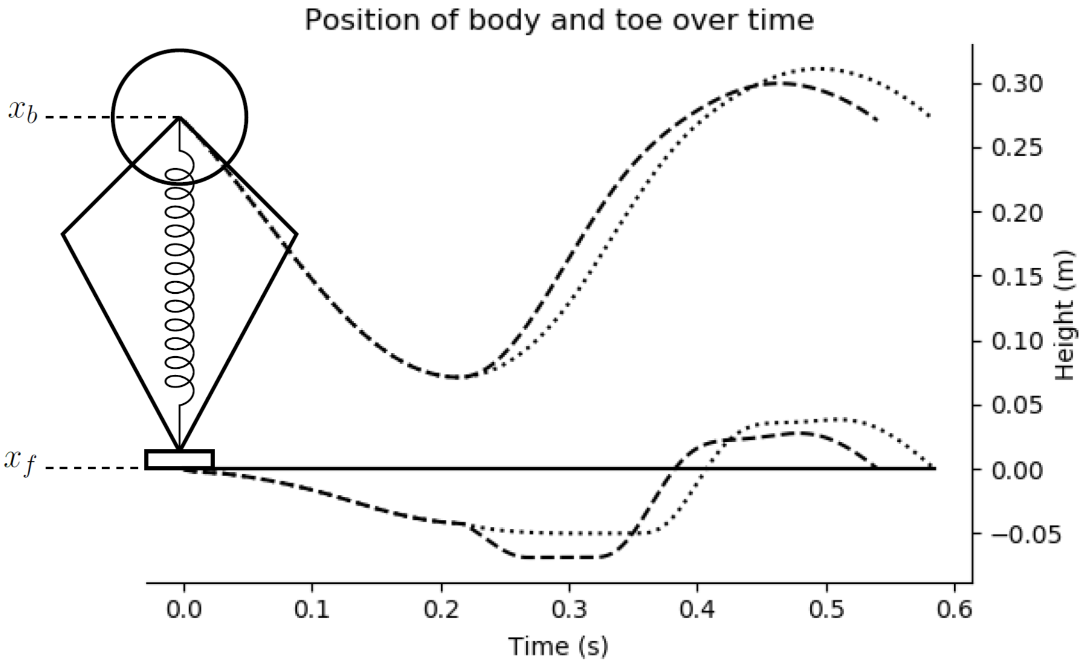

Figure 3.4: An example body and toe trajectory from the simulated robot using the compression-extension (dashed) and active damping (dotted) controllers. When the virtual leg spring switches from a soft compression gain to a stiff extension gain, the compression-extension controller pushes the foot further into the ground [109].

The total mechanical energy of the body, leg and foot is then

$$E_{bf} = LSP + KB + GB + KT + GT, \tag{3.3}$$

which is the sum of all of these energies except for the ground's "potential" energy, since the ground plastically deforms and any energy transferred to it is immediately lost.

The total energy for one jump in this simulation using the compression-extension and active damping controllers along with all component energies is plotted in Figure 3.5. The dissipation function of the ground contributes to the initial drop in total energy (black line in plot). The robot's leg, which has a very soft compliance gain during compression, initially deflects more quickly than the ground. This is reflected in the quantity of energy being stored in the robot's virtual leg spring (dotted magenta line), which is larger than the quantity lost to ground compression (solid magenta line). The trajectory of the body during compression is also reflected in the gravitational potential energy of the robot's body mass

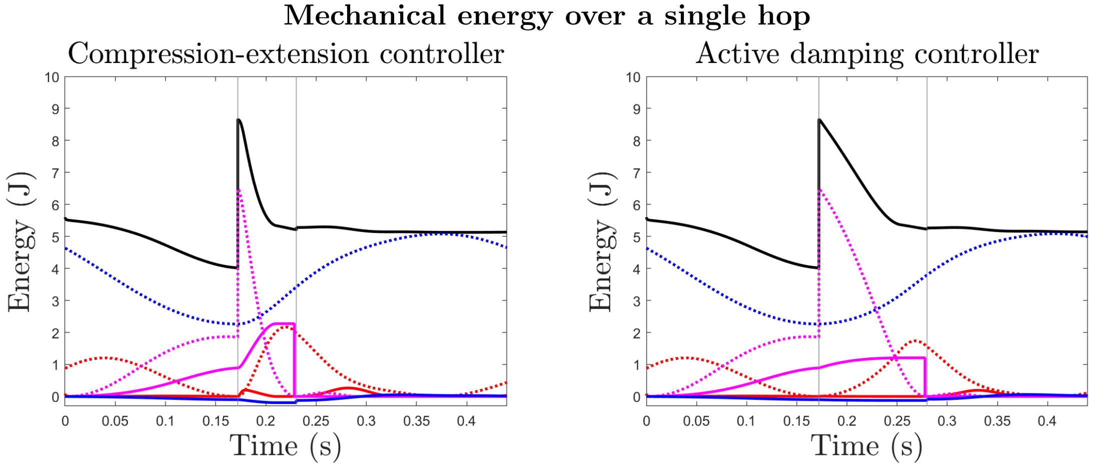

Figure 3.5: The total mechanical energy (Eqn 3.3; black line) during stance is plotted along with the component kinetic (red), spring potential (magenta), and gravitational potential (blue) energies for the body-leg (dotted) and foot-ground (solid) subsystems. The vertical thin gray lines indicate the switch from soft virtual leg spring to stiff at the midpoint of stance and back at toe liftoff [106].

(blue dotted line).

When the leg stops compressing, $\dot{x}_b - \dot{x}_f \rightarrow 0$ (first gray line), the compliance gain of its virtual spring suddenly changes to the extension value, injecting a large quantity of spring potential energy (dotted magenta line). Much of this energy is quickly lost to the ground, both through further compression (bump in the solid magenta line) and to the ground's dissipation function. Notice that a small amount of gravitational potential energy is gained by the foot at liftoff (second gray line), because negative gravitational potential energy is lost when the foot mass, which is below 0 height, is suddenly reduced to its nominal value.

Ultimately, the difference in mechanical energy loss between the compression-extension and active damping controllers is very similar, which is reflected in the similar apex heights (Figures 3.9, 3.12). Notice also that while from the point of view of the physical world the robot's leg looks like a spring-mass damper system, because the leg spring is virtual, the forces that produce this behavior will cost more or less energy from the battery to create depending on the leg's kinematics and the efficiency of its motors. The total mechanical energy is concerned only with the mechanical behavior of virtual springs.

3.1.6 Electrical energy cost of locomotion is mitigated by purposefully dissipating energy into the virtual leg damper

Recall that the ground is modeled as a transiently nonlinear spring with nonlinear dissipation (Sections 3.1.2, 3.1.2) and no restoring forces. Let us focus for a moment on the mechanical energy in the physical subsystem involving just the foot and ground. I conceptually isolate this subsystem by "zeroing out" the forces from the leg, F_{bf} (Eqn 3.1), and consider the energy just of the foot-ground subsystem, $E_f = KT + GT$, which interacts with the vector field defined over the foot dynamics, $\{x_f, \dot{x}_f\}$. The energy used to plastically deform the ground cannot be recovered, so there is only contribution from the kinetic and gravitational potential energy of the foot. The mechanical power loss function of the foot-ground subsystem (Figure 3.6) is then

$$\dot{E}_f = -d_g(x_f) \cdot |\dot{x_f}^3| - k_g(x_f)|\dot{x}_f|. \tag{3.4}$$

Since the dissipation function is quadratic in velocity, the power function is cubic and the ground will dissipate a large amount of energy when the velocity is high. The depth dependence of the first term is due to the formation of the cone of added material, so we expect to see a different slope to the power loss function for high velocities when depths are low. Notice too that this power loss function involves the stiffness function of the ground, $k_g(x_f)$, because the ground deforms plastically and does not store energy. Looking at the surface plot in Figure 3.6, we can see the appropriate dips in the power loss landscape as we vary the depth and the velocity of the foot. Qualitatively, we can surmise that if a robot can keep its foot away from these higher-cost parts of its state space in inertial world-frame coordinates, it will lose much less mechanical energy to the ground during stance.

Comparing sample trajectories of the robot's foot through its state space under the compression-extension and active damping controllers (Figure 3.6), the mechanism of the reported mechanical energy savings for the added damping controller becomes clear. Three sample initial conditions are plotted (black circles). In each initial condition, the initial

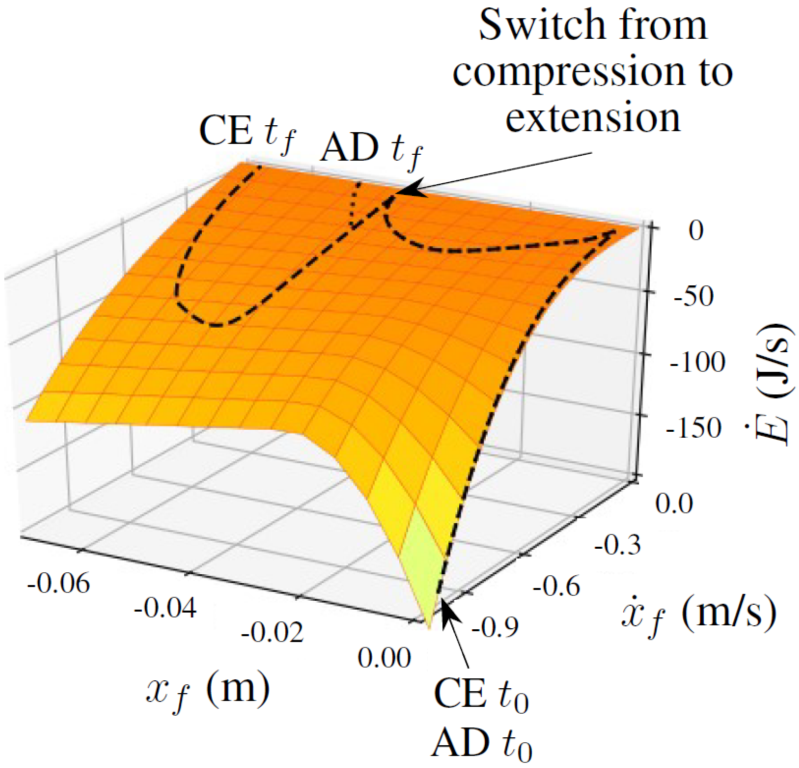

Figure 3.6: The compression-extension controller transfers more energy to the ground than the active damping controller during the extension mode. The surface indicates the rate of energy transfer between the robot's foot and the ground as a function of the state of the foot. It is the right side of Equation 3.4, the power function of state associated with the total energy function. The dashed line plots a typical trajectory of the foot through state space when jumping using the compression-extension controller, while the dotted line plots the trajectory of the same foot from the same initial conditions using the active damping controller (Equation 3.2 introduced in Section 3.1.4). The lines only diverge during the extension mode, when the active damping controller is active [109].

body and foot velocities are the same, the foot is just touching the ground, and the virtual leg spring is at its rest length. During compression mode, which is the same for the two controllers, the virtual leg spring compresses quickly and the foot's velocity quickly drops as it sinks into the granular media. The foot's velocity goes to zero when the granular media "jams" and returns an equivalent reaction force. When the leg length velocity goes to zero after this point, the virtual leg spring switches to its stiff extension gain, causing a sudden increase in velocity as the forces from the leg spring are now stronger than those exerted by the ground. This enables the foot to continue compressing the ground. The ground jams a second time when the foot's velocity again goes to zero, and the robot's foot begins to lift from the compressed ground, entering ballistic flight.

When the robot leg switches from compression to extension modes, its virtual spring changes stiffness instantaneously and exerts a large force to both push the body up and the foot down further into the ground, as reflected in the large swoop down into the high-depth, high-velocity portion of the foot's state space in the compression-extension trajectory plots in Figure 3.6. The compression-extension controller injects a large amount of energy into the foot-ground system when the velocity of the leg length goes to zero, but loses most of this energy immediately to the ground. In contrast, the active damping controller punishes negative foot velocities, pushing the state of the foot back towards zero velocity. Since the foot's velocity is negative for a smaller amount of time, it does not penetrate as far into the ground and does so less quickly, and thus loses less mechanical energy.

The energy being lost by the foot-ground subsystem during stance is largely energy that is injected into it by the leg spring force F_{bf} (Eqn 3.1). Kinetic energy losses to mechanical dissipation in the leg spring may be significant when its damping coefficient is high. However, recall that the spring and damper in the leg are both virtual, and all forces exerted by a virtual leg spring come at a cost from the battery. This includes leg spring potential energy storage, which in a mechanical system is free. Virtual damping forces acting in opposition to virtual spring forces that reduce the torque requested from the motors will therefore use less energy from the battery.

While the added damping force in the virtual leg spring does potentially come at a cost in kinetic energy, the investment is rewarded immediately in two ways: First, the ground compresses less, so that the robot does not need to jump as high from the point underneath the surface of the granular media at which it enters flight mode in order to achieve the same apex height in an inertial frame; and second, the power function of the ground has a lower magnitude when the foot's depth and velocity are lower, so less mechanical energy is dissipated to the ground. In fact, as we will see later in this chapter and in the next two chapters which describe experiments with a physical robot, the apex heights of the compression-extension and active damping controllers are comparable, and in some cases higher when active damping is used (see Figures 3.9, 3.12 in this chapter).

3.1.7 Analysis of the active damping controller provides insight for when it should provide benefit

To determine when the active damping controller should cost less energy than the compression-extension controller on granular media, we compared the rate at which energy is transferred from the toe to the ground (Eq. 3.4) under the two controllers. For k_l the stiffness coefficient of the virtual leg spring, x_b the body position, x_f the foot position, and l the nominal leg length, let $P_{k_l} = \dot{x}_f k_l (x_b - x_f - l)$, the power from the stiffness function of the leg. Then, for P_{CE} the power with the compression-extension controller and P_{AD} the power with the active damping controller including the force F_{AD} (Eq. 3.2), we have

$$
\begin{aligned}
P_{CE} &= P_{k_l} + \dot{x}_f b_l (\dot{x}_b - \dot{x}_f) - b_g \dot{x}_f^3 \\
P_{AD} &= P_{k_l} + \dot{x}_f (b_l - b_{AD} \dot{x}_f)(\dot{x}_b - \dot{x}_f) - b_g \dot{x}_f^3.
\end{aligned}
$$

Taking the difference to see the conditions under which the compression-extension power function will be larger than the active damping power function, we get

$$
P_{CE} - P_{AD} = b_{AD} (\dot{x}_b - \dot{x}_f) \dot{x}_f^2.
$$

Assuming negative foot velocity $\dot{x}_f$ and positive active damping gain b_{AD}, this quantity is greater than zero when $\dot{x}_f < \dot{x}_b$. This corresponds to a situation where the foot accelerates more quickly than the body in response to a change in virtual leg stiffness, for example in a robot with more mass in its body than its foot when switching from the soft compression gain to the stiff extension gain when the leg is compressed. When the foot velocity and active damping gain are both negative, this quantity is greater than zero when the body and foot velocity are both negative, and the body is moving faster than the foot ($\dot{x}_b < \dot{x}_f < 0$). This corresponds to a situation where the robot's body accelerates more quickly than its foot, for example if the foot mass is greater than the body mass, or (more likely) if the ground is very stiff. Under these conditions, adding energy to the leg with a negative velocity gain – as in the standard Ghost Minitaur bounding gait – will result in more energetically efficient locomotion than a naive compression-extension controller. However, on compliant ground, adding damping to reduce the foot's intrusion velocity saves energy.

3.2 First set of simulations, varying ground parameters and initial velocity

I performed the first set of computer simulations in Matlab using a discrete-time dynamical system with a small time-step (dt $= 1 \times 10^{-6}$s).[1] The added-mass bulk-behavior model uses measured parameters about the individual grains of the granular media, and has two additional scalars in the dissipation function describing the hydrodynamic-like forces: One a linear scaling parameter which was experimentally fitted in [57], and one a constant from integration. The constant from integration arises from the derivation of the added mass term in [1], which was integrated from a change in added mass and reflects the inertia of the

[1] In [1], where a Matlab simulation was also used to simulate the bulk-behavior of granular media using this added-mass model, Zeno-like switching between unjammed and jammed granular modes was addressed by switching the simulated granular media from a mode in which compression is allowed to a rigid "jammed" mode by watching the acceleration of the foot. I selected my time-step to be small enough that there was no Zeno-like switching in the behavior of the robot, but allowed Zeno-like switching from the granular media. I then recalculated the values of the ground's stiffness, dissipation, and added mass terms afterwards based on the robot foot's simulated behavior, which did not have this switching. This approach allowed the granular media to jam, unjam, and re-jam an arbitrary number of times during stance as the forces from the leg changed.

grains accelerated along with the intruding foot. To ease comparison with and extension from previous results, for the nominal granular media I used parameters that were measured for poppyseeds [76], and the same linear scaling parameter ($b_g = 17.2$) as in [57]. I set the integration constant $C = 1$. As the difference between the contributed and the nominal controllers occurs only after the transient nonlinearities during the formation of the cone of added material in the stiffness, dissipation, and added mass functions of the ground, these details do not greatly affect the results (see Section 3.2.3 and Figure 3.6). Finally, I arbitrarily set the active damping coefficient to the same value as the extension stiffness for these initial simulations.

The three component terms $k_g(x_f)$, $d_g(x_f)\dot{x}^2$, and $m_a(x_f)$ used to simulate the granular media response to intrusion by the robot's foot are plotted in Figure 3.2. The ground reaction model exerts no forces when the robot's foot velocity is positive, and all added mass is lost when the foot lifts off. This simulates the plastic deformation of the ground and allow for continued deformation during leg extension with a stiff virtual extension spring following the initial deformation under the soft virtual compression spring.

3.2.1 Kinematics and motor model used for energy estimates

I used the kinematics of the virtual leg spring created by the simple linkage to estimate the motor torques and therefore the current draw from the battery required to exert the forces at the foot in the simulated experiments. The kinematics were simplified by the assumption that the leg and foot are constrained to move vertically. For l_1, l_2 the leg linkage lengths, r the length from the center of mass of the motors to the foot, and β the angle of the first link relative to the vertical, the inverse kinematics are $\pi - \beta = \cos^{-1}\left(\frac{l_1^2 - l_2^2 + r^2}{2l_1 r}\right)$. The torque for leg spring force F_{bf} is then $\tau = Df|_r F_{bf}$. (See Figure 3.1.) To estimate losses, I assumed that the leg looked mechanically like a perfect linear spring, calculated the torques at the motors required to produce the forces at the foot, and then calculated the additional energy lost to heat and electromechanical drag in order to achieve those torques.

A simple motor model relating the current draw to the torque consisting of a linear portion with instantaneous saturation at the stall torque was used. For K_τ the motor torque constant, τ_n the torque from the motor at time-step n, and I_n the estimated current draw at time-step n, we have $\tau_n = K_\tau \cdot I_n$. For any torques requested by the simulation above the stall torque for two motors working together to rotate the first leg links, $2 \cdot \tau_s$, I provided the stall torque of the leg instead. Losses to heat were calculated as $P_{R_m} = I^2 R_m$ and losses to electromechanical drag were calculated as $P_v = \frac{K_\tau K_v}{R_m}\dot{\beta}^2$, for K_v $\frac{V}{\text{rad/s}}$ the motor velocity constant and R_m Ω the motor resistance. The electrical power converted to mechanical power was calculated as $\dot{\beta}\tau$. The values for $K_\tau = 0.0955\frac{\text{Nm}}{\text{A}}$, the stall torque $\tau_s = 3.5\text{Nm}$, and motor resistance $R_m = 0.186\Omega$ for the T-motor U-8 series motors used on Minitaur were reported in a previous study on actuator sizing [69].

With T the number of time-steps, I_n the current draw of the motor, β_n the motor angle, and τ_n the torque at the motor at time-step n, the energetic cost J of a single jump is then:

$$J = \text{dt} \sum_{n=1}^{T} \left[R_m I_n^2 + \dot{\beta}_n \tau_n + \frac{K_\tau K_v}{R_m} \dot{\beta}_n^2 \right]. \tag{3.5}$$

This is the sum of the losses to heat through the resistance of the motor, losses to electromechanical drag, and the mechanical energy converted from electrical energy over each time-step. Direct-drive motors operating at high torques and low velocities are inefficient, and the cost is dominated by the dissipation to heat.

3.2.2 Test of simulation by hopping a robot with different extension gains on a force plate

To validate the energy cost estimates of the simulated robot, I compared simulated costs with energy costs measured from a battery used to power a 2.0kg one-legged robot hopping on a Bertec force plate[2] while constrained to a vertical rail. These experiments serve as a ground truth for the robot model used in simulations. The robot was programmed to jump using the compression-extension controller with four extension virtual stiffness gains, and completed 80 jumps during each experiment. The battery used to power the robot was fully charged before and after each experiment, and the mAh required to fully recharge the

[2] Bertec FP4060-07 force plate, leveled to within 1 degree in either axis of the horizontal plane; data recorded using Bertec Acquire version 4.0.12.411.

battery after the experiment as reported by the ThunderPower charger was recorded as the cost of 80 jumps using that virtual stiffness gain during extension.

To control for variability due to changing motor resistance as the motors warm up, I allowed the robot to jump for approximately 2 minutes before any experimental data was taken. I also used block experiment ordering to prevent an interaction between time and leg stiffness. For extension gains $k_l = \{300, 400, 500, 600\}$, I performed experiments in this order: $\{300, 600, 500, 400\}$. Each experiment began with the robot leg held just above the force plate, such that when it was released the soft virtual leg spring immediately compressed under the weight of the body. When the robot's body velocity reached zero, the robot switched to its stiff extension gain and jumped. Within a few hops (two or three), the robot reached a consistent jumping height in all extension gain conditions. I allowed the robot to jump 80 times and then caught it during its flight phase after the 80th jump. The battery was immediately disconnected to avoid any additional power draw.

In addition to vertical axis force data (N) recorded from the force plate, I collected leg extension position and velocity data as reported by the Ghost SDK. For ground truth, I recorded the height of the robot's body through the SDK using a string potentiometer, and took record-keeping videos which were not analyzed as data. The force plate data was recorded at 1kHz, and robot data was logged at 333Hz. The force plate data was lightly smoothed with a low-pass filter to reduce noise (moving average filter, window size of 15 samples $=$ 0.015s). The window size was chosen by plotting the sum of absolute differences between filtered and unfiltered data for a range of window sizes, and picking the window size at which the difference between one filtered force profile and the next becomes (and stays) small.

The force plate and leg extension data were automatically aligned at the leg touchdown for each hop, which was automatically detected in the robot by leg deflection and on the force plate by a large spike in the raw force plate readings (Figure 3.7). The force plate data, which was zeroed from the mass of the robot resting on the force plate, was used to determine liftoff at the end of stance. For each hop, the leg lengths and ground reaction forces from the force plate were fed directly into the kinematic model and the motor model described in Section 3.2.1. An estimate for the number of joules required to exert the forces at the foot as reported by the force plate at the leg lengths reported by the SDK was calculated. Assuming the leg was moving only vertically, I first estimated $\hat{\beta}$ (see Figure 3.1) using the reported leg length r, and then calculated $\hat{\tau} = Df_rF_{fp}$ using the force plate data F_{fp}. (In computer simulations, the force exerted by the toe was determined by the leg spring constant and damping coefficient.) $\hat{\beta}$ was used to estimate the losses to electromechanical drag and I used the inverse motor model to calculate the estimated losses to heat $\hat{P}_{R_m}$. The motor models used for simulation and for validation experiments differed only in that I did not assume a stall torque in the validation experiments, so that the forces measured by the force plate could supersede the theoretical maximum forces the leg could exert based on the stall torque. This estimated joules $\hat{J}$ (see Eqn 3.5) for each hop was then plotted against the measured average joule cost $\bar{J}$ for a single jump in that condition (Figure 3.7). The measured and estimated joules had a strong correlation that was close to unity ($\hat{J} = 1.35\bar{J},\ \text{RMSE/IQR} = 0.63$). I should note that the size of the moving average window chosen to filter the force plate data had a significant effect on the slope. For example, a slightly higher moving average window resulted in a fit with slope equal to 1. The sensitivity of the slope to the moving average window size drove my decision to choose the moving average window in the manner that I did – that is, by looking for the "corner" after which the sum of absolute differences between filtered and unfiltered data stays small.

3.2.3 Computer simulations using the bulk-behavior force model show little effect of ground parameter or initial condition variation on energy savings

I performed computer simulations in Matlab of a one-legged hopper with a virtual leg spring performing a single jump on granular media using the added-mass bulk-behavior model, varying ground parameters and initial conditions.

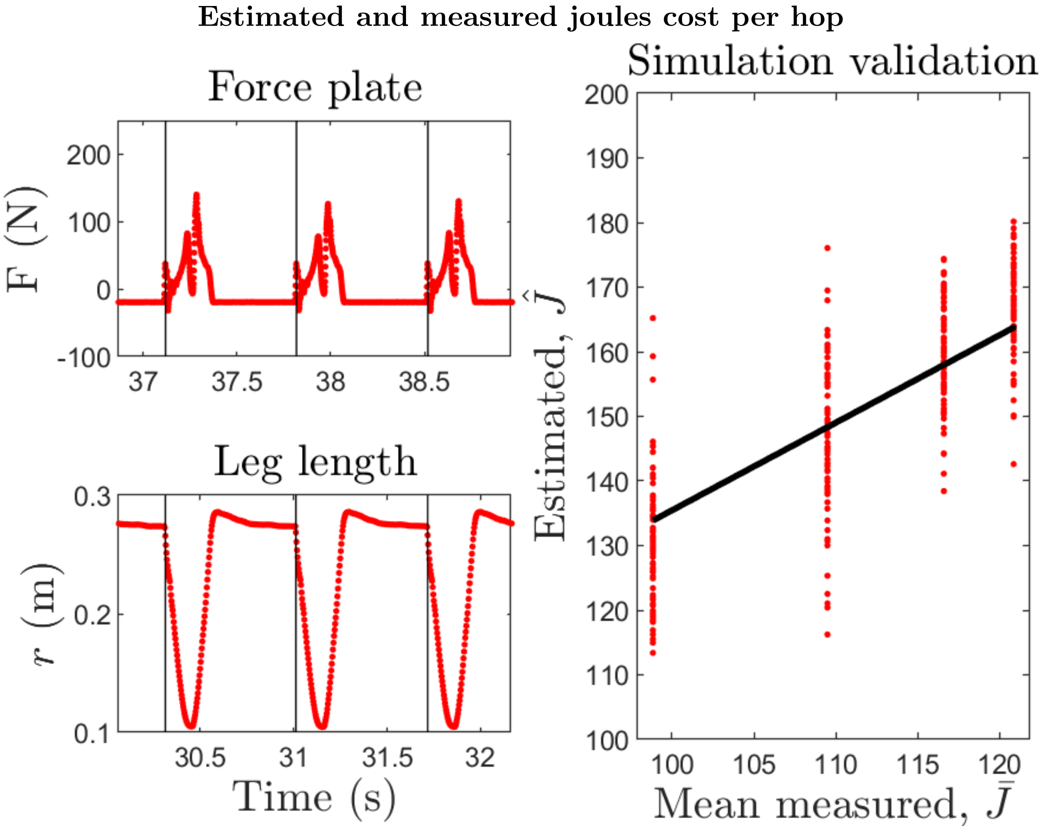

Figure 3.7: The force plate data (left, top) and leg position data (left, bottom) were both repeatable between jumps. The force plate readings were zeroed from the weight of the robot. The black vertical bars indicate the automatically detected onset of stance. The mean measured joules per hop $\bar{J}$ was well correlated with the estimate of the joules cost $\hat{J}$ (Eqn 3.5; Section 3.2.2) calculated using the forces measured by the force plate and the leg position data (right), $\hat{J} = 1.35\bar{J}$, RMSE/IQR $= 0.63$. The variability comes from the force plate data, which is only lightly filtered [106].

The active damping controller consistently loses less energy than the compression-extension controller under different initial conditions

I varied the initial velocity of the body and foot, assuming that both were starting at the same velocity and with a neutral leg length. Since the virtual spring stiffness gain during the initial compression phase of stance is very anemic, and the foot has only 10% of the mass of the body, there are only small effects on the estimated energy costs from varying either initial positions or different initial velocities for the body and foot, and the largest effects are seen by varying the amount of kinetic energy that the robot starts with at the beginning of stance.

Recall from Section 3.2.1 that P_{τ} is the power of mechanical output torque, or the electrical energy successfully converted to mechanical energy, while P_{R_m} is the eletrical energy lost to heat and P_v is the electromechanical drag. Plotting the energy cost of a jump using the active damping and compression-extension controllers with a variety of initial body velocities (Figure 3.8), I see a consistent savings of 20%. Notice that the efficiency of the active damping controller is lower than the efficiency of the compression-extension controller. Ordinarily one would expect the more efficient controller to be the better one for a given circumstance. However, if the robot efficiently produces a large quantity of mechanical energy at an inopportune time while jumping on granular media, that mechanical energy will be immediately dissipated by the media. This is counter-intuitive and important to keep in mind when considering locomotion on dissipative substrates.

The active damping controller consistently loses less energy than the compression-extension controller under different ground conditions

In the stiffness function, I varied σ, the parameter describing the stress in the vertical direction. Once the cone of added material is formed and the stiffness function becomes linear in depth, this parameter is the scalar coefficient determining the stiffness of the ground.

In the dissipation function, I varied the linear scaling parameter that multiplies the rate of change of the added mass, b_g. When the cone is fully formed and the dissipation function

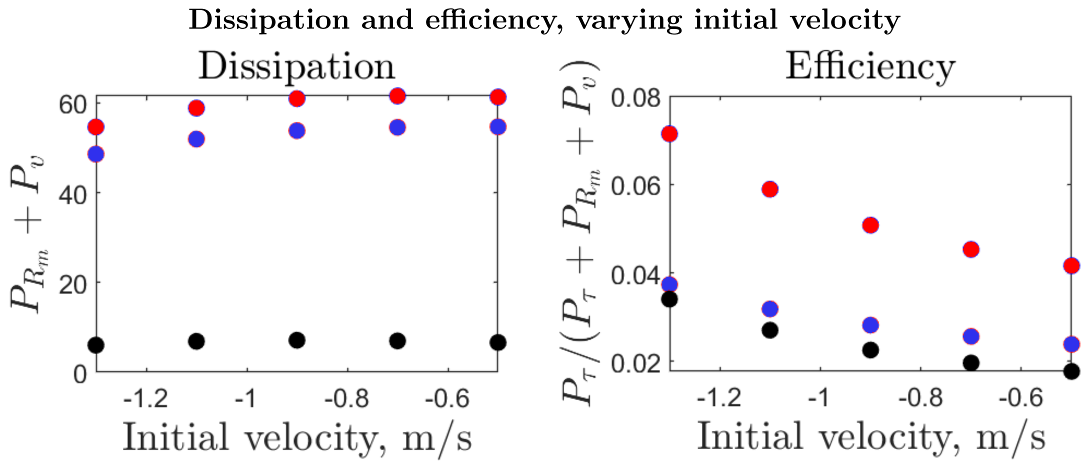

Figure 3.8: The simulated dissipation of energy (left; see Eqn 3.5) over a whole hop for the compression-extension (red) and active damping (blue) controllers is plotted under different initial velocities, with the difference between dissipated energy for the compression-extension and active damping controllers (black). The efficiency of the motors (right; Equation 3.5), is plotted for the compression-extension (blue) and active damping (red) controllers, with their difference (black) [106].

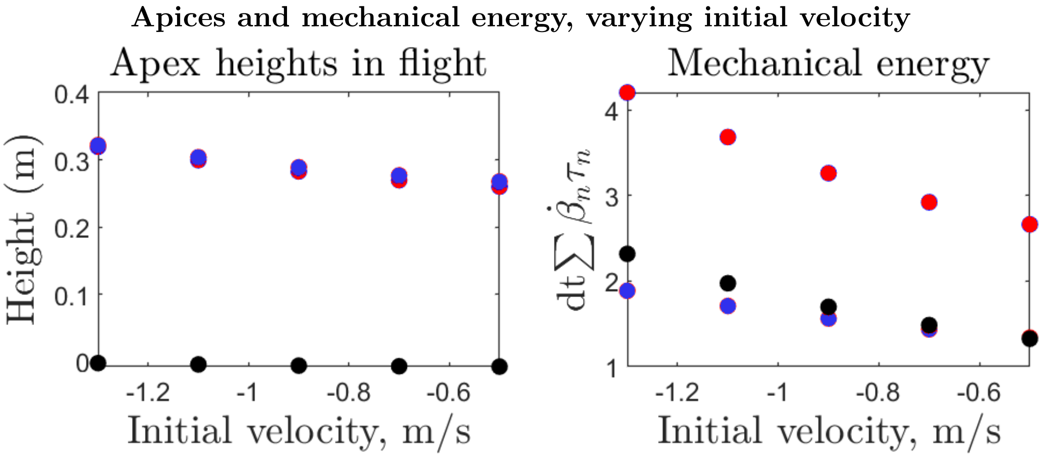

Figure 3.9: The apex heights of a simulated robot jumping with the compression-extension controller (red) and the active damping controller (blue; difference in black) are remarkably similar, though the compression-extension controller requires about twice as much mechanical energy to achieve these apex heights [106].

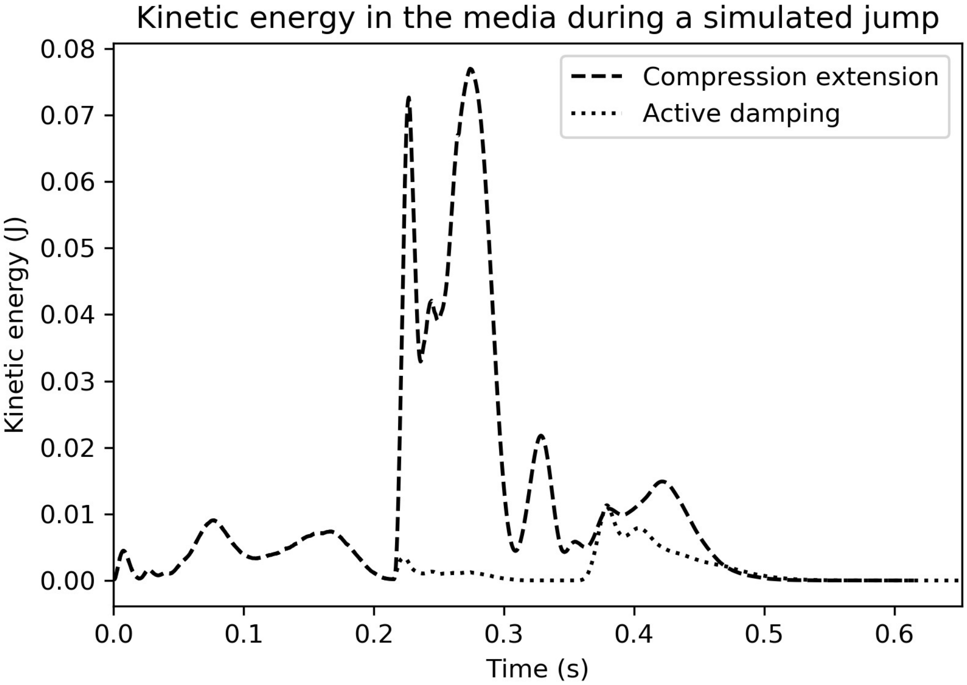

Figure 3.10: Discrete element model simulations run based on a trajectory produced in a simulation using the analytic force models. Notice how much more kinetic energy the ground absorbs under the compression-extension controller. See Section 3.1.7 for more information. Many thanks to Drs. Swapnil Pravin and Tonia Hsieh at Temple University for running my trajectories through their LIGGGHTS installation.

is quadratic in velocity, this parameter becomes a scalar directly multiplying $\dot{x}_f^2$. Using the same initial conditions (leg spring at rest length at start of stance, $-1\frac{\mathrm{m}}{\mathrm{s}}$ velocity at body and foot) for all simulations comparing ground conditions, the compression-extension controller uses about 20% more energy than the active damping controller (see Figure 3.11).

3.2.4 Discrete element model simulations show the mechanism of energy transference to the ground

To see what was happening in the granular media during jumps with the compression-extension and active damping controllers, I sent two sample trajectories to a colleague, Dr. Swapnil Pravin at Temple University, who ran them through a discrete element model simulation system that he already had installed. The simulations were performed using LAMMPS

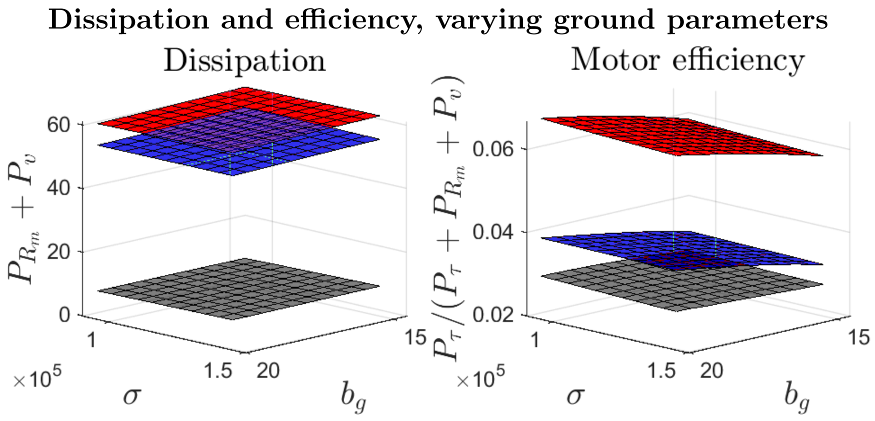

Figure 3.11: The simulated dissipated energy (left) over a whole hop for the compression-extension (red) and active damping (blue) controllers is plotted under different ground conditions, with their difference (gray). Here, σ indicates the stiffness of the ground, and b_g is the linear coefficient on the ground's dissipation function. The efficiency of the motors (right; see Eqn 3.5) is plotted for the compression-extension (red) and active damping (blue) controllers, with their difference (gray). As when varying initial conditions (Figure 3.8), we see that even though the compression-extension controller uses its motors more than twice as efficiently as the active damping controller, the compression-extension controller still dissipates almost 20% more energy [109].

Improved for General Granular and Granular Heat Transfer Simulations (LIGGGHTS)[3], an open-source discrete element modeling simulation tool. The effect of using active damping is clear in Figure 3.10. Under the compression-extension controller, the grains experienced a surge of kinetic energy when the robot enters its extension mode. In contrast, the active damping controller only imparted small amounts of kinetic energy to the ground over the course of its whole jump. These simulations provide additional corroboration for the empirical validity of the mathematical analysis in Sec 3.1.7. The active damping controller reduces the energy transfer from the robot to the ground according to the bulk behavior model of the substrate mechanics.

3.3 Second set of simulations, varying ground parameters, foot size, extension gain, and active damping coefficient

I ran a second set of simulations after already having tested the active damping controller using the physical emulation system described in Chapter 4. These simulations accompany the physical experiments described in Chapter 5 [109]. There are a few differences between

[3] https://www.cfdem.com/liggghts-open-source-discrete-element-method-particle-simulation-code

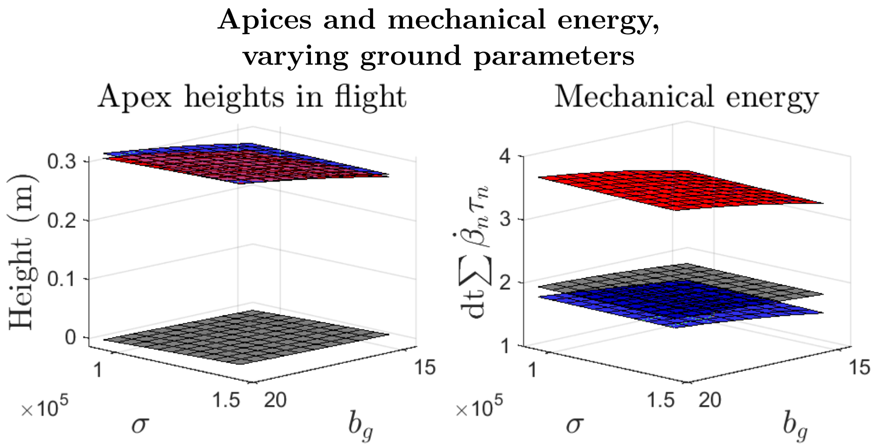

Figure 3.12: The apex heights of a simulated jump (left) under the compression-extension (red) and active damping (blue) controllers are almost indistinguishable (difference in gray). However, the mechanical energy output of the motors (right) required to achieve that height is more than twice as large when using the compression-extension (blue) controller as when using the active damping controller (red). Difference in gray.

these simulations and those described in the previous subsection.

First, the code to run this next set of simulations was written in Python, whereas the previous simulations were run in Matlab. The code is available for download on the KodlabPenn GitHub page.[4] Second, in the previous simulations, there was no limit on the forces that the robot could actually exert, only on the calculated energetic cost of a single jump. I made this choice for the previous simulations because anecdotal evidence from colleagues experimenting on the T-Motor U8 motors indicated that the datasheet under-predicted the maximum torque of those motors. I did not vary the extension gain or active damping coefficient in those simualtions, so I was able to choose conditions for which the peak forces were reasonable. In the Python simulations, I capped the forces that the robot could exert during the simulation. I made this choice because the requested torques in some of the simulated jumps in some combinations of extension gains and active damping coefficients were reaching extremely high peak forces, and I decided that slightly under-predicting the peak possible forces was a better modeling choice.

Finally, I did not model the electromechanical drag in the Python experiments (recall this term from Equation 3.5). The electrical energy transferred from the battery is com-

[4] The repository can be found at `https://github.com/KodlabPenn/jumping_on_granular_media`.

pletely described by the electrical energy successfully converted to mechanical energy and the electrical energy converted to heat, which are the other two terms. In adding the electromechanical drag (a mechanical loss) to this model, I was accounting for all of the losses the robot experiences instead of only the losses from the electrical power, which I decided was important to do because the active damping controller loses more energy in a mechanical sense relative to the compression-extension controller. However, it is cleaner to work only with the energy from the battery converted to mechanical energy or lost to heat. As the losses are dominated by the dissipation of electrical energy to heat, the qualitative results are not at all changed by this modeling choice: Using active damping still provides consistent benefits when jumping on granular media.

3.3.1 Simulation results and predictions for physical experiments

I ran simulations using the Python code varying the foot size, the active damping coefficient, and the virtual extension stiffness of the robot's leg to predict when the robot would be more likely to benefit from the active damping controller as compared with the compression-extension controller (Fig. 3.13). To account for different ground types, we also scaled the simulated stiffness and damping forces from the ground. The effect of reaching the robot's torque limit is evident in these simulations. Increasing the active damping coefficient initially increases the difference in the cost of a single jump relative to the compression-extension condition. However, after a certain point, the robot hits its torque limit more and more during its extension mode and gains no further benefit from increases to the active damping coefficient. There appears to be a trade-off with ground stiffness and foot size that affects the location of the "elbow" in the plot. The robot reaches the point of diminishing returns more quickly when the ground is less stiff and the foot is smaller.

A few more patterns emerge. In the compression-extension condition (active damping coefficient = 0), there is never a large difference between the joules cost for a smaller versus a larger foot. The maximum difference, in the softest ground condition with the stiff gain, was only 5 joules. In contrast, when using active damping, the difference between the joules cost for different foot sizes with all other conditions held constant can be quite large. This

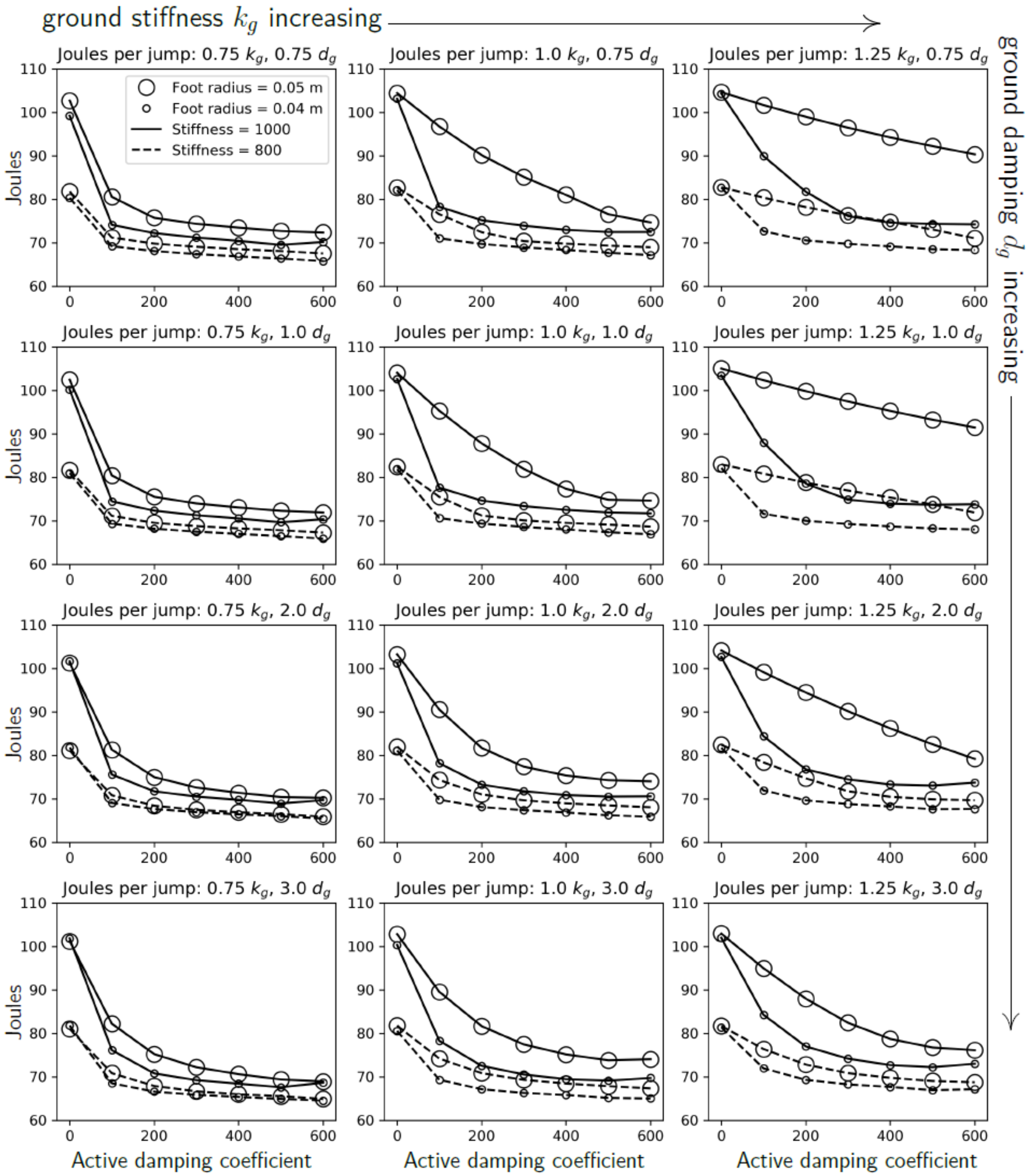

Figure 3.13: From simulations of the robot jumping on granular media, we expect that there should be a larger benefit to using active damping on a robot with a stiffer virtual extension spring and larger feet. These lines show the joules used in a simulation of a single jump with a range of active damping coefficients, foot sizes, extension stiffnesses, and scalings of the ground's stiffness and damping forces. The points corresponding to the compression-extension controller are those for which the active damping coefficient equals zero [109].

is particularly the case when the ground is stiff and has little damping. When the ground stiffness is low and has larger damping forces, there is less of a difference in the joules cost for a single jump with different foot sizes. The greatest benefit from using active damping is conferred when the robot has a small foot and a high virtual extension stiffness.

Based on these simulations, it is possible to make two general predictions about when the active damping controller will confer the most benefit:

1. Jumps using the compression-extension controller with the same virtual extension stiffness should have similar energetic cost regardless of the size of the foot.

2. Jumps using active damping should have the highest savings when using the small foot and stiff gain, and the lowest savings when using the large foot and soft gain.

3.4 Conclusion

In this chapter, I described the forces exerted by granular media in response to intrusion and discussed the performance of the well studied, robust compression-extension controller on granular media in simulation. I developed the active damping controller using the simulations to examine losses in different parts of the foot's state space and performed analysis on these losses relative to the compression-extension controller. Finally, I reported on two sets of simulations suggesting the utility of the active damping controller for reducing the energetic cost of transport on granular media. In the next chapter, I will discuss a series of physical experiments comparing the compression-extension and active damping controllers jumping on a robotic platform that emulates a granular media, providing the first physical demonstration of the utility of the active damping controller for locomotion on granular media.

Chapter 4

A physical emulation system for testing jumping controllers on arbitrary ground force profiles

4.1 Introduction

This chapter introduces a simple, robust physical substrate emulator that can be mechanically coupled to a physical one degree-of-freedom robot leg for vertical hopping experiments on "ground" with an arbitrary force-extension law for an arbitrary number of jumps [108]. I used this ground emulator to test whether the active damping controller developed in simulation and described in the previous chapter [106] could reduce the energetic cost of transport for a physical robot jumping on a dissipative ground. The results support the previous conclusion that virtual energy dissipation can be used to mitigate electromechanical energy loss to substrates exhibiting granular media mechanics.

4.2 Physical ground emulator and single-leg hopper design and setup

In this section, I will describe the design process and physical setup of the ground emulator robot and the single-leg robot that hopped on it. The next section will describe the experiments performed with this emulation system.

4.2.1 Simplified bulk-behavior model of granular media as a unidirectional Hooke's law spring with quadratic damping

During locomotion on granular media, stance under a compression-extension controller occurs in two stages: First, the soft virtual leg spring compresses under the weight of the body mass, simultaneously pushing the foot into the ground (see Figure 3.6). In previous simulations of single Minitaur legs hopping on granular media, the "cone" of added grains accelerated underneath the robot's foot was quickly formed during this time (Chapter 3). When the robot's leg length stops decreasing and its virtual leg spring switches to its stiff gain, causing the leg to extend and the robot to jump, the cone of grains is already fully formed, and the compliance and damping functions of the ground's force profile are already in their linear and quadratic regions, respectively. The assumption that the extension mode will occur after the initial nonlinearity in the forces from the ground is valid so long as the robot's foot size is relatively small. I assumed a foot diameter of less than 3 cm (about the size of the standard Minitaur foot), for which this assumption holds.

In the work presented in this chapter, I therefore employed a simplified granular media model in the present experiments that does not include the initial nonlinearity. I modeled the ground's stiffness function $k_g(x)$ as a Hooke's law spring with no restoring forces, $k_g(x) = kx \quad (\dot{x} \leq 0)$, and the drag term as a quadratic damping term, $d_g(x)\dot{x}^2 = d\dot{x}^2$, with no separately modeled added mass.

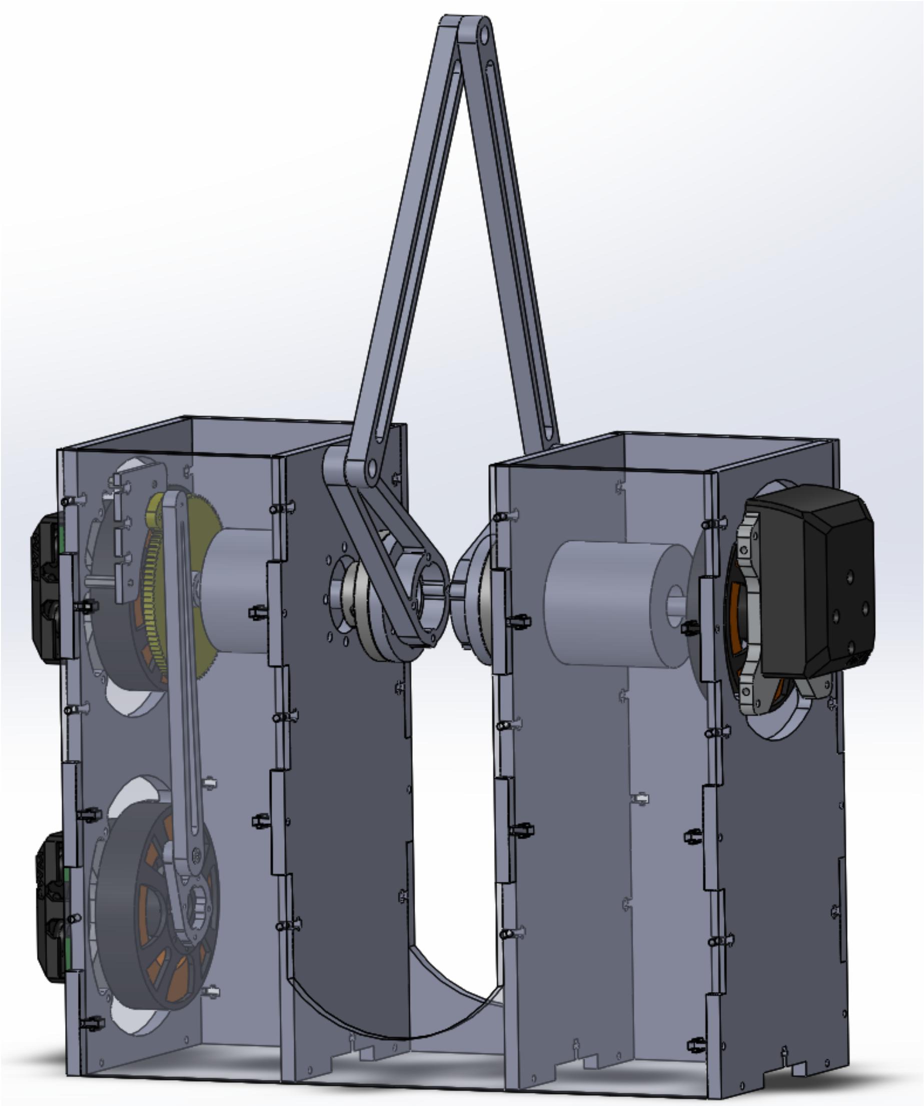

Figure 4.1: A semi-transparent CAD model of the ground emulator shows the ratchet gear (yellow) attached to one of the motors controlling the leg that moves the platform up and down the linear rail [108].

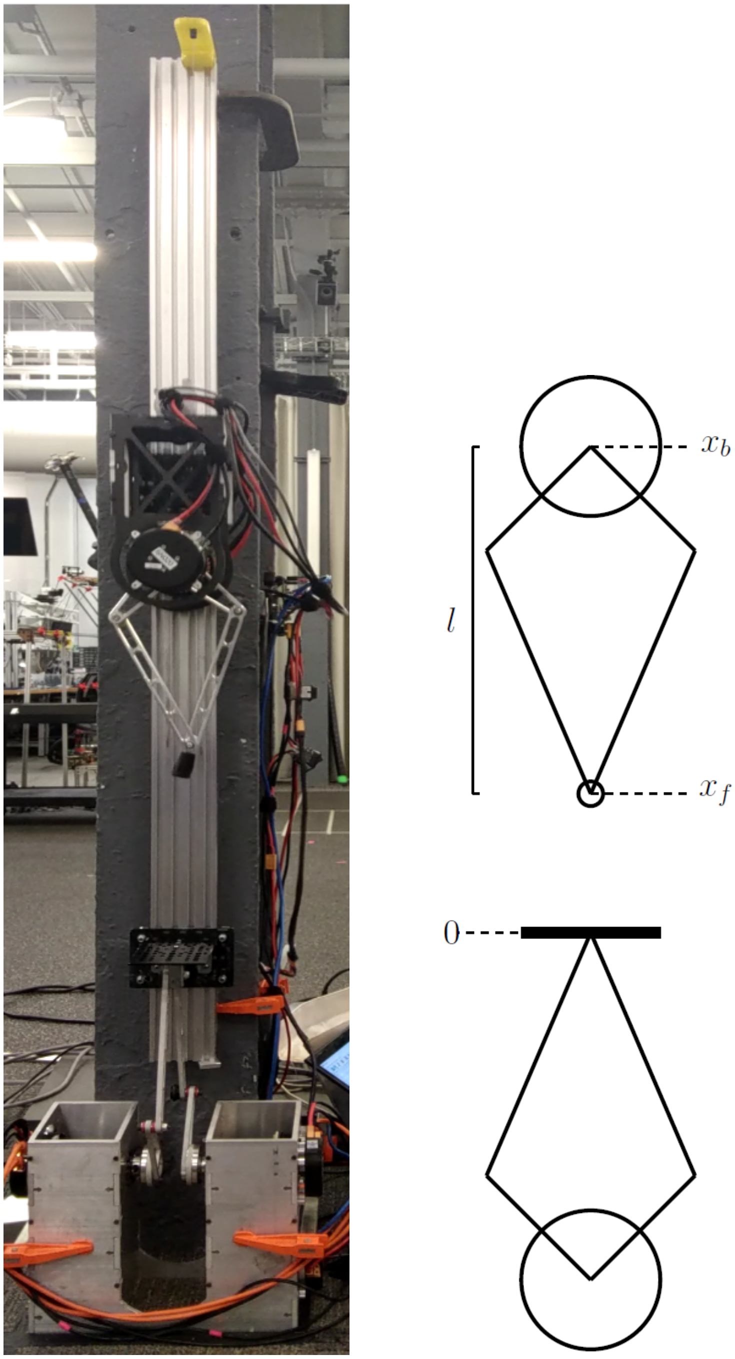

Figure 4.2: (Left) The ground emulator and hopper. (Right) A schematic of the hopper and the ground emulator [108].

4.2.2 Physical setup of ground emulator

The ground emulator used a modified Ghost[1] Minitaur leg to move a platform up and down a linear rail. The leg used two opposing T-motor U-8 motors driven by Ghost EtherCAT motor controllers, lightly geared to increase maximum torque while maintaining backdrivability [69] (4.3:1 reduction; Maxon ceramic planetary gearbox, PN 223081). The body of the emulator and linear rail were clamped to the same vertical I-beam, and both the body of the ground emulator and the vertical rail were leveled in two axes to within 1 degree of inclination. A releasable mechanical stop at the bottom of the vertical rail constrained the range of motion of the leg controlling the platform to prevent the leg from reaching a singularity. The programmed range of motion used for experiments was further restricted to between 20 and 27cm (possible range 10-30cm). This is the part of the robot's workspace where it has the least mechanical advantage, and where the mechanical advantage is relatively constant [68]. Because of the consistently low mechanical advantage within this range, the behavior of the limb overall will better emulate a linear spring. All parts used to build the linear rail were purchased from OpenBuilds.[2]

The force-extension behavior produced by the ground emulator was a composition of two simple physical actuation subsystems. The lightly geared leg emulated a spring with a linear stiffness function, $F_s(x_f) = kx_f$, and quadratic damping, $F_d(\dot{x}_f) = \alpha\dot{x}_f + \beta\dot{x}_f^2$, with α the native mechanical viscous damping in the system and β the programmed quadratic term. The linear damping modeled in coefficient α is due to friction from the linear rail, the 4.3:1 gearboxes, and the ratchet, as well as inefficiencies from the PWM motor controllers. A ratchet gear[3] attached to one of the paired motors controlling the lightly geared leg engaged with a pawl arm controlled by a third Ghost motor module (see Figure 4.2).

[1] Ghost Robotics, 3401 Grays Ferry Ave, Philadelphia, PA 19146 http://www.ghostrobotics.io

[2] OpenBuilds Part Store, https://openbuildspartstore.com/

[3] Ratchet gear and pawl arm purchased from Stock Drive Products/Sterling Instruments, http://sdp-si.com.

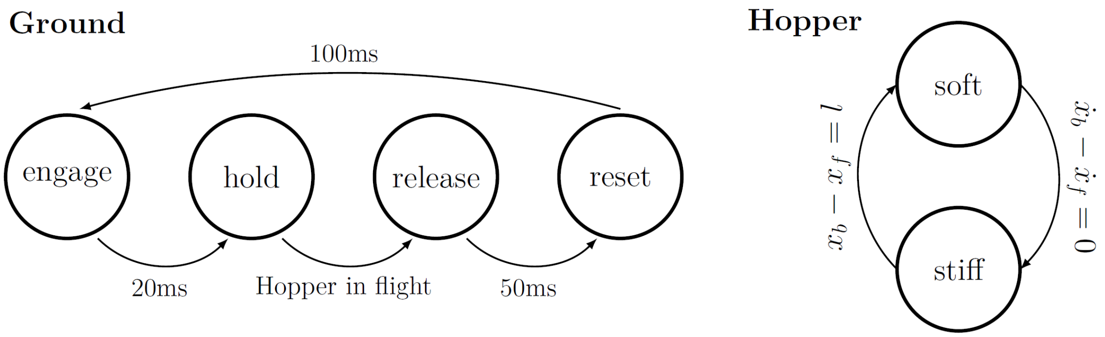

Figure 4.3: (Left) The state machine for the ground emulator *engaged* the ratchet when the hopper was in flight, then lightly *held* the ratchet's pawl arm down to engage with the gear while the hopper was in stance. When the hopper entered its flight mode, the ground emulator *released* the ratchet, allowing the platform to *reset* its position. (Right) The hopper's state machine was independent of the ground emulator's, and consisted of only two states: emulating a soft and a stiff virtual leg spring [108].

4.2.3 Control of ground emulator

The state machines for the emulator and hopper were both simple, and the hopper's state machine was independent of the ground emulator's. (See Figure 4.3 for details.) The ground emulation control entailed four states. While the hopper is in flight, the motor controlling the ratchet moved the pawl arm down to engage the gear. Once in position, the motor received a small constant open-loop command, which produced a small force to hold the pawl arm in place and keep it engaged as the gear rotated. While the emulator was in this state, the hopper entered stance mode, touching down and compressing its leg spring. When its leg spring was fully compressed, the hopper switched to a stiff extension spring, and rapidly pushed the emulator's platform down a second time before lifting off and entering its flight mode. The emulator was triggered to release the ratchet when the hopper's leg extension length was close to its rest length, the hopper leg was in its stiff state, and the "hold" state had lasted at least 50ms, with these conditions serving as a proxy for the hopper being in flight. The release was accomplished by changing the desired position of the platform to slightly below its current position, releasing pressure on the pawl arm, and moving the pawl arm up. Finally, while holding the pawl arm up, the emulator quickly pushed its platform back up to reset the emulated "ground" to its nominal height, and the hopping cycle was ready to repeat. For a visual representation, see Figure 4.4.

4.2.4 Physical setup of hopper

The one-legged hopper modeled one quarter of a Minitaur, using two opposing Ghost EtherCAT motor modules to control the motion of a toe through a symmetric four-bar linkage. The hopper was constrained to move its body center of mass vertically along the linear rail. A string potentiometer attached to the top of the hopper's body measured its height, with values recorded by the microcontroller running the hopper and ground emulator. All control software was written using the Ghost SDK. Although the emulator and the hopper were controlled by the same microcontroller, the hopper was powered from a separate battery.

4.2.5 Control of hopper

The hopper cycled between two states: emulating a virtual soft leg spring which compresses easily, and alternating with a stiff leg spring. When appropriately triggered and reset, the alternation of these two internal hybrid controller modes produced two physical robot modes: Stance, during which time the robot's foot is in contact with the ground; and flight, when it is not. The hopper switched from its soft programmed leg spring to stiff when the leg was compressed beyond a threshold and the velocity of the change in leg length was zero, $\dot{x}_b - \dot{x}_f = 0$. It switched from stiff to soft when the leg again achieved its neutral leg length l. (See Figure 4.3 for details.) The switch from soft spring to stiff injected a large quantity of potential energy when the leg is compressed, causing the robot to jump. For a visual representation, see Figure 4.4.

4.2.6 Characterization of ground emulator

To validate the assumption that the ground emulator would exert the programmed forces in the expected ways, I characterized the force response of the ground emulator's leg commanded to emulate a Hooke's Law compliance and viscous damping (i.e., completely linear) response, with different position and velocity gains under different neutral leg extension positions. To characterize the force response, I placed a mass on the platform, displaced the mass by pushing the platform down, and then recorded the extension position and velocity of the leg as the platform oscillated and came to rest. For these experiments, the ratchet

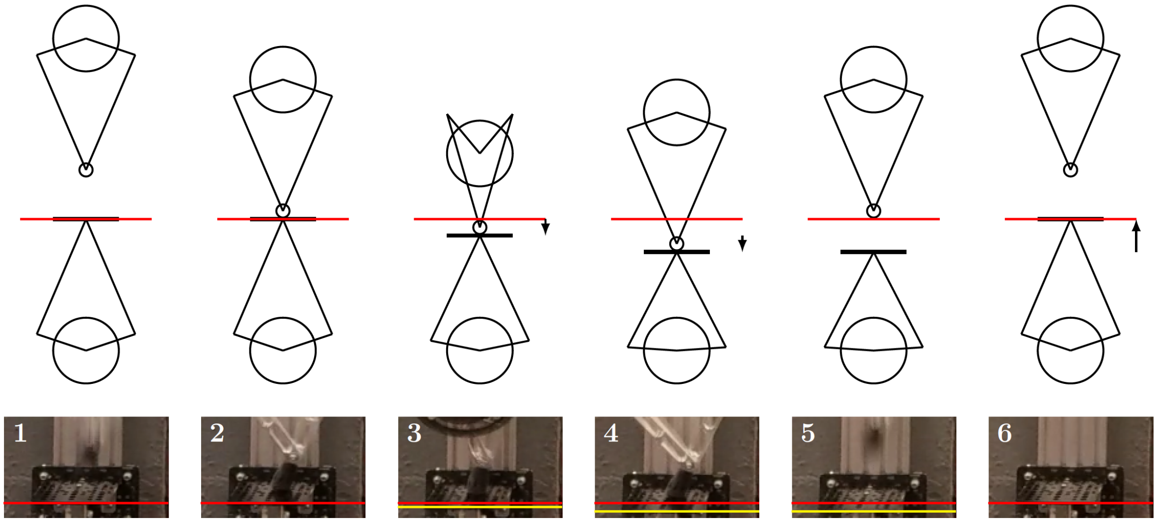

Figure 4.4: This sequence of video stills and corresponding schematic images shows how the hopper and ground emulator interact during a single jump. (1) The ground emulator engages its ratchet while the hopper is in flight. (2) The hopper touches down. (3) The hopper's soft leg spring compresses easily. Forces exerted by the soft leg spring through the hopper's toe compress the ground emulator and move the platform. (4) The hopper's leg stiffness increases, pushing both the hopper's body up and the platform further down. (5) When the hopper lifts off, the ratchet is still engaged, preventing the ground emulator from exerting restoring forces. (6) While the hopper is in flight, the ground emulator releases its ratchet and resets the platform height to the neutral position. The ground emulator is then ready for the hopper's next jump [108].

was disengaged, allowing the platform to oscillate up and down. In lieu of using a variety of initial conditions, I used a variety of masses with each position and velocity gain to achieve a range of trajectories through the platform's state space. At least ten sample trajectories through the state space under each combination of position gain, velocity gain, and mass were collected. The characterization experiments were performed with an older version of the Ghost motor controllers and firmware, but using the same motors and control software.

I calculated the acceleration of the platform at each time step from the extension velocities and time in milliseconds measured through the Ghost SDK at 300Hz. The force exerted by the virtual leg spring at each time step was then calculated by multiplying the acceleration by the total mass that the leg was pushing. Finally, I used simple linear regression (pseudoinverse on the position and velocity data) to fit a plane to the position and velocity measurements, predicting the force. The fitted coefficients on the position and velocity axes were taken as the physical stiffness and damping coefficients of the virtual spring. Planes were only fit to experimental conditions where I had at least 250 data points. (See Figure 4.5.)

4.2.7 Compression-extension and active damping controllers

As my nominal controller, I employed a Raibert-style compression-extension control law [100]. Recall from Section 3.1.4 that under this control law, a soft spring during the first half of stance mode allows the robot's leg to compress under the weight of its body and a sudden injection of potential energy in the form of a sudden switch to a stiff spring when the leg is fully compressed and the body mass velocity reaches zero causes the leg to extend and the robot to jump.

In comparison, I tested two versions of the *active damping* controller introduced and developed in Chapter 3. Recall that this controller adds a damping force to the stiff spring in proportion to the velocity of intrusion of the robot's toe into the ground. Here, "intrusion" is considered to be the vertical displacement of the ground emulator's platform. In the *constant* active damping controller, the same proportional damping gain is used for all stiff spring conditions tested. In the *scaled* active damping controller, the gain used in the active

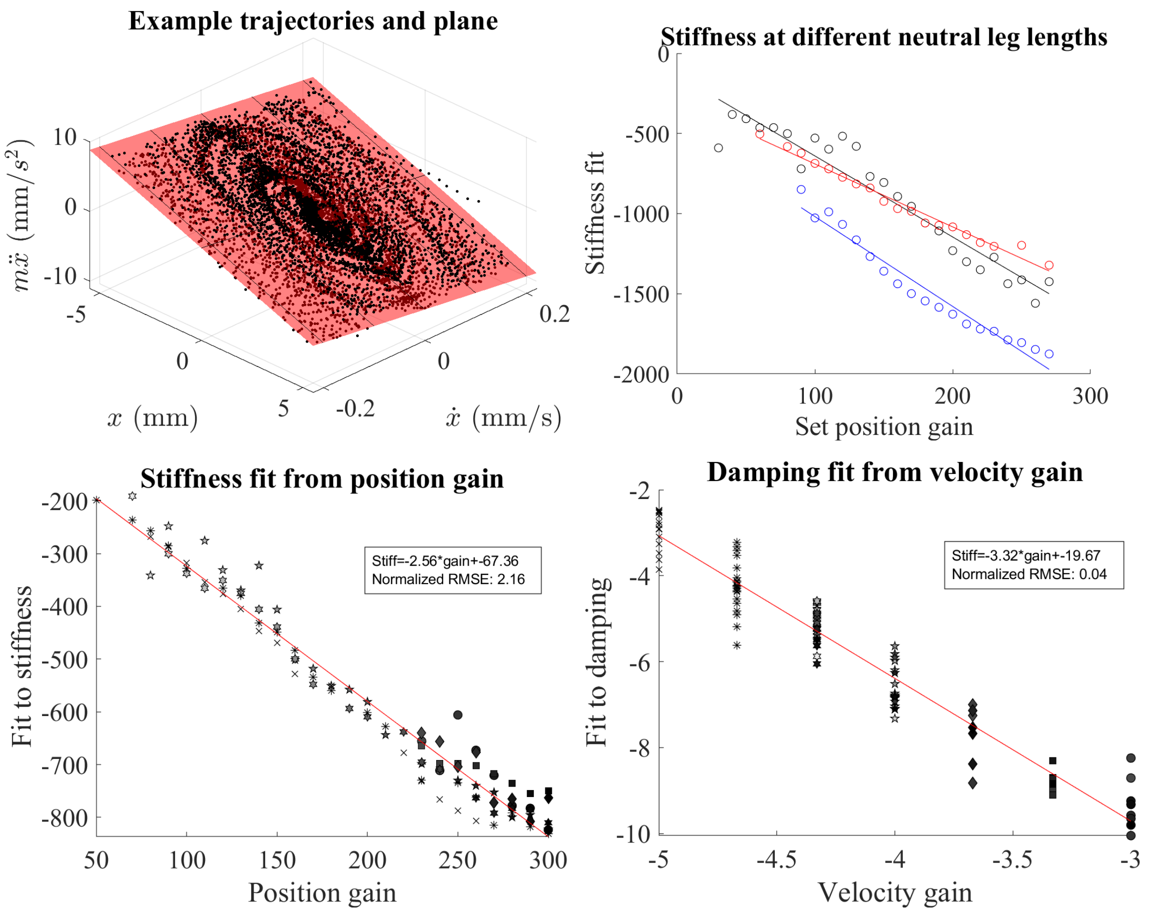

Figure 4.5: (Top left) Example data of trajectories through the platform's state space that were used to relate the acceleration of the platform to its position and velocity, and thus fit the physical values of the spring constant and damping coefficient. The fitted plane is in red. (Top right) The fits to physical stiffness were similar when the leg's neutral point was 20 (red) and 29 (black) cm, but the mechanical advantage conferred by the crouched posture when the leg was more compressed at 15cm (blue) resulted in stiffer physical springs from the same set gains. (Bottom) At neutral leg length 20cm, the set position gains vary linearly with measured stiffness and the set velocity gains vary linearly with measured damping. In both plots, different marker shapes correspond to experiments conducted with different masses [108].

damping controller was scaled proportionately with the extension position gain used for the stiff spring.

4.3 Experiments conducted and analysis of results

In this section, I will describe the experiments conducted using this physical emulation system and the results for both active damping conditions. In all conditions, active damping did improve energy efficiency of locomotion. However, the quantity of active damping had an effect on the percent of energy saved relative to the control condition.

4.3.1 Experiments comparing controllers

I jumped the hopper on the ground emulator under five different stiff spring extension position gain conditions (100, 200, 300, 400, 500) using two versions of the active damping controller: one in which the active damping gains were set to the same value (=50) for all stiff spring conditions, and one in which the active damping gains scaled linearly with the stiff spring's extension position gain at a ratio of 1:6. For example, for extension position gain 200, active damping gain $200/600 = 33$ was used; for extension position gain 400, the scaled active damping gain was 67. These values coincided for the condition with extension stiffness gain 300 ($= 6 \cdot 50$).

The experiments reported here were run over four non-consecutive days. On days where many experiments were run, the trial ordering was randomized. On days with only a few experiments, block ordering was used to prevent spurious correlations between time and extension gains or controller type. Every day that experiments were run, at least one control experiment for each extension condition was run using the nominal compression-extension controller.

The protocol for each experiment was as follows. First, a fully charged 4-cell lithium ion polymer battery (ThunderPower, Reaper series, 7200 mAh) was connected to the hopper. The ground emulator and microcontroller were connected to a separate power supply, and the whole system was turned on. The ground emulator moved the platform to its neutral position and the hopper was lowered by hand to where its toe just touched the platform. The

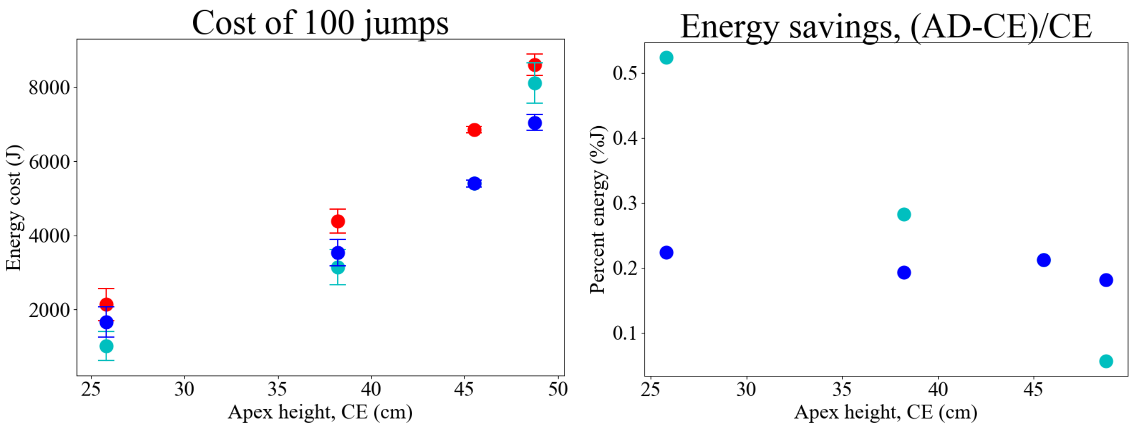

Figure 4.6: The compression-extension controller (red) consistently required more energy from its battery than the constant (cyan) or scaled (blue) active damping controllers to jump 100 times. Under a constant active damping controller, the percent energy savings scales linearly with jump height, but when the active damping gain scales, the percent savings is a consistent 20%. All error bars are the standard error of the mean [108].

hopper was then released, allowing its body mass to compress the soft leg spring and trigger a switch to the stiff leg spring, causing the robot to take its first jump. The hopper was allowed to complete 100 jumps before being caught and immediately turned off. Between four and seven repetitions of each experiment were conducted.

The battery was then recharged using a ThunderPower charger, and the mAh used to recharge the battery was recorded. The joules drawn from the battery assuming a full battery voltage of 16.8 was then calculated as the energy cost for the 100 jumps. In addition to the data recorded from the charger, some control and validation data (gains, current states, and positions and velocities of the hopper and ground emulator) was logged at 300Hz through a serial port connection to the microcontroller and at least one 60fps video was taken of each experimental condition. The only data logged through the serial port that is reported here is the apex heights for the different conditions, which were recorded using the spring potentiometer attached to the top of the hopper.

4.3.2 Active damping controller reduces energy cost for a variety of jump heights

The constant and scaled active damping controllers both consistently out-performed the compression-extension controller in terms of energy expenditure over 100 jumps, but exhibited different patterns of performance relative to the compression-extension controller (see Figure 4.6). For each of the two active damping controllers, I calculated the percent improvement between the compression-extension and active damping controllers, that is, the percent of the joules cost for 100 jumps with the compression-extension controller that was saved by using the active damping controller: $\frac{CE-AD}{CE}$. The constant active damping controller, which added the same damping force relative to the robot's intrusion velocity regardless of the stiffness of the emulated leg spring, gave extremely high relative improvement in the lowest stiffness condition and very little improvement in the highest stiffness condition, with an approximately linear relationship to apex jump height. The scaled active damping controller, which had a gain that scaled relative to the hopper's stiff spring gain, gave a consistent 20% improvement across all jump height conditions. See Figure 4.6 for more details.

4.3.3 Energy savings from active damping controller come with little cost to apex jump height

The apex center of body mass heights were determined by the spring potentiometer readings logged over a serial communications port to the microcontroller. Noting that there was no appreciable difference in jump height between the two stiffest conditions (gains = 400 and 500), I determined that the hopper's motors were already exerting their maximum torque in the second-stiffest condition and excluded the stiffest condition from further analysis.

Apex heights were determined to be the local maxima of the lightly smoothed spring potentiometer data (moving average, window size 10 points), excluding any hops where a dropped data packet obscured part of the aerial phase of the hop. The first two jumps of each experiment were also excluded. Because all experimental conditions had at least

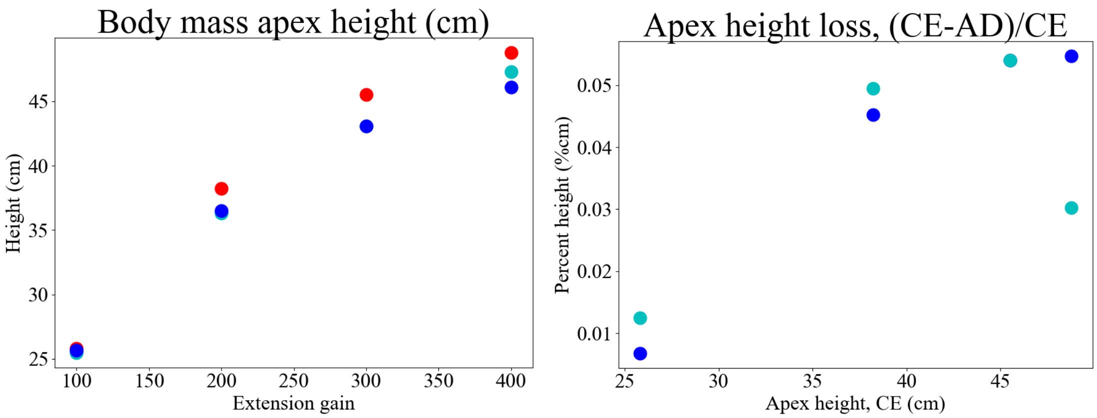

Figure 4.7: The consistent 20% energy savings come at a consistent $< 6\%$ cost in apex body center of mass height. In all plots, red indicates the compression-extension controller, cyan the active damping controller with the same active damping gain for different extension stiffnesses, and blue the active damping controller with an active damping gain that scales with the extension stiffness. Percent savings are calculated using sample averages. Each sample consists of between 200 and 700 apex heights.

200 data points, and jump heights were very regular, standard deviations were very small ($<$ 0.75cm for all conditions) and are not plotted. The apex heights varied approximately linearly with the extension position gain for all experimental conditions (Figure 4.7), and the percent difference between the apex center of body mass heights for the two active damping conditions and the control condition was consistently less than 6%.

4.4 Conclusion

In this chapter, I have introduced a ground emulator that can be used to test hypotheses about locomotion on dissipative compliant ground with arbitrary force extension laws, including generalized granular media models. I used this system to perform some preliminary tests in emulation of a hypothesis developed originally in simulation [106] (Chapter 3), that is, that the dissipation of virtual energy into a virtual damper in an electromechanical system before it is transferred to a nonlinear, unidirectional, and highly dissipative mechanical system can significantly reduce the energetic cost of transport.

As the neutral leg length for the hopper was set to 25cm, which is very close to the lowest apex jump height of 25.6cm, the lowest apex height condition represented a very modest “jump” which would be appropriate to use in the stance portion of a step in a walking gait.

The highest apex height, 49.3cm, represented a large jump that might be used to climb up a steep slope or run quickly over a long distance. The consistent 20% energy savings and low ($< 6\%$) cost to apex height across this large range of jump height conditions suggest that the choice to dissipate energy using virtual forces in electromechanical systems has potential to mitigate energy costs in a large variety of locomotion applications on dissipative ground. In the next chapter, I will discuss experiments on physical granular media using the same single-leg hopper.

Chapter 5

Jumping experiments on physical granular media

5.1 Introduction

In order to validate the simulation (Chapter 3) and emulation (Chapter 4) results, I performed jumping experiments on controlled physical granular media. Locomotion experiments on granular media are most often performed using poppyseeds in a bed which pumps air uniformly through the granular media to fluidize it in between experiments (e.g. [1]). The main advantage of such a bed is that the compaction and thus stiffness of the granular media can be determined programmatically by sending small puffs of air through the media after it is fluidized [121]. The fluidization process also makes consistent preparation of the same compaction simpler, as freshly fuidized media will have a flat top and be uniformly compact [120].

However, for small amounts of media, it is also possible to simply stir the media and smooth the top between experiments (e.g. [9, 47, 90]). The introduction of noise to the data by this less exact method of media preparation is mitigated in these experiments by the use of granular media with a relatively large diameter (3.4mm), which can only occupy a tight range of volume fractions (volume of solid media/total volume of container filled)

[32]. As the stiffness of the ground is determined by the volume fraction, this means that ground with a tight range of possible volume fractions will only be able to exert a limited range of stiffnesses. A fluidizing bed is necessary for multi-step locomotion experiments over a larger area, enables the same media to be prepared with different stiffnesses, and would certainly have eased the preparation of media for these experiments. However, for single jumps with large-diameter media to exert the same stiffness for every jump, it is possible to obtain consistent results without fluidizing the media.

5.1.1 Robot used in jumping experiments

The robot I used in these experiments was a single-leg hopper using the same motor controllers and basic hardware as the Ghost Minitaur and T-motor brand U8 motors, but with custom control code to implement the classical compression-extension controller and the active damping controller. The robot used two opposing motors to control the motion of its toe through a symmetric four-bar linkage. I powered the robot with a 4-cell LiPo battery[1] and charged it between experiments with a LiPo charger-balancer[2].

The robot's leg was modified to linearize the vertical motion of the foot (see Fig. 5.1. The foot was attached to an aluminum rod which passes through a linear bearing housed in the 3D-printed top plate of the robot's chassis, preventing any rotation of the foot as the motors move the foot vertically through the leg linkages. The rod was lubricated with machine oil at the start of each day that experiments were performed. The robot's foot was 3D printed from ABS. Two foot sizes were used in these experiments: One with a radius of 0.051 m, and one with a radius of 0.038 m. The robot weighed 2 kg, accounting for the force exerted by the string potentiometer. The leg's maximum length was 0.3 m and its minimum length, when fully compressed, was 0.1 m. The robot was attached to a gantry plate and free to move up and down along a vertical rail[3]. The angle of the vertical rail was checked using an analog angle gauge at least once per day of experiments.

[1] ThunderPowerRC, 3550 East Post Road Suite 500 Las Vegas, NV 89120, Reaper series, part number TP6600-4SR70

[2] ThunderPowerRC, part number TP610HVC

[3] OpenBuilds, 719 Whig Ln, Monroeville, NJ, 08343

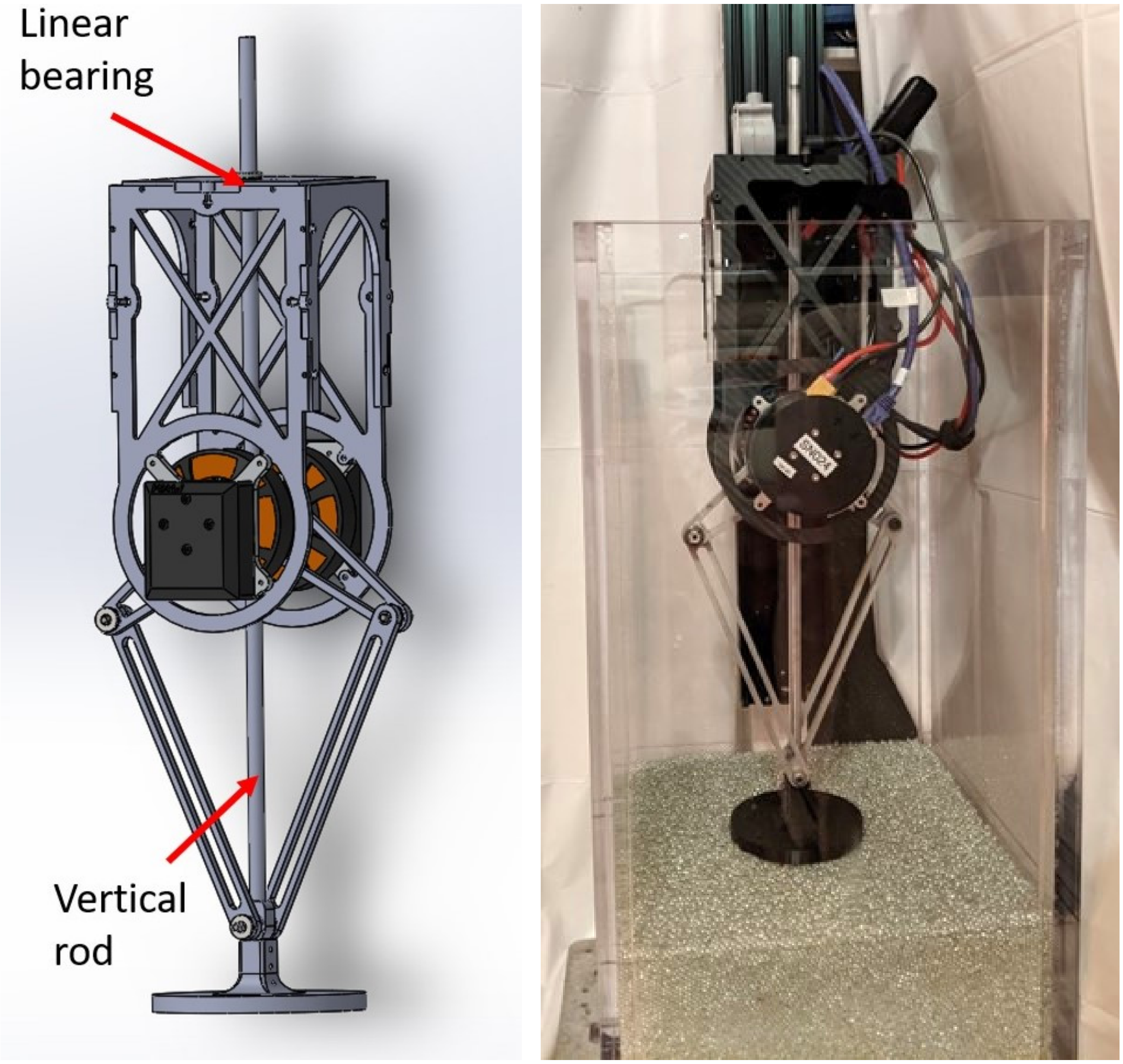

Figure 5.1: Left: The one-legged robot which was adapted for vertical jumping experiments on prepared granular media. Right: The full setup, with robot attached to linear rail in the sandbox. See Section5.1.1 for more information.

The robot was programmed with a simple hybrid controller which cycled between two states: *compresssion*, in which the robot's leg emulated a soft virtual spring through a low proportional and derivative gain on the motors through the leg kinematics, and *extension*, in which the leg emulated a stiff virtual leg spring. The robot switches from compression to extension when the leg is compressed beyond a small threshold (0.05 m) and the rate of change of its leg length goes to zero, $\dot{x}_b - \dot{x}_f = 0$. The switch from extension back to compression occurs when the leg reaches its neural leg length l (0.27 m for these experiments). The active damping controller added a force during extension, but did not change the otherwise change the control. The injection of energy caused by a sudden change from a soft to a stiff virtual leg spring is what causes the robot to jump (Fig. 3.4).

I tested two virtual extension stiffnesses and five active damping gain conditions. The extension gains (300 and 400) were converted to stiffness coefficients (units: N/m) and the active damping gains (50, 100, 150, 200, 250) were converted to damping coefficients (units: kg/s) using a least-squares fit I performed in a previous study on a similar leg [108]. For a stiffness coefficient k, stiffness gain g_k, damping coefficient d, and damping gain g_d, the formula for stiffness is $k = 2.56g_k + 67.36$ and the formula for the damping coefficient is $d = 3.32g_d + 19.67$. The plots in this paper use the fitted stiffness and damping coefficients to ease comparison with the simulations and enable other researchers to more easily extend my results to their own robot platforms.

5.1.2 Controlled granular media bed

The controlled granular media bed consisted of a clear acrylic box with a 0.3 x 0.3 m base and 0.6 m walls. I filled the box with 3.4 mm glass beads[4] to a depth of 0.16 m. Before each jump, I lightly stirred the media and smoothed the surface. The surface smoothing was performed with a slider cut to the inside shape of the box from a sheet of thick cardboard. Wings at the top of the slider hooked over the top of the box as it was moved back and forth, ensuring that the bottom of the slider prepared the surface at the same depth for each jump.

[4] Jaygo, Inc., 7 Emery Ave, Randolph, NJ, 07869

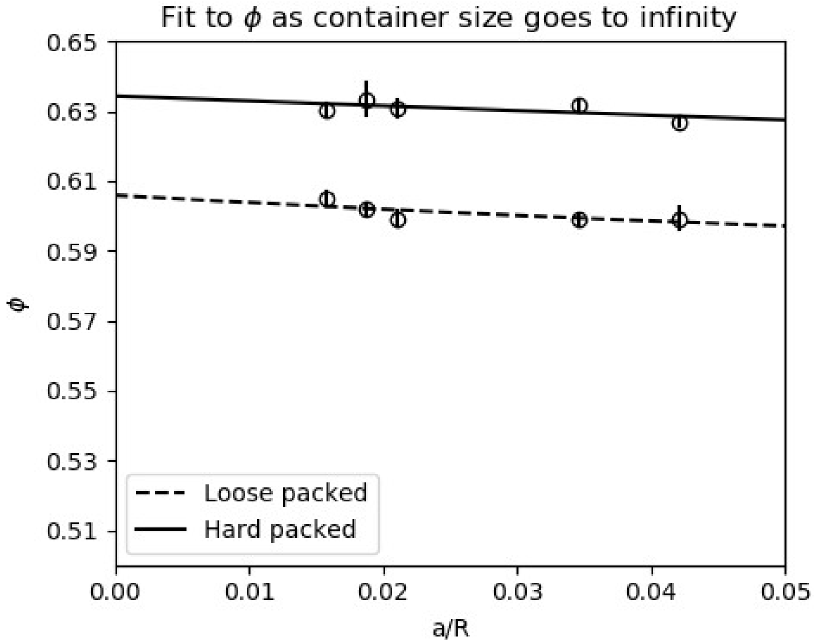

Figure 5.2: The difference between the minimum and maximum possible compactions ϕ, and therefore forces exerted by the ground, was 2%. The x-axis on this plot describes the ratio of the size of the grains (a = 3.4 mm) to the container radius. The y-axis corresponds to the volume fraction of the media, that is, the percentage of space occupied by the grains. The y-intercepts on this plot therefore correspond to the volume fractions when the radius of the container goes to infinity. The range of the y-axis is determined by the possible range of granular media compactions. The vertical bars indicate one standard deviation [109]. See Section5.1.2 for more information.

I tested the range of compactions that the 3.4 mm glass beads could occupy by pouring grains loosely into spherical flasks of five different diameters, filling the remaining space with water, and then compacting grains and removing water until no more grains could be added. Water volume measurements were collected for both the initially poured loose packed state and the final maximum compaction state. I then fit a model which estimates the compaction at the center of a spherical container filled with media as the percent of media in the boundary layer goes to zero for both the loose packed and hard packed states using the method described in [84].

The estimated volume fractions for the loose packed and hard packed states were 0.61 and 0.63, respectively (see Fig. 5.2). To determine whether this variation was acceptable, I considered how the variation would affect the conclusions of my data. Since the maximum random close packing of a homogeneous granular media with spherical grains is about 0.64 [32], in the 0.61-0.62 range, an impacting leg should not be able to substantially increase the compaction. Considering the force response from the granular media as a function of the compaction, the forces from the granular media should level off as the compaction approaches the maximum random closed packing.[5] In [1], the experimenters jumped a robot on a controlled granular media bed with a range of compactions. The expected relationship between compaction and jump height emerged, with the jump heights levelling off as the compaction exceeded 0.61. In the 0.61-0.63 range, the difference in jump heights is small and close to within experimental noise.[6] This maximum 2% possible range of compactions in the granular media in my preparation was therefore deemed acceptable for my physical experiments.

5.1.3 Experimental protocol for robot jumping on controlled granular media bed

The full setup, with the robot constrained to a linear rail in the sandbox, is pictured in Fig. 5.1. The robot's foot was centered in the middle of the box to avoid boundary conditions during jumps, meaning that there was a minimum of about 0.1 m between the edge of the foot and any side wall during the experiment.

The energy consumption for the cost of transport measurements was calculated by recharging the battery after use and recording the mAh reported by the charger. The battery was recharged to the storage voltage of 15.4 V (3.85 V per battery) instead of the maximum voltage of 16.8 V because the relationship between percent of charge and voltage for lithium ion polymer batteries is nonlinear at the top of the voltage range. Keeping the battery close to the storage voltage avoids this nonlinearity.

I took several additional precautions to reduce noise in the energy consumption measurements. First, if experiments had not been run the previous day, the battery was discharged by jumping the robot 20-50 times and then recharged before starting experiments for the

[5] Marc Miskin, personal communication, July 7th, 2021.

[6] Tonia Hsieh, personal communication, July 7th, 2021.

day. This mitigated the effect of passive self-discharge. Second, I either randomized the order of experiments in each day or used block ordering, depending on how many experiments were to be conducted. Experiments were, however, performed in a rough ordering of foot size and extension gain: All experiments with the larger foot were performed first, and all experiments with the stiffer extension spring were performed first for a given foot size.

I also used a timer to ensure that all of the experiments took the same length of time (12 minutes). This was necessary because resetting the ground between jumps took significantly longer than the time the robot spent jumping. The passive power consumption of the robot's electronics, even when the motors were not powered, added significant noise to the energy cost measurements if this was not held constant. Sometimes, the motor controllers would report the incorrect leg configuration, and the robot would need to be restarted up to 3 times. When this happened, I quickly flipped the switch on and off, and noted how many starts were required. I was not able to detect a difference in the power consumption between trials with multiple starts versus one start.

I prepared and checked the experimental setup to ensure that it was consistent from day to day. Before starting experiments each day, I checked the angle of the robot's vertical rail to make sure that it was within 1 degree of vertical. I added machine oil to lubricate the linearizing rod attached to the robot's foot which passes through a linear bearing in the 3D-printed top of the robot's chassis.

Each experiment proceeded as follows:

1. Connect battery to robot and turn the hard switch on, providing power to the robot's electronics but only zero gain to the motors.

2. Start the timer.

3. Connect the robot's microcontroller board to the laptop and extend and compress the leg to ensure that the robot is booted up and transferring data correctly.

4. Repeat steps 1 and 3 as many times as necessary to get accurate length readings.

5. Begin logging data to the laptop.

6. Remove the clamp that the robot is resting on and move the robot down until it is just past a mark on the string potentiometer indicating the start position (0.42 m).

7. Drop the robot.

8. Catch the robot before it touches down a second time.

9. Replace the clamp and allow the robot to rest while resetting the ground.

10. Repeat steps 7-9 for a total of 25 jumps.

11. Allow the robot to rest on the clamp until the full 12 minutes have passed.

12. Cut power to the battery and place it to charge. Stop logging data and upload the code for the next experiment.

I performed at least one control experiment per day, and almost always at least one from all of the same extension gains as the experiments with active damping that I tested that day. At least 10 experiments were performed for each combination of foot size, extension gain, and active damping gain, with more experiments performed for some control conditions.

5.1.4 Analysis of energy consumption data

I first subtracted the passive power consumption over the 12 minutes of experiments. The passive power consumption was estimated by collecting datapoints at 20, 24, 30, 40, 50, and 60 minutes by letting the robot hang from a clamp for the length of the trial and then disconnecting and recharging the battery to its storage voltage. Obtaining a linear fit to this data ($R^2 = 1$), I estimated that the passive power draw over a 12-minute experiment added 86.183 to the mAh reported by the charger. The stance duration for a typical jump is less than 0.5 s and each experiment consisted of only 25 jumps, meaning that the robot spent only about 10 s in stance during each experiment. The time spent during stance was therefore considered trivial relative to the estimated passive power consumption, and 86.183 was subtracted from each measurement recorded from the charger.

5.1.5 Analysis of jump height data

The robot's height during each jump was measured with a string potentiometer attached to the top of the robot, with its string attached to the top of the vertical rail the robot jumped up and down along. The data was captured by the robot's controller board and passed to the experimenter's laptop through a serial-to-USB connection.

After all experiments were complete, I used a custom script to display the logs and allow the experimenter to visually check each jump before accepting it as a data point. I rejected jumps where the log had a dropped packet or the script failed to correctly identify the apex of the jump. For a single condition, the minimum number of accepted jumps was 185 and the maximum number was 272.

5.2 Results

5.2.1 Energy consumption measurements for jumps on physical granular media

The data from the physical experiments is plotted in Fig. 5.3. For each pairing of a control compression-extension condition and active damping conditions, I first used an F-test to check for equal variances and then used a T-test to compare the conditions using the appropriate assumption about equal or unequal variances. Across all combinations of foot radius and virtual extension stiffness, the robot used less energy to jump with active damping than with the compression-extension controller. Most of these comparisons were statistically significant. From the simulations, I expected that the active damping controller should save more energy relative to the compression-extension controller when either the foot is smaller, or the virtual extension stiffness is greater. Therefore the combination of foot radius and extension gain that should have the largest difference between compression-extension and active damping is the smaller foot with the stiffer extension spring, and the combination with the smallest difference should be the larger foot with the softer extension spring. These predictions were consistent with the results of my statistical analysis. The difference between the control and each active damping coefficient was statistically significant for the smaller

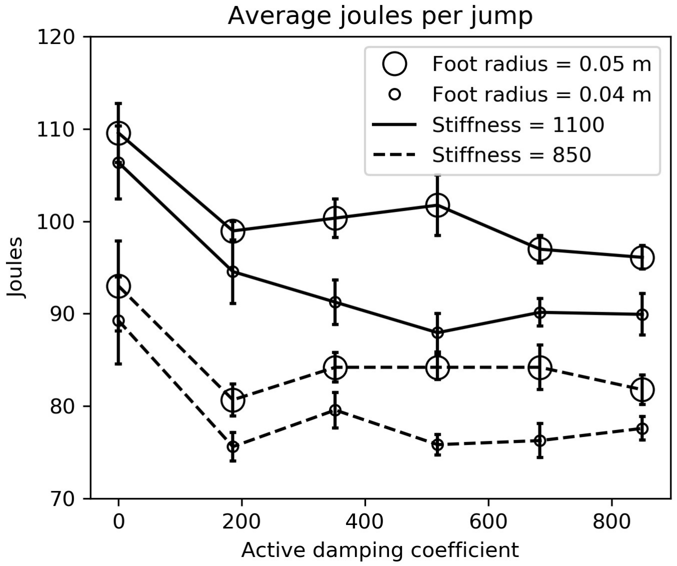

Figure 5.3: The robot used more energy with the compression-extension controller than the active damping controller when jumping on the granular media bed. The foot radius had a larger effect on the joules per jump than the leg's virtual spring stiffness during its extension mode. In this plot, the size of the circle indicates the foot's radius, the line style indicates the stiffness gain during extension, and the horizontal bars indicate standard error [109]. See Section5.2.1 for more information.

foot and stiffer extension spring combination (p = 0.041, 0.006, 0.001, 0.002, 0.002 for active damping coefficients in increasing order). The combination of the smaller foot and stiffer leg spring, and the larger foot and softer leg spring, both were statistically significantly different from the control in 4/5 cases. For the smaller foot and softer spring, the p-values were 0.019, 0.081, 0.019, 0.025, 0.037; for the larger foot and stiffer spring, the p-values were 0.007, 0.028, 0.103, 0.003, 0.002. In the combination where I expected the least benefit from the active damping controller, the difference between the compression-extension and active damping controllers was only statistically significant in one case, for the lowest active damping coefficient (p = 0.035).

I did not see a relationship between the active damping coefficient and reduced energetic cost to jump. The simulations (Section3.3) indicate that there is a point of diminishing returns for the active damping coefficient. Assuming that the model is correct, all of my physical experiments appear to have active damping coefficients beyond this point. I used a one-way ANOVA to check for an overall relationship between active damping coefficient and energy consumption, which was not significant for any combination of foot size and virtual extension stiffness ($p > 0.15$ for all conditions). I pooled all of the active damping conditions together and used a t-test to compare the pooled with active damping condition to the control condition. There was a statistically significant difference between all of the pooled active damping conditions and their respective control conditions ($p < 0.05$) except for the large foot, soft spring condition ($p = 0.071$). When comparing the pooled active damping conditions to control conditions for the same virtual leg extension stiffness but pooled across foot size, all comparisons were statistically significant ($p < 0.05$). Calling CE the cost to jump under a compression-extension controller with a certain foot size and extension stiffness and AD the average cost to jump under the active damping controller with any coefficient for that same foot size and extension stiffness, the percent savings afforded by the active damping controller is (CE-AD)/CE. The highest percent savings, about 15%, was in the small foot, stiff extension spring condition.

From the simulations (see Fig. 3.13), I expected that there should be a negligible difference between the joules per jump for a robot using the same virtual extension stiffness with different sized feet, and that there should be a larger reduction in the joules per jump for the same active damping coefficient when using a smaller foot. These patterns are supported by the data. Using the same method of first testing for equal varianc with an F-test and then performing a t-test, I found that differences between the joules per jump for the same virtual extension stiffness but different foot sizes were not statistically significant for the compression-extension condition ($p > 0.5$ for both). However, seven of the ten extension stiffness-active damping pairs were statistically significant ($p < 0.05$). One of the three which were not statistically significant was from the smallest active damping coefficient with the stiffer leg ($p = 0.024$) and the other two were from the softer spring condition (active damping gain = 100, $p = 0.079$; active damping gain = 250, $p = 0.057$). Comparing the larger and smaller foot sizes for the pooled active damping condition, both the stiffer and softer extension springs had a significant difference for joules per jump with foot size ($p < 0.0001$ for both virtual extension stiffnesses).

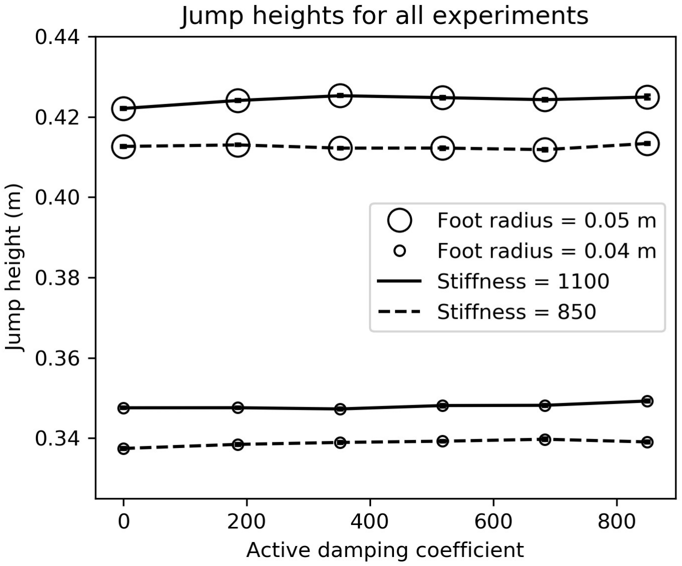

Figure 5.4: Using the active damping controller did not change the jump height. In most conditions, the robot jumped slightly higher (up to 3mm) on average when using active damping. Open circles indicate the average height of the robot's center of mass at the apex of the jump and horizontal lines indicate standard error. Line style indicates the leg spring's stiffness during extension [109]. See Section5.2.2 for more information.

5.2.2 Jump heights on physical granular media

Previous experiments [106, 108] suggested that the robot should jump slightly less high when using the active damping controller than when using the compression-extension controller, with a maximum height loss of less than 5%. I did not see that loss in these experiments (see Fig. 5.4). Repeating my procedure of performing an F-test for equal variance and then a t-test with the appropriate assumptions, I found either a statistically significant *increase* in jump height when using active damping compared with the compression-extension controller, or no statistically significant difference. However, the largest increase in jump height measured was only 3 mm. Although the difference in height was statistically significant, it is small enough to be negligible.

5.3 Conclusion

With these physical experiments, I have demonstrated the utility of the active damping controller in reducing energetic cost of transport without reducing the effectiveness of locomotion using a combination of simulations, analysis, and experiments in physical granular media. In other words, the number of joules required to take a single jump is significantly reduced without any loss to the height of the jump. This method of reducing energy cost has benefit over optimization and reinforcement learning based control methods because it uses basic principles of the energetic properties of sand. Data-driven, non-analytical methods may be more effective in specific conditions where there is data available, but this method should be reliably effective in any previously unencountered situation where the ground exerts bulk behavior forces like a granular media. Building an accurate and useful representation of a truly unknown environment is a very difficult task which I suggest is not necessary for many basic locomotion behaviors [114].

Since the active damping controller provides more benefit with smaller foot sizes, it will be most effective when the robot's feet cannot be significantly enlarged. For example, if the robot needs to walk over a mixed terrain with both sandy portions and rocky portions that would be more easily traversed with a smaller foot that can hook into crevices and lift over rocks without getting stuck, it might be more useful to use active damping than to increase the foot size. For our application, in which the robot's foot size cannot be significantly increased without reducing the utility of its feet as force sensors, the active damping controller is also an approach well suited to increasing endurance without diminishing capability.

The results in this chapter warrant a further discussion about the previous results from [108] discussed in Chapter 4, in which I jumped the same physical robot on top of a lightly geared robot emulating the forces from a compressible ground. In [108] I found that a higher active damping coefficient relative to the virtual extension stiffness resulted in a higher energy savings, which I did not replicate in these results on physical granular media, finding instead that varying the active damping coefficient did not change the energetic savings. The most likely explanation is that the robot's motors are hitting their torque limits during the extension mode in my experiments on physical granular media, meaning that there is very little difference from the motors' point of view between the different active damping coefficients. As we saw in the simulations in Section 3.3, Fig. 3.13, when we reach the artificially set torque limits, there is no further benefit from increasing the active damping coefficient after a certain point. In [108], the most significant increases from increasing the active damping gains were in the low virtual extension stiffness conditions, when a higher damping gain would not cause the robot to reach a torque limit. I was not able to test those low extension stiffness conditions on the physical setup due to the softness of the granular material and the necessity of the experimenter to be able to catch the robot while in flight. In the minimum stiffness, minimum foot size condition tested in this paper, the robot's foot achieved a height of only about 0.02 m from the undeflected surface of the ground.

Part III

Contextualization and discussion of the work

Chapter 6

Conceptual foundations and direction of future work

This chapter contextualizes the contributions of the thesis into a broader project of building robust, explainable robot behavior using compositions of mostly reactive controllers. The first section relates the work presented in this thesis to other, closely related work in robotics and to the work of the influential ecological psychologist James J. Gibson. His concept of "affordances" can be used to describe robot behaviors at many levels of abstraction. It is possible to implement affordance-exploiting behaviors in the morphology of a robot, in a low-level controller on the legs, or in a high-level navigation controller. This first section arose from a collaboration between myself, my adviser Dan Koditschek, and a philosopher affiliated with the GRASP Lab, Lisa Miracchi. The second section explores the trade-off between the robustnessness conferred by implementing aspects of control in the morphology of a robot versus the plasticity gained by implementing a controller in software, using the example of adapting the RHex and Minitaur robots for desert locomotion.

6.1 Behaviors as exploitations of opportunities

Consider our application: a collaborative team of humans and robots performing fieldwork in a desert [97] (Chapter 2). The environment is highly unpredictable, and the robot may not behave predictably: end effectors break, and sensors can be damaged in the field. Outside of a highly structured factory setting, attempting to produce desired behaviors by precisely controlling and modeling the environment, then using an intricate recreation of a task in an agent's associated internal representation in order to execute it, is empirically unworkable. It is computationally costly, inherently specialized, and inevitably brittle.

Equally unworkable is the opposite extreme of design: A dogmatic commitment to reject internal representation altogether [12], using only layers of reactive architectures to attempt to confer robustness [11]. This approach may be sufficient for certain tasks in specific settings, but is unnecessarily limiting, and does not confer robustness even in those cases if the layers are not well composed. Thus, there is need for more considered approaches which promote formal reasoning about how agent architectures can recruit preexisting affordances to generate desired behaviors.

An attractive middle ground is an empirically driven rather than dogmatically Gibsonian approach to design that uses structured compositions of sensory-driven controllers arranged to produce a coupled agent-environment system that achieves desired tasks. This research program is built on the two most vitally Gibsonian notions of affordance [18]: that perception is direct, with the consequence that we minimize representations where the task does not explicitly involve representation generation; and that the agent and environment comprise one indivisible system that admits analysis. This section reviews specific design episodes from a longstanding program of research in legged robotics that implicitly investigates affordances in the more formal but empirically grounded way we endorse.

This approach has two benefits which are not immediately obvious. First, it facilitates exploration of empirical possibilities that are Gibsonian in spirit: What representations are *needed* to produce the desired behavior? And second, if effort need not be spent to create representations that are useful for the robot to perform its basic behaviors, then the effort can be spent to create useful representations for communication between collaborating robots and humans. For example, a map of the ground stiffness in different locations in the desert would be a very useful representation for a team of robots tasked with helping geomorphologists studying erosion [97]. It is still useful even if the robots are able to navigate and locomote with reactive control that allows each robot to continue functioning normally even when it loses signal connection to team members, damages an end effector, or experiences a sensor glitch.

6.1.1 Affordances and their relationship to robotics

The ecological psychologist James J. Gibson [43] describes an *affordance* as a perceptually reliable feature of the environment that presents an agent with an opportunity for purposeful action. Autonomous robotics research can then be conceived as the process of designing a robot to systematically exploit the available opportunities for action in order to accomplish a specified overall task or tasks. In a complex, uncertain, and changing world, it is not obvious what design strategies will be most effective. It is therefore of general interest to ask how the explicit study of affordances might facilitate robotics research, and what the empirical study of affordances involves.

Ecological psychologists and philosophers have in general argued that perception and exploitation of affordances need not require the construction and manipulation of complex internal representations. Here, a “representation” refers to a model used in the control policy. For example, while a reactive controller could be argued to in some way represent the problem it is designed to solve, the system itself only senses and represents the variables used for feedback control. Beginning with the observation that agents have bodies [20, 123] and environments [25, 146], and considering affordances to be properties of the embodied agent-environment system [18, 128], the argument is that the agent already has all of the action-relevant properties of the world available to it. It thus does not need complex internal representations, either of the world or of the affordances it exploits.

Others — even those sympathetic to the cause of embodied cognition [23, 24] — have argued that complex representations are necessary for basic cognitive skills. It is elementary that some representation of internal state is necessary to achieve feedback stabilization of many control systems, and more comprehensive analyses suggest that robustness to complex perturbations in a complex world requires an agent to have complex internal representations of the environment and the perturbations [27, 39, 151]. The role of internal models for limbs and their environmental loading in animal motor activity is widely accepted by many neuroscientists [67]. Deep learning [45, 74] offers a modern version of this argument: The complexity of the problem a neural net can solve is in many ways limited by the size of the net and the amount of data, and thus the complexity of the model the net can build.

However, taking an ecological view, it may instead be the case that the agent needs only representations of "essential variables" which describe the relevant features of the activity the agent is involved in [41]. Representations using only these essential variables may be of much lower dimensionality than representations of the full system. Seemingly complex behaviors can then be built from structured compositions of such simpler controllers operating on the variables essential to their component behavior. The behavior resulting from such compositions of simpler controllers has the added benefit of increased explainability [26, 48, 117] since the expected behavior of the component parts is known and, when properly conceived, their composition follows formal mathematical properties [15, 33].

6.1.2 Application to locomotion science

Legged locomotion is one example of such a behavior. Robots are able to locomote using both very strong feed-forward control methods such as central pattern generators [59, 60, 118] as well as more distributed control [30, 36, 88, 89] and many roboticsts employ combinations thereof [37, 80]. Legged animals appear to pragmatically combine feedforward [44, 46, 81, 145] and feedback [92, 93, 127] controllers, implemented physically in both the mechanics of the body and in the nervous system [29, 31, 63, 126].

Research on insect navigation provides some support for the potential robustness and flexibility of coordinated systems of simple controllers, even for behaviors that had been previously believed to require cognitive maps [130]. Despite compelling evidence of complex cognition in invertebrate species [62], recent studies of insect navigation (for a review: [152]) suggest that insects integrate information from multiple simple navigation systems [56]. These could include a path integration system [144]; visual cues, with motivation controlling the switch between relevant cues [28]; reactive collision avoidance [7]; and a highly conserved systemic search mechanism when other mechanisms fail [19]. Each of these simple mechanisms for navigation operates in a relatively decentralized manner and requires little internal representation. Properly coordinated, together they are sufficient to produce robust navigation.

The literature on vertebrate navigation suggests that even animals which do seem to build complex spatial maps of their environments for navigation using special neural structures [49, 86, 119] still rely on the coordination of multiple navigation systems [85] – perhaps one solving the problem of local navigation with landmarks, and the other providing directional bearing [62]. It has even been suggested that primates navigate available affordances and choose between them in virtue of neurally implemented competing feedback controllers [21, 94].

However, the robotics research often considered to exemplify the application of ecological concepts like affordances to robotics is generally either oriented towards building representations of affordances [2, 51, 116, 153] or towards biomimetic implementations of specific animal behaviors or capabilities [6, 30, 58, 143] which then act as models for testing biological hypotheses [141, 142]. When non-biomimetic robotics research oriented towards coordinating simple controllers is considered [e.g., 3, 10, 11, 100], it is inevitably decades old. This motivates a reconsideration of how affordances are — and can be — studied in robotics, one that examines how simpler component processes and behaviors might be coordinated to explainably produce more complex and robust affordance exploitation.

6.1.3 The generative framework for robotics research

We find the application of Miracchi's [82, 83] *generative framework* useful for this discussion. The generative framework is designed to separate descriptions of a target behavior (in our case affordance exploitation) from commitments about the details of robot morphology, programming, or environment necessary to accomplish the task. The framework consists of three parts. The *basis* model describes aspects of the robot, including its methods of information processing, and relevant properties of the environment. The *emergent* model specifies the target behaviors in the relevant contexts. These behaviors operate at a larger spatiotemporal scale than those of the basis model, characterizing more global patterns and abstracting away from the details of implementation. Emergent behaviors are thus likely not to be obvious consequences of the basis model. The *generative* model specifies how features of the basis model determine ("generate") features of the emergent model, thus explaining the emergent behavior in terms of the implementation details at the basis level.[1] (See Table 6.1.3.)

This separation of the basis and emergent models can be demonstrated with an example application to two types of feedback controller. Say we have a proportional-derivative (PD) controller on the speed of a steam engine that operates by powering a motor to open or close a valve based on a reading given by an electronic velocity sensor such as an inertial measurement unit (IMU). The emergent model would then be the stable operation of the engine at the set point speed. The basis model would then include the engine dynamics, the way it is influenced by powering the valve, and the properties of the velocity sensor. Formal analysis on the stability of the PD controller would constitute the generative model. With properly set gains and an assumption that the sensor is within a certain percentage error, the controller would be guaranteed to bring the engine to the set speed. Now say the speed controller used a Watt governor instead [135], which raises and lowers the arms controlling the amount of steam allowed through the valve using centrifugal forces determined by the speed of the prime mover. The emergent model would be the same, but the basis model would substitute the governor's mechanical equations of motion for the electronic signal processing model of the IMU. Similarly, we can consider what representations are sufficient to effectively exploit the target affordance specified by an emergent model.

The next section applies this framework to six case studies of legged locomotion involving reactive controllers in order to demonstrate how these projects can be usefully conceptualized as designing robots to exploit affordances without complex internal representations. We choose work that uses reactive controllers to generate affordance exploitation, not only

[1] [83] uses the term "agent" model because of her focus on agency and intentionality. Here we use the term "emergent" both for increased generality and because we do not wish to take a stand on whether the target behaviors are agential in any important sense.

Term	Definition
basis model	describes relatively more concrete aspects of the robot and environment relevant to the target behavior (e.g., equations of motion)
emergent model	describes relatively more abstract behavior qualifying as systemic, effective affordance exploitation (e.g., fixed point location)
generative model	formal analysis linking features of the basis and emergent models (e.g., stability analysis of fixed point)
Gibsonian affordance	an opportunity for action in an agent-environment system (emergent-level property)
reactive control	responsive to robot-environment system's state, with little or no memory
parallel composition	controllers operating simultaneously in the same basis level, interacting according to formally described rules
sequential composition	"chains" of controllers, with the successful execution of one sub-behavior setting up the next sub-behavior
hierarchical composition	controllers operating at different levels of abstraction, e.g. on a single limb, coordination of limbs, center of mass trajectory, or to set a global goal

Table 6.1: Definitions of terms used to describe the case studies under the generative framework. An example application to a simple reactive controller represented with a dynamical system is provided in parentheses.

because they are often referenced in research on affordances in animals (see above), but also because robotics research has long demonstrated their utility. Reactive controllers respond to the state of the robot-environment system with little or no memory; are robust; typically require modest explicit internal world models, if at all; can often be formally analyzed with tools from dynamical systems theory; and — correctly designed and implemented — must indefatigably steer the coupled robot-environment system towards an appropriate goal. Such controllers can also be composed into more complex systems [3, 11], though it is vital to the explainability of the emergent behavior that these compositions follow formal mathematical rules [e.g., 15]. Compositions can be made in parallel [33, 36, 100], in sequence [13–15, 78], and hierarchically [40], which requires proper coordination of more primitive subcomponents whose isolated behavior and interactions are both mathematically understood. These interactions generate the required emergent behavior [138, 139] (see Table 6.1.3).

The case studies are drawn from one research group that typically provides formal generative explanations, easing the application of the generative framework. Focusing on one group also enabled us to quickly and deeply examine the ways in which systems can be designed to exploit affordances at multiple levels of abstraction from implementation details without introducing many different kinds of research problems, and to discuss each project with the primary and senior authors to ensure that the researchers agreed with this characterization of their work. Similar analysis would be interesting to apply to a variety of other robotics research programs [e.g., 13, 14, 52, 55, 79].

6.1.4 Case Studies

The six examples in this section are arranged in order of abstraction from the physics governing the robot's limb-ground interactions. Parallel, sequential, and hierarchical compositions of controllers will be mentioned where appropriate. The *emergent* and *basis* models (EM, BM) refer to the target behavior and implementation details of the paper cited in the last column. The *generative model* (GM) describes the formal analytical link, a mathematical explanation of how the target behavior emerges from the basis model (Table 6.1.3). The *Gibsonian affordance* (GA) describes in functional terms the designers' selected opportunity for action provided by the interaction of the robot's physical implementation with its environment, and the *agent-environment interaction* (AEI) specifies the perceptually reliable information or energetic exchange between the robot and the environment that makes this affordance possible to exploit.

Energetic cost of running on sand

This is the project described in the second section of this thesis. In this work, I aim to increase the capabilities of robots working alongside geoscientists studying erosion in environments like deserts [97].

Emergent behavior under study: The authors reduce the energetic cost of transport for a robot locomoting in the desert without sacrificing speed. Sand is highly dissipative, with a reaction force approximately linear in depth and quadratic in velocity, and no restoring forces [1] (Section 3.1.2).

Basis-level robot-environment pair: Minitaur [70] is a quadrupedal direct-drive robot that can be programmed for locomotion using parallel compositions of PD controllers that emulate damped springs [36]. Vertical hopping control for a single leg is thus decoupled from pitch control or coordination between legs. Deriving from Raibert's pioneering initial designs [100], a typical vertical hopping controller has a soft compliance gain during the first half of stance, allowing the leg "spring" to deflect under the weight of the body, and a stiff compliance gain during the second half of stance that causes the leg to extend and push the body up. When this type of controller is used on a compliant substrate like sand, the sudden injection of energy into the leg spring causes the foot to penetrate deeper into the sand at high velocity before the body moves up [106] (see Section 3.1.4. The authors target the vertical hopping controller and model its interaction with a bulk-behavior granular media model [1].

Generative relationship: Because the dissipation function of the sand is quadratic, most of the energy that a robot transfers to the ground through forces exerted at its foot will be quickly lost. The authors significantly reduce the energetic cost of a single jump to a given height [106, 108, 109] (Chapters 3, 4, 5) by adding a virtual damping force in proportion to the velocity of intrusion of the foot into the granular media. The virtual damper is only active during the second half of stance, when the robot's leg spring switches from soft compliance gain to stiff. By punishing high-speed intrusions, this virtual damping force prevents the foot from entering the dangerous high-velocity regimes in which large amounts of energy are quickly transferred to the ground, significantly reducing the energetic cost of a single step without reducing apex height.

Use of Gibsonian affordances: The robot does not model the ground in any control loop running at the time of execution. Rather, at every timestep, it interrogates the state of the agent-environment system – its body and foot position and velocity – and reacts to this information by changing its leg gain in the next timestep. To implement this controller on a behaving robot, the robot need only have position encoders on its motors to sense leg length, and a sensor to detect the distance between the robot's body and the ground. To motivate the controller, the agent-environment system is considered as one indivisible system – a vertical hopper interacting with granular media. The quantity of interest is the work transferred between the robot's foot and the ground.

Manipulating a robot's body pose using its limbs

[64] develops a controller that distributes effort between limbs of a six-legged robot standing on rigid, uneven terrain. Statically stable poses require the projected center of mass to lie within a polygon defined by the toes, which typically requires much more torque from some motors than others on uneven surfaces. Distributing effort between legs reduces the maximum torque requirement, lowering the overall energetic cost of standing and avoiding damage to the motors from overheating (EM).

To develop the controller, the authors build a "landscape" describing the energetic cost to stand as a function of body pose for a robot with a given legged morphology and a given toe placement (GA). They show formally that an effective descent direction towards a local minimum can be determined at every location on the landscape (GM) by the current draw from the motors, a direct measurement requiring no additional modeling (AEI).

Since the landscape can be expressed as the sum of costs due to the legs fighting each other in stance (internal forces) and the effort of the limbs to support the body mass (external forces), these two systems can be decoupled. The authors exploit this decomposition to implement the behavior on a physical six-legged robot as a parallel composition of two controllers: One to relax the internal forces by driving down the torque of legs operating in opposition to each other, and one to center the body mass over the toe polygon by driving down the body-averaged torques in parallel (BM).

Characterizing interactions with obstacles

Obstacles in a robot's environment could be used as opportunities for the robot to perturb its trajectory towards a desired direction. [95] walk a small robot with four legs and a fast-manufacturable body through a periodic obstacle field consisting of evenly spaced half-cylinders. By systematic experimentation, they observe the emergence of a yaw angle that locks the robot's steady-state trajectory over the obstacles in a manner relatively invariant to the robot's initial conditions upon entering the field (EM). This locked angle is an empirically stable function of body aspect ratio, the spacing between the obstacles, and the robot's gait (GA).

The authors develop an abstract representation of the effective yawing disturbance field resulting from the interaction between the robot's body aspect ratio and the spacing between the obstacles, which is a selectable consequence of gait (BM). The result is a dynamical model whose equilibrium states predict the resulting steady-state body yaw angle of the robot — and thus its steady-state locked heading (GM). The only feedback signals used by the robot are position and velocity measurements on the rotation of the legs, which are used for feedback control on the clock-driven position and velocity commands sent to the legs. These are sufficient to recruit the desired interaction between the body morphology and the environment structure, and the robot's heading stabilizes in absence of any body-level sensing (AEI).

Reactive control on a global scale

[61] develop a controller that drives a robot towards the locally most elevated position from any start location in a gentle hillslope environment punctured by tree-like, disk-shaped obstacles (EM). They test their controller on a physical six-legged robot walking on unstructured, forested hillslopes, using the top of the hillslope as the goal location. The robot uses an inertial measurement unit to acquire the local gradient, and a laser range finder to detect obstacles which are likely to be insurmountable (AEI).

A reactive "navigation"-level controller takes information about the local gradient and the presence of local obstacles, and produces a summed vector indicating the direction that increases the robot's elevation while avoiding a collision (GA). The coordination of the limbs to execute these commands is handled by a lower-level controller in a hierarchical composition.

The authors present multiple options of such compositions that assume different degrees of actuation authority for the lower-level controller. The strongest conclusions from formal analysis (global stability; GM-1) come from assuming the robot can be treated as a fully velocity-controlled two degree-of-freedom point particle (BM-1). More realistic models of outdoor mobility, which have more conservative guarantees (GM-2), assume that the robot can be treated as a non-holonomically constrained, velocity-controlled unicycle, or – when running at speed – a force-controlled unicycle.

Using recognition of complex obstacles to create abstract spaces conditioned for reactive control schemes

In contrast to the previous case study, which had a perceptually detected environmental feature as the goal location and a purely reactive control scheme, [138, 139] develop a controller that governs navigation in an environment with perceptually intricate obstacles towards an arbitrary, user-selected goal (EM). Obstacles may be highly complex, but if non-convex or densely packed then they are expected to be "familiar." The robot is assumed to have access to its global position and to an oracle with a catalogue of non-convex obstacles on which it was previously trained [91] (BM). When an obstacle enters the robot's sensory footprint at execution time, the obstacle can thus be instantaneously recognized and localized. Unrecognized obstacles are presumed to be convex and suitably sparse.

Once recognized, non-convex obstacles are abstracted to a generic round shape using a smooth change of coordinates, and if densely packed, may be conglomerated into one large obstacle. The result is a geometrically simple, abstracted space. A purely reactive navigation controller [4] closes the loop to guarantee obstacle free convergence to the goal location within the geometrically simplified but topologically equivalent environment (GA). Actuation commands for the geometrically detailed physical environment with non-convex obstacles are obtained by pushing forward the abstracted navigation commands through this change of coordinates (AEI). The authors perform a formal analysis of the overall dynamical system describing the closed-loop controller navigating reactively through the abstracted space as it is updated by the robot's perception of new obstacles. Proofs of correctness (GM-1, GM-2) are provided for two actuation schemes: A fully actuated point particle robot (BM-1), and a kinematic unicycle (BM-2). In a recent extension [137], the composed controller is implemented on a physical legged robot, with the unicycle commands interpreted by a lower-level controller for the robot's gait in a hierarchical composition.

The contribution of this project may at first seem to be at odds with our interpretation of affordances, but this project demonstrates how two very different methods can usefully complement one another. The problems of obstacle perception and navigation can be separated by the judicious use of a previously learned library of objects. This separation reduces the navigation problem to one which can be solved with reactive navigation control, about which formal guarantees can be provided. Methods like deep learning can then be used to produce the necessary library of objects. A careful composition of the navigation capability provided by the reactive controller and object recognition capabilities provided by the learning methods then produces the emergent behavior described in this project.

Layering deliberative and reactive controllers

[139] build on the previously described navigation system to develop a deliberative (offline) planning and reactive (online) control architecture which enables a robot to rearrange multiple objects in its imperfectly known environment. During execution of each deliberatively sequenced sub-goal, the combined controller produces reactive commands (GA) as a function of the recognized obstacle's boundary shape. Theoretical work [2018] assumes a robot constrained to move as a kinematic unicycle, with a globally known position, and an omnidirectional LIDAR producing a dense local depth map (BM). Physical experiments [2018] are performed with a four-legged direct-drive robot, with a hierarchically arranged composition of controllers coordinating the robot's legs to produce the kinematic unicycle-like behavior. The emergent model of the velocity-controlled unicycle is generated by a subcomponent ba-

sis model consisting of properly coordinated parallel and sequential compositions of hybrid Lagrangian stance dynamics [133]. The velocity-controlled unicycle then becomes the basis model of the reactive controller in this project, producing the whole-robot behavior.

Formal generative analysis (GM) in these papers addresses only the interaction between the deliberative planner and the reactive controller. The former breaks down the task of moving multiple objects to multiple goals into an ordered set of subtasks assigned to the latter. The reactive controller, which is endowed with the same oracle as the previous case study, is able to drive the robot around unanticipated obstacles (AEI) as needed in order to execute subtasks as they are assigned by the deliberative symbolic controller. The robot is then able to grab and move each object towards its planned subgoal location (EM).

The use of a reactive layer to handle obstacle interactions significantly simplifies the control problem, and allows the authors to provide formal guarantees about the conditions under which this combined controller should be expected to succeed. The offline, symbolic deliberative layer effectively solves the abstracted task planning problem. High-level commands from this layer drive the reactive manipulation and navigation layer, which can use realtime signal processing and control to readily handle unexpected geometric and topological complexities which would seriously challenge a symbolic planner.

6.1.5 Discussion

A major contribution of engineering to the understanding of affordances more generally is the formal methods which are used to describe the generative relationships between the implementation details and the desired behavior. The clear separation of the specified target behavior from the implementation details provided by a generative framework is helpful for cross-disciplinary discussion. The use of affordances in robotics research need not include the development of computational models of those affordances for robots to identify and thus exploit. Instead, consideration of the mutuality of the agent-environment system during robot behavior design can be used to develop robust and explainable architectures which implicitly exploit affordances. Roboticists can and do use systematic, empirical practice to apply Gibson's philosophy of affordances – just without naming them.

Considerations of engineering design and the practicability of abstraction from the environment at different levels of planning and control can determine the mix of endowed prior knowledge, representation building, and sensory dependence. For example, the last case study suggests that methodological commitment to use *only* reactive controllers [as by e.g. 11, 12] distracts from the potential benefits of combining a focus on affordances during robot behavior design with a cautionary approach to internal representations.[2] If effort need not be spent to create representations that are useful for the robot to perform its basic behaviors like locomotion and navigation, then the effort can be spent to create useful representations for tasks which do require them, such as to enable better communication between collaborating robots and humans. For example, a team of robots tasked with helping geomorphologists study erosion in the desert might build a map of the ground stiffness in different locations [97]. Such a map would be useful even if the robots are able to navigate and locomote completely with reactive control, which allows each robot to continue functioning normally even when it loses signal connection to team members, damages an end effector, or experiences a sensor glitch. Why not reserve the difficult task of building good representations for behaviors that require them, and use affordance-based reactive control for behaviors that don't?

6.2 The trade-off between robustness and plasticity: Mechanical and virtual compliance for locomotion in a compliant world

This section discusses an empirical question that is Gibsonian in spirit: Where should we place the line between the aspects of behavior we implement physically in a robot's body versus virtually in its software? The specific aspect of behavior under discussion here is compliance in the legs while locomoting on compliant ground: sand.

[2] As formalized by [116], this is similar to taking the "observer" perspective rather than the "agent" perspective.

6.2.1 Introduction

With improvements in additive manufacturing, programmable materials, and meta-materials that exhibit complex behaviors, the choice of where to place the line between control implemented in the robot's morphology and in its programming is becoming more and more available to the designer [72]. A useful way to place this line is by considering the aspects of control for which the designer needs more *plasticity* of behavior in terms of sensory capability or responsiveness to changing environments, or more *robustness* of behavior in terms of sensitivity to perturbations, sensor noise, and energy efficiency. The example of compliance in robot locomotion over complex, yielding terrain highlights the trade-off between robustness and plasticity.

Locomotion in a compliant world

As part of a collaboration with geoscientists and cognitive scientists, we take our robots to natural deserts, complex environments with compliant substrates that exhibit unpredictable behavior. Dry, relatively homogeneous granular media with known parameters like grain density and friction exerts forces in response to intrusion that are well characterized by bulk-behavior models [1, 66]. Of course, a natural desert environment will contain significant variation in packing density, grain size, and moisture content, even within the length of a single robot (or human) stride [110, 111]. Bulk-behavior models cannot therefore be relied upon to provide accurate predictions of the behavior of natural desert sand in response to intrusion.

It is intuitive to increase the forces applied to the ground in order to either offset the energy lost to this highly dissipative substrate, or to achieve a stronger reaction force from the ground. However, competent interaction with ground of this type, whether "competence" means control over height, use of minimal effort, or some other metric, cannot be accomplished this way. Exerting more force simply further excites the granular media, losing more energy without necessarily resulting in a higher jump [1, 106, 108].

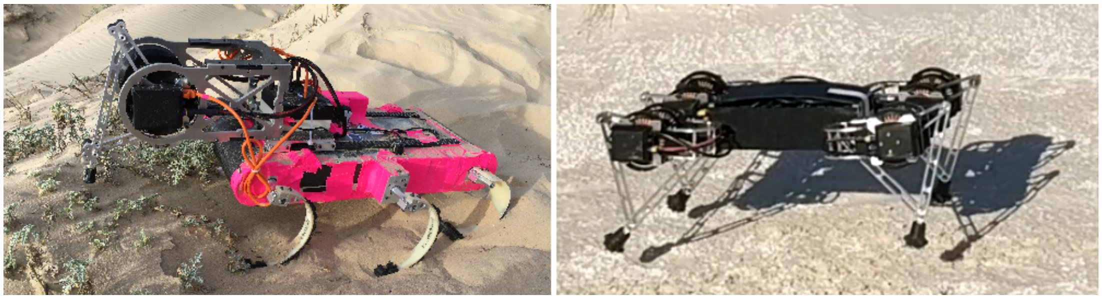

Figure 6.1: RHex [54] (left) and Minitaur [70] at Oceano Dunes and White Sands.

Locomotion using compliance

One method of programming locomotion is to use the Spring-Loaded Inverted Pendulum (SLIP) model [122]. RHex [54] and Minitaur [70] (Fig. 6.1) both run using SLIP-like dynamics, but the compliance in RHex is implemented mechanically in its springy C-shaped legs, and the compliance in Minitaur is implemented in software using proportional-derivative (PD) control on the two opposing motors in each leg.

Mechanical compliance: RHex exhibits SLIP-like dynamics when it runs by loading potential energy into its legs during the first half of stance, and releasing this potential energy to propel itself forward during the second half of stance [71]. The mechanical springs in the C-legs implement a PD controller on the leg extension by virtue of the spring force exerted by the legs in response to displacement. This controller takes trivial time and power to compute the restoring force and does not rely on any sensors other than the motors' encoders. Furthermore, until the legs reach mechanical failure, they store and release energy at no cost from the robot's power supply.

Virtual compliance: Each of Minitaur's four legs emulates a linear spring using PD control on two opposing direct-drive (no gearbox) motors through a four-bar linkage [70]. Exerting this emulated spring force costs energy from the robot's power supply. However, perturbations of the leg's position and velocity are "visible" to the robot, meaning that it can respond to this information as a sensory input.

Robustness and plasticity

The locomotion capability (*robustness* of behvaior) can be contrasted to the sensory capability and adaptability (*plasticity*) conferred by mechanical and virtual compliance in our robots.

Sensing capability: A single direct-drive Minitaur leg has recently been developed as mechanical shear stress sensor that can be used to study erosion processes [97]. Because the compliance in the Minitaur robot's legs comes entirely from software, it is able to sense perturbations at its toe – information that is not available to the RHex robot, which has mechanical compliance that hides information about its interactions with its environment from its motors.

Locomotion capability: In general, predictable morphological adaptations like wider feet that reduce the foot pressure of the locomotor [96] provide advantage in natural desert environments. A RHex with legs twice as wide as the standard 2.6 cm walked faster than a RHex with standard-issue legs while following the same path over 430 meters in the Tengger desert, and had a lower specific resistance [110]. The robot with wider legs also turned further in a single maneuver [110]. Both of these improvements to performance may be explained by the reduction in foot pressure causing an increase in "effective" leg length, that is, the length of the leg that does not intrude into the sand and over which the leg is able to pivot [75]. The mechanical implementation of RHex's compliance enabled us to further improve RHex's locomotion in desert environments by increasing the gear ratio nearly three times, from 28:1 to 79:1, without altering the compliance of its legs [97].

When tested in White Sands, Minitaur overheated quickly and was not able to transport itself for more than a few minutes without needing to cool down. The interventions used for RHex would severely limit Minitaur's utility for desert research: Increasing the foot mass by too much or gearing down the robot both reduce the sensing capability of the robot.

Adaptability: The natural environment is inherently unpredictable. While in general wider legs improved RHex's performance in natural deserts, there are specific situations in which this seeming adaptation is not advantageous. On a 30-degree dune that had recently experienced rainfall at the Tengger, we were unable to climb a dune with the wide-legged robot, which could not find purchase on the dry sand near the surface of the dune. The robot using standard-issue legs penetrated past the soft, dry sand and was able to ascend the dune by walking on the damp, cohesive sand underneath the surface [110]. The mechanical compliance in RHex's legs produces *robust* behavior that is consistent in execution and requires no sensory input or extra power, but the robot is unable to adapt to unpredictable situations: it is not *plastic*.

In contrast, a Minitaur leg, which has programmable compliance, can reactively change its compliance properties. By considering the compliant robot leg interacting with a compliant, highly dissipative ground as a two-spring system in which the ground's "spring" has no restoring motion, it is possible to mitigate the transfer of energy from the robot's leg to the sand, and thus the transfer of energy from the robot's battery to the ground. Since the compliance of the leg is created in software it can be changed to adapt to the changing environment. By adding a virtual damper and "dissipating" energy into the robot's leg "spring" in proportion to the intrusion velocity of the robot's foot into the sand, it was possible to reduce the mechanical energy required to jump to a fixed height by 50% and the losses to Joule heating in the motors by 20% in simulation [106] and emulation [108] with a single, vertically hopping direct-drive leg.

6.2.2 Discussion

Where do we put the line between mechanical and virtual implementations of compliance? Compliance created through PD control comes at a cost from the robot's power supply, but it confers the advantages of sensory capability and adaptability. The robot is able to sense features of its environment through its motors that may be useful both for the human experimenters and for its own locomotion. It is also able to change aspects of its compliance in response to its environment. If it is not necessary to change behavior in response to a changing situation, a designer can implement many aspects of control in the morphology of the robot and benefit from the robustness to perturbations and noise and the energy efficiency that such morphological implementations provide for "free". In a compliant world with unpredictable bulk-behavior forces, the ability to sense perturbations and plastically change behavior in response may be more important.

6.3 Conclusion

In this chapter, I have contextualized the contributions of my thesis into a broader project of building robust, explainable robot behaviors. I argued for moderation in the building and use of abstract representations for the use of programming robot behavior. Building good representations is difficult and certainly necessary for some tasks, such as to communicate relevant information to humans, but it does not appear to be necessary for mission-critical behaviors like locomotion or basic navigation. This discussion was guided by the notion of an affordance, which I suggest is a useful concept for robot behavior designers.

In the last section, I briefly described a trade-off between plasticity and robustness of behavior, using the example of mechanical and virtual compliance in the RHex and Minitaur robots, respectively. A task with a greater risk of catastrophic failure may require a robust behavior, even at the cost of the ability to change this behavior to respond optimally as the environment changes. I suggest that the application described in Chapter 2 falls under this category, as might applications to remote-operated rovers on distant planets or self-driving cars.

Chapter 7

Conclusion

In this thesis, I developed a reactive controller to reduce the energetic cost of transport for a direct-drive robot jumping on granular media in comparison to a well studied and robust controller for jumping on rigid ground. Whereas the nominal Raibert-style compression-extension controller transfers a lot of energy to a dissipative, deformable substrate when the robot pushes off in the second half of stance, my active damping controller slows down the leg extension in proportion to the foot intrusion velocity. As the highest energetic losses to the ground occur during high-speed foot intrusions, this should reduce the energetic cost of transport. Through a combination of simulation (Chapter 3), emulation (Chapter 4), and physical experiments in granular media (Chapter 5), I suggested that this active damping controller does in fact result in significant energy savings across a variety of dissipative ground conditions, jump heights, and gain choices.

There are several important implications of this finding. The reactive controller switches on automatically when used on soft ground because the added force is only nonzero when the foot intrusion velocity is nonzero. Thus, the successful use of a reactive controller for this task which switches on automatically suggests that the performance of a jumping robot can be significantly improved through behavioral adaptations without building a complex internal model of the granular media (Chapter 6). The consistency of energetic savings across a wide range of jump heights, ground conditions, and active damping gains suggests that this finding may not be limited to the specific conditions studied in this thesis. Instead, the results are likely to extend to other types of fragile, dissipative ground like wet sand, leaf litter, snow, and so on. Finally, the active damping controller was developed by examining trajectories of the robot's foot on the surface defined by the transfer of energy from the robot to the ground. The consistent results provided in this thesis by such a simple controller support the notion that robust, reliable control can be achieved by identifying a surface defined by the robot-environment interaction and using reactive control to push the robot towards favorable states.

There are also limitations to the results presented in this thesis. The primary limitation is that I only consider flat granular media being penetrated vertically. I do not consider the role of shearing forces or inclination in the granular media force responses. Shearing is an important part of locomotion, and more work in granular media physics is required to accurately model the forces in response to concurrent shearing and vertical intrusion. Work on angled intrusions [76] suggests that the force response from the granular media is lessened as the angle of attack rotates from the vertical, but it keeps a similar overall form. Similarly, work on inclined granular media [38, 50] suggests that the force response is similar in form but reduced in comparison to the force response of flat media. However, in neither case are the forces sufficiently well understood to perform the same sort of analytic simulations and modeling used in this thesis.

Future work in this project could include repeating the experiments in Chapter 5 with angled intrusions, rotating intrusions more similar to a footstep, and intrusions on an angled substrated. Once the force responses and efficacy of the active damping controller are better understood in this context, the controller could be implemented on a freely behaving Minitaur robot in a natural desert or dune system.

Other future work along this research program will include novel experimental protocols for comparing vastly different approaches to robot behavior design, such as an adversarial neural network which generates ground force profiles that cause a robot using a given controller to fail to jump; theoretical work suggesting structured methods to compose simple controllers; and new controllers designed to drive the state of a robot's foot, leg, or body towards a desired interaction with its environment, similarly to how the active damping controller drives the robot's foot state into a less dissipative region of surface defined by the energetic transfer between the leg and the ground.

Appendices

Appendix A

Contributions to the literature

The following table summarizes my contributions to the literature over the course of my thesis. The section in which the work is presented is indicated in the last column, where appropriate.

Title	Type (Ref'd)	Sec.
Virtual energy management for physical energy savings in a legged robot hopping on granular media [109]	Journal (Y)	3.3, 5
Reactive velocity control increases energy efficiency of jumping on granular media [104]	Poster (Y)	3.3, 5
Spatially and temporally distributed data foraging decisions in disciplinary field science [150]	Journal (Y)	
Technical report: Control and design of an open-source two-degree-of-freedom hopping robot [129]	Tech. report (N)	
Examples of Gibsonian affordances in legged robotics research using an empirical, generative framework [114]	Journal (Y)	6.1
Assimilating real-time measurements when making sampling decisions [149]	Presentation (Y)	
Using mobile robotic platforms to improve decision-making in geoscience field resarch [147]	Presentation (Y)	
Systematizing Gibsonian affordances in robotics [113]	Workshop paper (Y)	6.1
Mechanical and virtual compliance for robot locomotion in a compliant world [107]	Poster (Y)	6.2
Mitigating energy loss in a robot hopping on a physically emulated dissipative substrate [108]	Conference paper (Y)	4
Technological strategies for debiasing decision making in the geosciences [148]	Poster (Y)	
Improving decision making efficiency in field data collection using a heterogeneous group of legged robots [99]	Poster (Y)	
Using the art practice of play to communicate legged robotics research concepts [73]	Poster (Y)	
Determination of erosion thresholds and aeolian dune stabilization mechanisms via robotic shear strength measurements [98]	Poster (Y)	2.1
Reactive velocity control reduces energetic cost of jumping with a virtual leg spring on simulated granular media [106]	Conference paper (Y)	3
Mobile characterization of wind flow fields around solid and porous objects [136]	Conference poster (Y)	
Ground robotic measurement of aeolian processes [97]	Journal (Y)	2.1
Robotic measurement of aeolian processes [102]	Poster (Y)	2.1
Desert RHex Technical Report: Jornada and White Sands trip [112]	Tech. report (N)	2.2
Desert RHex Technical Report: Tengger desert trip [101]	Tech. report (N)	2.2

Table A.1: Table of all publications and presentations

Bibliography

[1] Jeffrey Aguilar and Daniel I Goldman. Robophysical study of jumping dynamics on granular media. *Nature Physics*, 12(3):278, 2016.

[2] Mihai Andries, Ricardo Omar Chavez-Garcia, Raja Chatila, Alessandro Giusti, and Luca Maria Gambardella. Affordance equivalences in robotics: a formalism. *Frontiers in neurorobotics*, 12:26, 2018.

[3] Ronald C Arkin, Ronald C Arkin, et al. *Behavior-based robotics*. MIT press, 1998.

[4] Omur Arslan and Daniel E Koditschek. Sensor-based reactive navigation in unknown convex sphere worlds. *The International Journal of Robotics Research*, 38 (2–3):196–223, Mar 2019. ISSN 0278-3649. doi: 10.1177/0278364918796267.

[5] Grover Beach. Oceano dunes in the guadalupe-nipomo dunes complex. *California Coastal Commission*, 2021. URL `https://documents.coastal.ca.gov/reports/2021/4/Th13a/th13a-4-2021-exhibits.pdf`.

[6] Randall D Beer. The dynamics of adaptive behavior: A research program. *Robotics and Autonomous Systems*, 20(2-4):257–289, 1997.

[7] Olivier JN Bertrand, Jens P Lindemann, and Martin Egelhaaf. A bio-inspired collision avoidance model based on spatial information derived from motion detectors leads to common routes. *PLoS computational biology*, 11(11):e1004339, 2015.

[8] Cacey Stevens Bester and Robert P Behringer. Collisional model of energy dissipation in three-dimensional granular impact. *Physical Review E*, 95(3):032906, 2017.

[9] SPD Birch, M Manga, B Delbridge, and M Chamberlain. Penetration of spherical projectiles into wet granular media. *Physical Review E*, 90(3):032208, 2014.

[10] Valentino Braitenberg. *Vehicles: Experiments in synthetic psychology*. MIT press, 1986.

[11] Rodney Brooks. A robust layered control system for a mobile robot. *IEEE journal on robotics and automation*, 2(1):14–23, 1986.

[12] Rodney A Brooks. Intelligence without representation. *Artificial intelligence*, 47(1-3): 139–159, 1991.

[13] Michael Burke, Yordan Hristov, and Subramanian Ramamoorthy. Hybrid system identification using switching density networks. *arXiv preprint arXiv:1907.04360*, 2019.

[14] Michael Burke, Svetlin Penkov, and Subramanian Ramamoorthy. From explanation to synthesis: Compositional program induction for learning from demonstration. *arXiv preprint arXiv:1902.10657*, 2019.

[15] Robert R Burridge, Alfred A Rizzi, and Daniel E Koditschek. Sequential composition of dynamically dexterous robot behaviors. *The International Journal of Robotics Research*, 18(6):534–555, 1999.

[16] Alexander H Chang, Christian M Hubicki, Jeff J Aguilar, Daniel I Goldman, Aaron D Ames, and Patricio A Vela. Learning to jump in granular media: Unifying optimal control synthesis with Gaussian process-based regression. In *Robotics and Automation (ICRA), 2017 IEEE International Conference on*, pages 2154–2160. IEEE, 2017.

[17] Alexander H Chang, Christian M Hubicki, Jeffrey J Aguilar, Daniel I Goldman, Aaron D Ames, and Patricio A Vela. Learning terrain dynamics: A gaussian process modeling and optimal control adaptation framework applied to robotic jumping. *IEEE Transactions on Control Systems Technology*, 2020.

[18] Anthony Chemero and Michael T Turvey. Gibsonian affordances for roboticists. *Adaptive Behavior*, 15(4):473–480, 2007.

[19] Ken Cheng, Patrick Schultheiss, Sebastian Schwarz, Antoine Wystrach, and Rüdiger Wehner. Beginnings of a synthetic approach to desert ant navigation. *Behavioural processes*, 102:51–61, 2014.

[20] Hillel J Chiel and Randall D Beer. The brain has a body: adaptive behavior emerges from interactions of nervous system, body and environment. *Trends in neurosciences*, 20(12):553–557, 1997.

[21] Paul Cisek. Cortical mechanisms of action selection: the affordance competition hypothesis. *Philosophical Transactions of the Royal Society B: Biological Sciences*, 362 (1485):1585–1599, 2007.

[22] Abram H Clark and Robert P Behringer. Granular impact model as an energy-depth relation. *EPL (Europhysics Letters)*, 101(6):64001, 2013.

[23] Andy Clark. The dynamical challenge. *Cognitive Science*, 21(4):461–481, 1997.

[24] Andy Clark. *Being there: Putting brain, body, and world together again.* MIT press, 1998.

[25] Andy Clark and David Chalmers. The extended mind. *analysis*, 58(1):7–19, 1998.

[26] Paul R Cohen. *Empirical methods for artificial intelligence*, volume 139. MIT press Cambridge, MA, 1995.

[27] Roger C Conant and W Ross Ashby. Every good regulator of a system must be a model of that system. *International journal of systems science*, 1(2):89–97, 1970.

[28] Holk Cruse and Rüdiger Wehner. No need for a cognitive map: decentralized memory for insect navigation. *PLoS computational biology*, 7(3):e1002009, 2011.

[29] Holk Cruse, Ch Bartling, M Dreifert, Josef Schmitz, DE Brunn, Jeffrey Dean, and Thomas Kindermann. Walking: A complex behavior controlled by simple networks. *Adaptive behavior*, 3(4):385–418, 1995.

[30] Holk Cruse, Thomas Kindermann, Michael Schumm, Jeffrey Dean, and Josef Schmitz. Walknet—a biologically inspired network to control six-legged walking. *Neural networks*, 11(7-8):1435–1447, 1998.

[31] Holk Cruse, Volker Dürr, and Josef Schmitz. Insect walking is based on a decentralized architecture revealing a simple and robust controller. *Philosophical Transactions of the Royal Society A: Mathematical, Physical and Engineering Sciences*, 365(1850): 221–250, 2006.

[32] DJ Cumberland and Roy James Crawford. *The packing of particles.* Elsevier Science Pub. Co. Inc., New York, NY, 1987.

[33] A. De and D.E. Koditschek. Parallel composition of templates for tail-energized planar hopping. In *2015 IEEE International Conference on Robotics and Automation (ICRA)*, page 4562–4569, May 2015. doi: 10.1109/ICRA.2015.7139831. URL `http://ieeexplore.ieee.org/lpdocs/epic03/wrapper.htm?arnumber=7139831`.

[34] Avik De and Daniel E Koditschek. Parallel composition of templates for tail-energized planar hopping. In *Robotics and Automation (ICRA), 2015 IEEE International Conference on*, pages 4562–4569. IEEE, 2015.

[35] Avik De and Daniel E Koditschek. The Penn Jerboa: A platform for exploring parallel composition of templates. *arXiv preprint arXiv:1502.05347*, 2015.

[36] Avik De and Daniel E Koditschek. Vertical hopper compositions for preflexive and feedback-stabilized quadrupedal bounding, pacing, pronking, and trotting. *The International Journal of Robotics Research*, 37(7):743–778, 2018.

[37] Kenneth S Espenschied, Roger D Quinn, Randall D Beer, and Hillel J Chiel. Biologically based distributed control and local reflexes improve rough terrain locomotion in a hexapod robot. *Robotics and autonomous systems*, 18(1-2):59–64, 1996.

[38] Yoël Forterre and Olivier Pouliquen. Flows of dense granular media. *Annu. Rev. Fluid Mech.*, 40:1–24, 2008.

[39] Bruce A Francis and Walter Murray Wonham. The internal model principle of control theory. *Automatica*, 12(5):457–465, 1976.

[40] Robert Full and Daniel Koditschek. Templates and anchors: Neuromechanical hypotheses of legged locomotion on land. *J. of Experimental Biology*, 202(23):3325–3332, 1999.

[41] Martin Fultot, P Adrian Frazier, MT Turvey, and Claudia Carello. What are nervous systems for? *Ecological Psychology*, 31(3):218–234, 2019.

[42] K.C. Galloway, G. C. Haynes, B. Deniz Ilhan, A. Johnson, R. Knopf, G. Lynch, B. Plotnick, M. White, and D. E Koditschek. X-RHex: A highly mobile hexapedal robot for sensorimotor tasks. *University of Pennsylvania Electrical and Systems Engineering Technical Reports*, 2010. URL `http://kodlab.seas.upenn.edu/Kod/Xrhextech`.

[43] James J Gibson. *The ecological approach to visual perception*. Psychology Press, 1979.

[44] Martin Golubitsky, Ian Stewart, Pietro-Luciano Buono, and JJ Collins. Symmetry in locomotor central pattern generators and animal gaits. *Nature*, 401(6754):693, 1999.

[45] Ian Goodfellow, Yoshua Bengio, and Aaron Courville. *Deep learning*. MIT press, 2016.

[46] Sten Grillner. Neurobiological bases of rhythmic motor acts in vertebrates. *Science*, 228(4696):143–149, 1985.

[47] François Guillard, Yoël Forterre, and Olivier Pouliquen. Lift forces in granular media. *Physics of Fluids*, 26(4):043301, 2014.

[48] David Gunning and David W Aha. Darpa's explainable artificial intelligence program. *AI Magazine*, 40(2):44–58, 2019.

[49] Torkel Hafting, Marianne Fyhn, Sturla Molden, May-Britt Moser, and Edvard I Moser. Microstructure of a spatial map in the entorhinal cortex. *Nature*, 436(7052):801, 2005.

[50] Endao Han, Liang Zhao, Nigel Van Ha, S Tonia Hsieh, Daniel B Szyld, and Heinrich M Jaeger. Dynamic jamming of dense suspensions under tilted impact. *Physical Review Fluids*, 4(6):063304, 2019.

[51] Mohammed Hassanin, Salman Khan, and Murat Tahtali. Visual affordance and function understanding: A survey. *arXiv preprint arXiv:1807.06775*, 2018.

[52] Ross L Hatton and Howie Choset. Sidewinding on slopes. In *2010 IEEE International Conference on Robotics and Automation*, pages 691–696. IEEE, 2010.

[53] KM Havstad, WP Kustas, Albert Rango, JC Ritchie, and TJ Schmugge. Jornada experimental range: A unique arid land location for experiments to validate satellite systems. *Remote Sensing of Environment*, 74(1):13–25, 2000.

[54] G. Clark Haynes, Jason Pusey, Ryan Knopf, Aaron M. Johnson, and Daniel E. Koditschek. Laboratory on legs: an architecture for adjustable morphology with legged robots. May 2012. doi: 10.1117/12.920678. URL `http://spie.org/x648.html?product_id=920678`.

[55] Neville Hogan and Dagmar Sternad. Dynamic primitives in the control of locomotion. *Frontiers in computational neuroscience*, 7:71, 2013.

[56] Thierry Hoinville and Rüdiger Wehner. Optimal multiguidance integration in insect navigation. *Proceedings of the National Academy of Sciences*, 115(11):2824–2829, 2018.

[57] Christian M Hubicki, Jeff J Aguilar, Daniel I Goldman, and Aaron D Ames. Tractable terrain-aware motion planning on granular media: an impulsive jumping study. In *Intelligent Robots and Systems (IROS), 2016 IEEE/RSJ International Conference on*, pages 3887–3892. IEEE, 2016.

[58] Auke J Ijspeert. Biorobotics: Using robots to emulate and investigate agile locomotion. *science*, 346(6206):196–203, 2014.

[59] Auke Jan Ijspeert. Central pattern generators for locomotion control in animals and robots: a review. *Neural networks*, 21(4):642–653, 2008.

[60] Auke Jan Ijspeert, Alessandro Crespi, Dimitri Ryczko, and Jean-Marie Cabelguen. From swimming to walking with a salamander robot driven by a spinal cord model. *science*, 315(5817):1416–1420, 2007.

[61] B Deniz Ilhan, Aaron M Johnson, and Daniel E Koditschek. Autonomous legged hill ascent. *Journal of Field Robotics*, 35(5):802–832, 2018.

[62] Lucia F Jacobs and Randolf Menzel. Navigation outside of the box: what the lab can learn from the field and what the field can learn from the lab. *Movement Ecology*, 2 (1):3, 2014.

[63] Devin L Jindrich and Robert J Full. Dynamic stabilization of rapid hexapedal locomotion. *Journal of Experimental Biology*, 205(18):2803–2823, 2002.

[64] Aaron M Johnson, G Clark Haynes, and Daniel E Koditschek. Standing self-manipulation for a legged robot. In *2012 IEEE/RSJ International Conference on Intelligent Robots and Systems*, pages 272–279. IEEE, 2012.

[65] Ken Kamrin. A hierarchy of granular continuum models: Why flowing grains are both simple and complex. In *EPJ Web of Conferences*, volume 140, page 01007. EDP Sciences, 2017.

[66] Wenting Kang, Yajie Feng, Caishan Liu, and Raphael Blumenfeld. Archimedes' law explains penetration of solids into granular media. *Nature communications*, 9(1), 2018.

[67] Mitsuo Kawato. Internal models for motor control and trajectory planning. *Current Opinion in Neurobiology*, 9(6):718–727, Dec 1999. ISSN 0959-4388. doi: 10.1016/S0959-4388(99)00028-8.

[68] Gavin Kenneally and Daniel E Koditschek. Leg design for energy management in an electromechanical robot. In *2015 IEEE/RSJ International Conference on Intelligent Robots and Systems (IROS)*, pages 5712–5718. IEEE, 2015.

[69] Gavin Kenneally, Wei-Hsi Chen, and Daniel E. Koditschek. Actuator transparency and the energetic cost of proprioception. In *International Symposium on Experimental Robotics*, page 485–495. Springer, 2018.

[70] Gavin D Kenneally, Avik De, and Daniel E Koditschek. Design principles for a family of direct-drive legged robots. *IEEE Robotics and Automation Letters*, 1(2):900–907, 2016.

[71] D. E. Koditschek, R. J. Full, and M. Buehler. Mechanical aspects of legged locomotion control. *Arthropod Structure and Development*, 33(3):251–272, 2004. URL `https://pdfs.semanticscholar.org/02b6/2bbf1c361a27f76beb251a27dc077e64d463.pdf`.

[72] Daniel E Koditschek. What is robotics? why do we need it and how can we get it? *Annual Review of Control, Robotics, and Autonomous Systems*, 4:1–33, 2021.

[73] Diedra Krieger and Sonia F Roberts. Using the art practice of play to communicate legged robotics research concepts. *Science Through Narrative Symposium, Society for Integrative and Comparative Biology (SICB) Annual Meeting 2018*, 2018.

[74] Yann LeCun, Yoshua Bengio, and Geoffrey Hinton. Deep learning. *nature*, 521(7553): 436–444, 2015.

[75] Chen Li, Paul B Umbanhowar, Haldun Komsuoglu, Daniel E Koditschek, and Daniel I Goldman. Sensitive dependence of the motion of a legged robot on granular media. *Proceedings of the National Academy of Sciences*, 106(9):3029–3034, 2009.

[76] Chen Li, Tingnan Zhang, and Daniel I Goldman. A terradynamics of legged locomotion on granular media. *Science*, 339(6126):1408–1412, 2013.

[77] XR Li, Zh Sh Zhang, JG Zhang, XP Wang, and XH Jia. Association between vegetation patterns and soil properties in the southeastern Tengger Desert, China. *Arid Land Research and Management*, 18(4):369–383, 2004.

[78] Tomas Lozano-Perez, Matthew T Mason, and Russell H Taylor. Automatic synthesis of fine-motion strategies for robots. *The International Journal of Robotics Research*, 3(1):3–24, 1984.

[79] Anirudha Majumdar and Russ Tedrake. Funnel libraries for real-time robust feedback motion planning. *The International Journal of Robotics Research*, 36(8):947–982, 2017.

[80] Josh Merel, Matthew Botvinick, and Greg Wayne. Hierarchical motor control in mammals and machines. *Nature Communications*, 10(1):1–12, 2019.

[81] Karen Minassian, Ursula S Hofstoetter, Florin Dzeladini, Pierre A Guertin, and Auke Ijspeert. The human central pattern generator for locomotion: Does it exist and contribute to walking? *The Neuroscientist*, 23(6):649–663, 2017.

[82] Lisa Miracchi. Generative explanation in cognitive science and the hard problem of consciousness. *Philosophical Perspectives*, 31(1):267–291, 2017.

[83] Lisa Miracchi. A competence framework for artificial intelligence research. *Philosophical Psychology*, 32(5):589–634, 2019.

[84] Marc Z Miskin and Heinrich M Jaeger. Evolving design rules for the inverse granular packing problem. *Soft Matter*, 10(21):3708–3715, 2014.

[85] Edvard I Moser, Emilio Kropff, and May-Britt Moser. Place cells, grid cells, and the brain's spatial representation system. *Annu. Rev. Neurosci.*, 31:69–89, 2008.

[86] John O'Keefe and Neil Burgess. Geometric determinants of the place fields of hippocampal neurons. *Nature*, 381(6581):425, 1996.

[87] Ratan Othayoth, George Thoms, and Chen Li. An energy landscape approach to locomotor transitions in complex 3d terrain. *Proceedings of the National Academy of Sciences*, 117(26):14987–14995, 2020.

[88] Dai Owaki and Akio Ishiguro. A quadruped robot exhibiting spontaneous gait transitions from walking to trotting to galloping. *Scientific reports*, 7(1):277, 2017.

[89] Dai Owaki, Takeshi Kano, Ko Nagasawa, Atsushi Tero, and Akio Ishiguro. Simple robot suggests physical interlimb communication is essential for quadruped walking. *Journal of The Royal Society Interface*, 10(78):20120669, 2013.

[90] Andreea Panaitescu, Xavier Clotet, and Arshad Kudrolli. Drag law for an intruder in granular sediments. *Physical Review E*, 95(3):032901, 2017.

[91] Georgios Pavlakos, Xiaowei Zhou, Aaron Chan, Konstantinos G Derpanis, and Kostas Daniilidis. 6-dof object pose from semantic keypoints. In *2017 IEEE International Conference on Robotics and Automation (ICRA)*, pages 2011–2018. IEEE, 2017.

[92] Keir G Pearson. Proprioceptive regulation of locomotion. *Current opinion in neurobiology*, 5(6):786–791, 1995.

[93] Keir G Pearson. Generating the walking gait: role of sensory feedback. In *Progress in brain research*, volume 143, pages 123–129. Elsevier, 2004.

[94] Giovanni Pezzulo and Paul Cisek. Navigating the affordance landscape: feedback control as a process model of behavior and cognition. *Trends in cognitive sciences*, 20 (6):414–424, 2016.

[95] Feifei Qian and Daniel E. Koditschek. An obstacle disturbance selection framework: emergent robot steady states under repeated collisions. *International Journal of Robotics Research (in revision)*, 2019.

[96] Feifei Qian, Tingnan Zhang, Wyatt Korff, Paul B Umbanhowar, Robert J Full, and Daniel I Goldman. Principles of appendage design in robots and animals determining terradynamic performance on flowable ground. *Bioinspiration & biomimetics*, 10(5), 2015.

[97] Feifei Qian, Douglas Jerolmack, Nicholas Lancaster, George Nikolich, Paul Reverdy, Sonia Roberts, Thomas Shipley, R Scott Van Pelt, Ted M Zobeck, and Daniel E Koditschek. Ground robotic measurement of aeolian processes. *Aeolian research*, 27: 1–11, 2017.

[98] Feifei Qian, Dylan Bentley Lee, Sophie Bodek, Sonia Roberts, T Turner Topping, Yosef Robele, Daniel E Koditschek, and Douglas J Jerolmack. Determination of erosion thresholds and aeolian dune stabilization mechanisms via robotic shear strength measurements. *AGUFM*, 2017:EP51C–1663, 2017.

[99] Feifei Qian, Cristina G Wilson, Thomas F Shipley, Douglas J Jerolmack, Sonia Roberts, Julia Messick, and Daniel E Koditschek. Improving decision making efficiency in field data collection using a heterogeneous group of legged robots. In *AGU Fall Meeting 2018*. American Geophysical Union, 2018.

[100] Marc H Raibert. *Legged robots that balance*. MIT press, 1986.

[101] S. F. Roberts, J. M. Duperret, Xinwan Li, Hesheng Wang, and Daniel E Koditschek. Desert RHex technical report: Tengger desert trip. 2014.

[102] S. F. Roberts, D J Jerolmack, N Lancaster, G Nikolich, P B Reverdy, T F Shipley, R S Van Pelt, T M Zobeck, and D E Koditschek. Robotic measurement of aeolian processes. In *AGU Fall Meeting 2015*. American Geophysical Union, 2015.

[103] Sonia Roberts and Jeff Duperret et al. Desert rhex technical report: Jornada and white sands trip. Technical report, University of Pennsylvania, November 2014.

[104] Sonia Roberts and Daniel E Koditschek. Reactive velocity control increases energy efficiency of jumping on granular media. In *Dynamic Walking 2021*. Dynamic Walking, 2021.

[105] Sonia Roberts, Jeff Duperret, Xinwan Li, Hesheng Wang, and D. E. Koditschek. Desert RHex technical report: Tengger Desert trip. Technical report, University of Pennsylvania, November 2014.

[106] Sonia F Roberts and Daniel E Koditschek. Reactive velocity control reduces energetic cost of jumping with a virtual leg spring on simulated granular media. *Proceedings of the 2018 IEEE International Conference on Robotics and Biomimetics (ROBIO)*, 2018.

[107] Sonia F. Roberts and Daniel E. Koditschek. Mechanical and virtual compliance for robot locomotion in a compliant world. Poster presented at Robot Design and Customization workshop at ICRA, 2019.

[108] Sonia F Roberts and Daniel E Koditschek. Mitigating energy loss in a robot hopping on a physically emulated dissipative substrate. *Proceedings of the 2018 IEEE International Conference on Robotics and Automation (ICRA)*, 2019.

[109] Sonia F Roberts and Daniel E Koditschek. Virtual energy management for physical energy savings in a legged robot hopping on granular media. Submitted to Frontiers in Robotics and AI., 2021.

[110] Sonia F Roberts, J Duperret, Xinwan Li, Hesheng Wang, and D Koditschek. Desert RHex technical report: Tengger desert trip. *ESE Department Technical Report*, 2014.

[111] Sonia F Roberts, Jeff Duperret, Aaron M Johnson, Scott van Pelt, Ted Zobeck, Nick Lancaster, and Daniel E Koditschek. Desert RHex technical report: Jornada and White Sands trip. *ESE Department Technical Report*, 2014.

[112] Sonia F. Roberts, Jeff M. Duperret, Aaron M Johnson, Scott van Pelt, Ted Zobeck, Nick Lancaster, and Daniel E Koditschek. Desert RHex technical report: Jornada and white sands trip. 2014.

[113] Sonia F. Roberts, Daniel E. Koditschek, and Lisa J. Miracchi. Systematizing Gibsonian affordances in robotics: an empirical, generative approach derived from case studies in legged locomotion. Poster presented at 2nd International Workshop on Computational Models of Affordances at ICRA, 2019, `https://r1d1.github.io/iwcmar/papers/RobertsKM2019.pdf`, 2019.

[114] Sonia F. Roberts, Daniel E. Koditschek, and Lisa J. Miracchi. Examples of gibsonian affordances in legged robotics research using an empirical, generative framework. *Frontiers in Neurorobotics*, 14:12, 2020. ISSN 1662-5218. doi: 10.3389/fnbot.2020.00012. URL `https://www.frontiersin.org/article/10.3389/fnbot.2020.00012`.

[115] LOUIS SAHAGuN. Off-road vehicles to be banned at oceano dunes within three years. *LA Times*, 2021. URL `https://www.latimes.com/california/story/2021-03-19/off-road-vehicles-will-be-banned-at-oceano-dunes-within-three-years`.

[116] Erol Şahin, Maya Çakmak, Mehmet R Doğar, Emre Uğur, and Göktürk Üçoluk. To afford or not to afford: A new formalization of affordances toward affordance-based robot control. *Adaptive Behavior*, 15(4):447–472, 2007.

[117] Wojciech Samek, Thomas Wiegand, and Klaus-Robert Müller. Explainable artificial intelligence: Understanding, visualizing and interpreting deep learning models. *arXiv preprint arXiv:1708.08296*, 2017.

[118] Uluc Saranli, Martin Buehler, and Daniel E Koditschek. Rhex: A simple and highly mobile hexapod robot. *The International Journal of Robotics Research*, 20(7):616–631, 2001.

[119] Francesco Savelli and James J. Knierim. Origin and role of path integration in the cognitive representations of the hippocampus: computational insights into open questions. *Journal of Experimental Biology*, 222(Suppl 1):jeb188912, 2019.

[120] Matthias Schröter, Daniel I Goldman, and Harry L Swinney. Stationary state volume fluctuations in a granular medium. *Physical Review E*, 71(3):030301, 2005.

[121] Matthias Schröter, Sibylle Nägle, Charles Radin, and Harry L Swinney. Phase transition in a static granular system. *EPL (Europhysics Letters)*, 78(4):44004, 2007.

[122] William J. Schwind and Daniel E. Koditschek. Control of forward velocity for a simplified planar hopping robot. volume 1, pages 691–696. IEEE, 1995. URL `http://ieeexplore.ieee.org/xpls/abs_all.jsp?arnumber=525364`.

[123] Lawrence Shapiro. *Embodied cognition*. Routledge, 2011.

[124] James Slonaker, D Carrington Motley, Qiong Zhang, Stephen Townsend, Carmine Senatore, Karl Iagnemma, and Ken Kamrin. General scaling relations for locomotion in granular media. *Physical Review E*, 95(5):052901, 2017.

[125] Jochen Smolka, Marcus J Byrne, Clarke H Scholtz, and Marie Dacke. A new galloping gait in an insect. *Current Biology*, 23(20):R913–R915, 2013.

[126] S Sponberg and RJ Full. Neuromechanical response of musculo-skeletal structures in cockroaches during rapid running on rough terrain. *Journal of Experimental Biology*, 211(3):433–446, 2008.

[127] Inge Steuer and Pierre A Guertin. Central pattern generators in the brainstem and spinal cord: an overview of basic principles, similarities and differences. *Reviews in the Neurosciences*, 30(2):107–164, 2019.

[128] Thomas A Stoffregen. Affordances as properties of the animal-environment system. *Ecological psychology*, 15(2):115–134, 2003.

[129] Weiyi Tang, Sonia F. Roberts, and Daniel E. Koditschek. Technical report: ODrive hopper: control and design of an open-source two-degree-of-freedom hopping robot. Technical report, 2020.

[130] Edward C Tolman. Cognitive maps in rats and men. *Psychological review*, 55(4):189, 1948.

[131] T Turner Topping, Vasileios Vasilopoulos, Avik De, and Daniel E Koditschek. Towards bipedal behavior on a quadrupedal platform using optimal control. In *Unmanned Systems Technology XVIII*, volume 9837, page 98370H. International Society for Optics and Photonics, 2016.

[132] T Turner Topping, Gavin Kenneally, and Daniel E Koditschek. Quasi-static and dynamic mismatch for door opening and stair climbing with a legged robot. In *2017 IEEE International Conference on Robotics and Automation (ICRA)*, pages 1080–1087. IEEE, 2017.

[133] T. Turner Topping, Vasileios Vasilopoulos, Avik De, and E. Koditschek, Daniel. Composition of templates for transitional pedipulation behaviors. page (in press), 2019.

[134] Thomas Topping and D. E. Koditschek. Composition of templates for transitional legged behaviors. *Dynamic Walking*, 2020.

[135] Tim Van Gelder. What might cognition be, if not computation? *The Journal of Philosophy*, 92(7):345–381, 1995.

[136] Robert S Van Pelt, Ted M Zobeck, Tarek Kandakji, Dan Koditschek, Feifei Qian, Paul Reverdy, and Sonia Roberts. Mobile characterization of wind flow fields around solid and porous objects. In *AGU Fall Meeting Abstracts*, volume 2016, pages EP21A–0850, 2016.

[137] V. Vasilopoulos and D. E. Koditschek. Reactive Navigation in Partially Known Non-Convex Environments. In *13th International Workshop on the Algorithmic Foundations of Robotics (WAFR)*, 2018.

[138] Vasileios Vasilopoulos, T Turner Topping, William Vega-Brown, Nicholas Roy, and Daniel E Koditschek. Sensor-based reactive execution of symbolic rearrangement plans by a legged mobile manipulator. In *2018 IEEE/RSJ International Conference on Intelligent Robots and Systems (IROS)*, pages 3298–3305. IEEE, 2018.

[139] Vasileios Vasilopoulos, William Vega-Brown, Omur Arslan, Nicholas Roy, and Daniel E Koditschek. Sensor-based reactive symbolic planning in partially known environments. In *2018 IEEE International Conference on Robotics and Automation (ICRA)*, pages 1–5. IEEE, 2018.

[140] Theodore Von Karman and G Gabrielli. What price speed? Specific power required for propulsion of vehicles. *Mechanical Engineering*, 72:775–781, 1950.

[141] Barbara Webb. Can robots make good models of biological behaviour? *Behavioral and brain sciences*, 24(6):1033–1050, 2001.

[142] Barbara Webb. Validating biorobotic models. *Journal of Neural Engineering*, 3(3): R25, 2006.

[143] Barbara Webb and Thomas Consilvio. *Biorobotics*. Mit Press, 2001.

[144] Rüdiger Wehner, Mandyam V Srinivasan, et al. Path integration in insects. *The neurobiology of spatial behaviour*, pages 9–30, 2003.

[145] Patrick J Whelan. Control of locomotion in the decerebrate cat. *Progress in neurobiology*, 49(5):481–515, 1996.

[146] Andrew D Wilson and Sabrina Golonka. Embodied cognition is not what you think it is. *Frontiers in psychology*, 4:58, 2013.

[147] C. G. Wilson, F Qian, T. F. Shipley, D. J. Jerolmack, S. F. Roberts, and D. E. Koditschek. Using mobile robotic platforms to improve decision-making in geoscience field research. In *Proceedings of the 2019 Geological Society of America (GSA)*, 2019.

[148] Cristina G Wilson, Thomas F Shipley, Feifei Qian, Douglas J Jerolmack, Sonia Roberts, Julia Messick, and Daniel E Koditschek. Technological strategies for debiasing decision making in the geosciences. *AGUFM*, 2018:IN21C–0715, 2018.

[149] Cristina G Wilson, Feifei Qian, Thomas F Shipley, Douglas J Jerolmack, Sonia Roberts, Anmol Kathail, and Daniel E Koditschek. Assimilating real-time measurements when making sampling decisions. *AGUFM*, 2019:IN44A–05, 2019.

[150] Cristina G Wilson, Feifei Qian, Douglas J Jerolmack, Thomas F Shipley, Sonia F Roberts, Jonathan Ham, and Daniel E. Koditschek. Spatially and temporally distributed data foraging decisions in disciplinary field science. *Cognitive Research: Principles and Implications (under review)*, 2020.

[151] Walter Murray Wonham. Towards an abstract internal model principle. *IEEE Transactions on Systems, Man, and Cybernetics*, (11):735–740, 1976.

[152] Antoine Wystrach and Paul Graham. What can we learn from studies of insect navigation? *Animal Behaviour*, 84(1):13–20, 2012.

[153] Philipp Zech, Simon Haller, Safoura Rezapour Lakani, Barry Ridge, Emre Ugur, and Justus Piater. Computational models of affordance in robotics: a taxonomy and systematic classification. *Adaptive Behavior*, 25(5):235–271, 2017.